ISSN 1512-1127

საქართველოს გეოფიზიკური საზოგადოების ჟურნალი

სერია ა. დედამიწის ფიზიკა

JOURNAL OF THE GEORGIAN GEOPHYSICAL SOCIETY

Issue A. Physics of Solid Earth

ტომი 19ა **2016**

vol. 19A **2016**

ISSN 1512-1127

საქართველოს გეოფიზიკური საზოგადოების ჟურნალი

სერია ა. დედამიწის ფიზიკა

JOURNAL OF THE GEORGIAN GEOPHYSICAL SOCIETY

Issue A. Physics of Solid Earth

ტომი 19ა **2016**

vol. 19A **2016**

საქართველოს გეოფიზიკური საზოგადოების ჟურნალი

მთავარი რედაქტორი: თ. ჭელიძე

სერია ა. დედამიწის ფიზიკა

სერიის შინაარსი:

ჟურნალი (ა) მოიცავს მყარი დედამიწის ფიზიკის ყველა მიმართულებას. გამოქვეყნებულ იქნება: კვლევითი წერილები, მიმოხილვები, მოკლე ინფორმაციები, დისკუსიები, წიგნების მიმოხილვები, განცხადებები.

ЖУРНАЛ ГРУЗИНСКОГО ГЕОФИЗИЧЕСКОГО ОБЩЕСТВА

Главный редактор: Т. Челидзе

Серия А. Физика Твердой Земли

Содержание журнала:

Журнал (А) Грузинского геофизического общества охватывает все направления физики твердой Земли. В журнале будут опубликованы научные статьи, обозрения, краткие информации, дискуссии, обозрения книг, объявления.

JOURNAL OF THE GEORGIAN GEOPHYSICAL SOCIETY

Editor-in-chief: T. Chelidze

Issue A. Physics of Solid Earth

Scope of the Journal:

The Journal (A) is devoted to all branches of the Physics of Solid Earth. Types of contributions are: research papers, reviews, short communications, discussions, book reviews, and announcements.

მისამართი:

საქართველო, 0160, თბილისი, ალექსიძის ქ. 1, მ. ნოდიას გეოფიზიკის ინსტიტუტი

ტელ.: 233-28-67; Fax; (995 32 2332867); e-mail: tamaz.chelidze@gmail.com

გამოქვეყნების განრიგი და ხელმოწერა

სერია (ა) გამოიცემა წელიწადში ერთხელ. ხელმოწერის ფასია (უცხოელი ხელმომწერისათვის) 30 დოლარი, საქართველოში – 10 ლარი, ხელმოწერის მოთხოვნა უნდა გაიგზავნოს რედაქციის მისამართით. შესაძლებელია ონლაინ წვდომა: http://openjournals.gela.org.ge/index.php/GGS/index

Адрес:

Грузия, 0171, Тбилиси, ул. Алексидзе, 1. Институт геофизики им. М. З. Нодия

Тел: 233-28-67; 294-35-91; Fax: (99532)2 332867; e-mail: root@geophy.acnet.ge

Порядок издания и условия подписи:

Том серии (А) издается по одному номеру в год. Подписная цена 30 долларов США. Заявка о подписке высылается в адрес редакции. Возможен онлайн доступ http://openjournals.gela.org.ge/index.php/GGS/index

Address:

M. Nodia Institute of Geophysics, 1 Alexidze Str., 0160 Tbilisi, Georgia

Tel.: 233-28-67; Fax: (99532) 2332867; e-mail: root@geophy.acnet.ge

Publication schedule and subscription information:

One volume of issue (A) per year is scheduled to be published. The subscription price is 30 $.

Subscription orders should be sent to editor's address. Online access is possible: http://openjournals.gela.org.ge/index.php/GGS/index

Journal of Georgian Geophysical Society,
Issue(A), Physics of Solid Earth, v.19A, 2016, pp. 3-34

Georgian-European Center "Geodynamical Hazards of High Dams" at the Council of Europe: 20 years of activity.

T. Chelidze, V.Abashidze, T. Matcharashvili, T. Tsaguria, T. Tsamalashvili, A. Amiranashvili, N. Zhukova, Z. Chelidze, N. Varamashvili

Georgian-European Center "Geodynamical Hazards of High Dams"

M. Nodia Institute of Geophysics

Abstract

In 1987 by the resolution of the Council of Europe the EUR-OPA Major Hazards Agreement was created. EUR-OPA Major Hazards Agreement is a platform for co-operation in the field of major natural and technological disasters between Europe and the South of the Mediterranean. The Georgian-European Centre on Geodynamical Hazards of High Dams - GHHD (Tbilisi, Georgia) was founded in 1996. The paper considers the main results of GHHD activity obtainedduring 20 years after its foundation.

1. Introduction.

EUR-OPA Major Hazards Agreement is a platform for co-operation in the field of major natural and technological disasters between Europe and the South of the Mediterranean. Its field of competence covers the major natural and technological disasters - knowledge, prevention, risk management, post-crisis analysis and rehabilitation.The main objectives of the EUR-OPA Major Hazards Agreement are to reinforce and to promote co-operation between Member States in a multi-disciplinary context to ensure better prevention, protection against risks and better preparation in the event of major natural or technological disasters.

The important component of EUR-OPA is the network of 27 specialized centers. The Georgian-European Centre on Geodynamical Hazards of High Dams - GHHD (Tbilisi, Georgia) was founded in 1996 (http://www.coe.int/t/dg4/majorhazards/centres/presentation/ghhd_fr.asp).

The 271 m high Enguri arch dam, still one of the highest arch dam in operation in the world, was built in the canyon of the Enguri river (West Georgia) in the 1970s. It is located in a zone of high seismicity (MSK intensity IX) and close to the Ingirishi active fault. The high seismic and geodynamical activities together with the large number of people living downstream of the dam made the Enguri dam a potential source of a major catastrophe in Georgia. Of course, the Enguri Dam with its 1 billion cubic meters water reservoir is a potential source of large man-made catastrophe and it should be under permanent monitoring. At the same time this it is an amazing natural laboratory, where we can investigate tectonic and geotechnical strains/processes and response to the lake load-unload impact, i.e. the reaction to a controllable loading of Earth crust. This is an important scientific issue, connected with such problem as Reservoir Triggered Earthquakes.

All these factors conditioned foundation of Georgian-European Centre on Geodynamical Hazards of High Dams. The President of the Scientific Committee of GHHD is Dr. Martin Wieland (Switzerland), Director: is Academician Tamaz Chelidze, the Chairman of the Administrative Council: Prof. Vakhtang Abashidze.

Generally the hazards, such as extreme strains in the dam body, due to aging, damage or overloading can be monitored (Wieland, Mueller 2009) and in some cases even predicted by networks of special sensors (strainmeters, tiltmeters, etc).

The stability of a dam can be tested by its long-term and short-term response to the water load. The dam as a whole or its individual elements may respond to certain loading conditions through time-dependent elastic and inelastic deformations. For each action a safety limit can be determined, which must not be exceeded. Due to unusual or extreme loadings or due to accumulation of damage critical conditions may occur, which are jeopardizing the safety of dam.

The Centre is created for development of multinational, multidisciplinary approach to the problems of geodynamical hazards, generated by high dams, including:

i. development and testing of modern methods of multidisciplinary monitoring of local and regional geodynamical processes in the proximity of large dams on the basis of Enguri Dam International Test Area (EDITA).
ii. mathematical modeling of geodynamical processes at large dams,
iii. prediction of impending geodynamical events (earthquakes, tectonic deformations, landslides) and prognosis of response of large dams to these impacts
iv. monitoring of physical-chemical processes and associated variations in physical properties of foundation rocks
v. creation of databases of geodynamical observations on large dams
vi. analysis and generalization (in collaboration with other European centers) of possible natural and manmade hazards, creation of scenarios of possible damage and instructions for public education on what to do in case of alarm, during and after the disaster.
vii. active participation in international, regional and national projects related to major disasters and environmental problems.
viii. development of real time automatic telemetric monitoring and early warning systems for control of stability of large engineering objects.

By the funding of the EUR-OPA Major Hazards Agreement we realizedmore than 20 projects. The most important projects are shortly considered below:

2. *Real-time telemetric monitoring system of large dams (DAMWATCH): the case of the Enguri Dam International Test Area (EDITA).*

The M. Nodia Institute of Geophysics (MNIG) and Georgian-European Centre ”Geodynamical Hazards of High Dams” operating in the frame of Open Partial Agreement on Major Disasters at the Council of Europe developed the <u>real-time geotechnical telemetric monitoring system of large dams</u>

(DAMWATCH). This low-cost early warning system designed by MNIG and "ALGO Ltd" (Tbilisi) consists of sensors (tiltmeters, APPLIED GEOMECHANICS Model 701-2), which are connected to terminals and central controllers and by a GSM/GPRS modem transmits the data to the diagnostic center.

Fig. 1. Google view of Enguri Dam International Test Area (EDITA) territory. The arrow shows position of major Ingirishi fault.

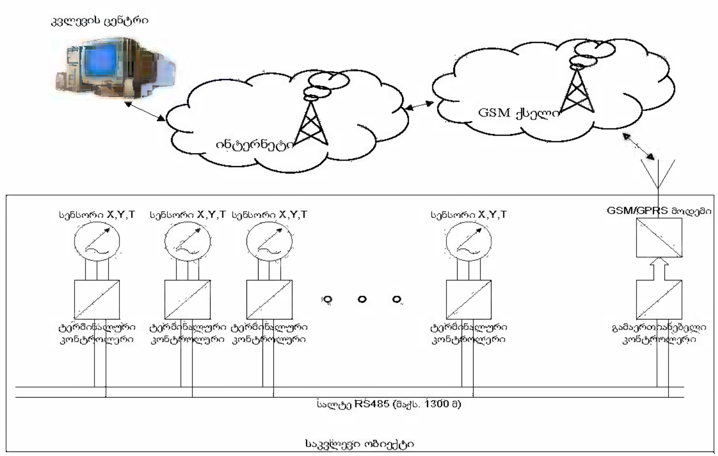

Fig.2. The cost-effective early warning system designed by MNIG and "ALGO Ltd" (Tbilisi) consists ofsensors (tiltmeters, APPLIED GEOMECHANICS Model 701-2), which are connected to terminals and central controllers and by a GSM/GPRS modem transmits the data to the diagnostic center.

The simplest approach to dam safety problem is to compare response of real strain/tilt data with design values, which as a rule use Hook's rheology (static, linear elasticity approach). If measured characteristics, e.g. strains are close to or larger than theoretically predicted limit deformations, some preventive measures will be realized. Of course, predictions of the model have to be compared with monitoring data (Table 1).

Table 1. Comparison of observed plumbline horizontal displacements (Bronshtein, 2008) and corresponding tiltmeters data (horizontal displacements in mm and tilts in seconds, with Root Mean Square) at maximal water level in the lake (510 m) for three sections of Enguri HPP (Abashidze et al. 2008) with theoretical (critical) admissible values of plumblines calculated by (Emukhvari, Bronshtein, 1991).

Level	Section 12			Section 18			Section 26		
	Observed plumbline data	Observed tiltmeter data	Critical Admissible values	Observed plumbline data	Observed tiltmeter data	Critical Admissible values	Observed plumbline data	Observed tiltmeter data	Critical Admissible values
360 m	20 mm	11 mm (38±5.1)"	89 (122)"	35 mm			15 mm	14 mm (46±5.6)"	88 mm
402 m	40 mm	32 mm (63±4.5)"	59 (112)"	60 mm	55 mm (70±3.9)"'	55 mm	30 mm	37 mm (74±4.1)'	58 mm
475 m	60 mm	48 mm (56±8.7)"	31 (182)"	65 mm			55 mm	42 mm (55±5.5)"	26 mm

The Table 1 presents observed data: plumbline horizontal displacements (Bronshtein, 2008) and corresponding tiltmeters data (horizontal displacements in mm and tilts in seconds, with Root Mean Square) at maximal water level in the lake (510 m) for three sections of Enguri HPP (Abashidze et al. 2008) and theoretical (critical) admissible values of plumblines calculated by (Emukhvari, Bronshtein, 1991). The generally accepted approach is to compare the observed stress (strain) to calculated stresses, which correspond to some fraction of yield strength or of the ultimate strength of the material, which the construction is made of.

Analysis of the Table leads to following conclusions: i. at the level 360 m all displacements are less than critical values; ii. at the level 402 m only in the central 18-th section the displacements are close to critical ones; iii. at the highest level (475 m) displacement of the side sections are larger than critical, i.e. at this level the state should be considered as diagnosis MAS or "faulty". According to Emukhvari and Bronshtein (1991) in this case it is necessary to carry out repeated diagnostics of construction on the basis of re-examination of monitoring data and correction of theoretical predictions of response of the dam to loads. The displacement observation data obtained by two different methods are in satisfactory agreement. Besides, the dam performs normally and there are no visual signs of significant damage.

This means that the theoretical model needs some corrections, possibly taking into account complexity of construction structure (lifts, joints, inhomogeneity etc).

Indeed, the real engineering structures manifest deviations from this simple model, which can be used for diagnostics. From above it follows that a promising technique could be analysis of deviations from static elasticity model, namely, analysis of nonlinearity of stress-strain relation such as hysteretic behavior during load-unload cycle. Figure 3 (left) shows how two components of tilts of dam body, along (X) and normal (Y) to the dam crest at Enguri Dam respond to the seasonal recharge-discharge cycle of the reservoir; on the right the hysteresis in seismic velocities of foundation section for the same cycle is shown.

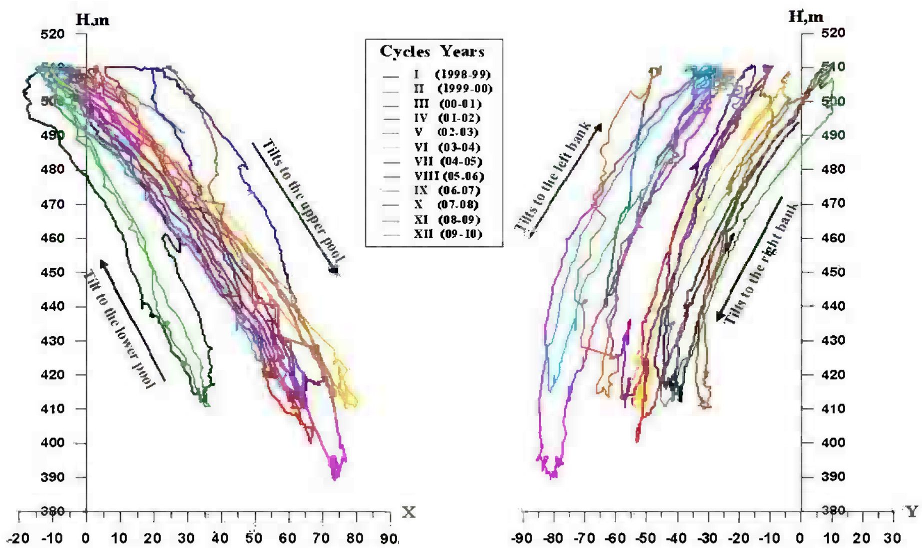

Figure 3. Left: Tilts in sec, registered in the body of Enguri High Dam, Georgia (section 12, mark 402) intwo directions, along (X) and normal (Y) to the dam crest versus water level in the lake H in meters, during12 seasonal cycles (1998-2009). Note hysteresis in load-unload response.

The interpretation of observed hysteretic stress-strain or tilt-stress diagrams (Fig.3) can be accomplished by the theory of mesoscopic elasticity (McCall&Guyer 1994, Guyer&Johnson 2009). The matter is that heterogeneous materials such as mass concrete and rocks are nonlinear and their behavior is very different from this of its homogeneous components: for example, stress-strain (or tilt) dependences manifest nonlinear hysteretic elastic behavior, namely, asymmetric response to loading and unloading of so called mesoscopic structural features (mainly compliant microcracks) to stress variation. Heterogeneous materials contain an enormous number (10^9-10^{12}) of such defects per square centimetre, which means that macroscopic elastic properties of the material depend strongly on behavior of microcracks. Thus parameters of hysteretic cycle can be used for diagnostics of material: in the absence of cracks the brittle solid manifests linear elasticity without any hysteresis, appearance of cracks leads to hysteresis and the opening of hysteresis curve increases with the number of defects.

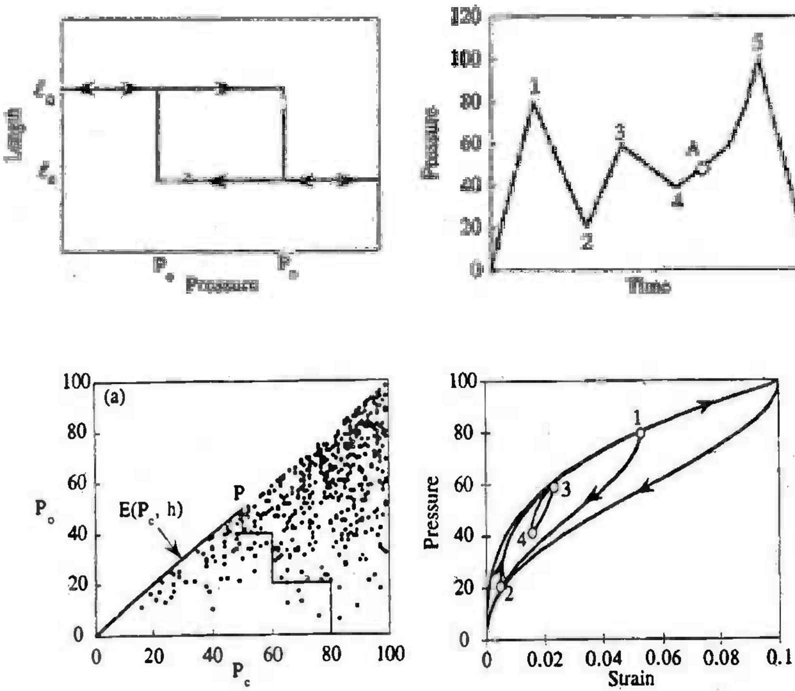

Fig.4. The approximation of hysteretic data by Preisach-Mayergoyz (P-M) phenomenological model. In the P-M model the system is represented by complex of hysteretic elastic units or hysterons, which manifest asymmetric response to loading-unloading cycle

The approximation of hysteretic data can be accomplished using the Preisach-Mayergoyz (P-M) phenomenological model. In the P-M model the system is represented by complex of hysteretic elastic units or hysterons, which manifest asymmetric response to loading-unloading cycle (Fig.4).

Comparing outputs of Preisach-Mayergoyz (P-M) model (Fig.3) with annual hysteresis loops of Enguri dam tilts (Fig.2)we can mark close similarity between model and observed data, i.e. P-M approach can be used in dam diagnostics. The successive annual Enguri tilt loops are shifted, which means that seasonal loading and unloading cycles involve the appearance of some residual strain. This shift also can be a diagnostic sign for aging effects (e.g. thermal cracking, freezing-thawing cycles, chemical processes in mass concrete or foundation rock etc.).

As a rule nonlinear contributions to well-designed and well-constructed dam strains are small, so it can be concluded that the dam design based on linear approach works quite well, but the analysis of relatively small nonlinear effects can produce promising methods of dam safety diagnostics due to high sensitivity of nonlinear systems to small external impacts.

Short-term diagnostic tools. The main short-term diagnostic tool is the analysis of the eigenfrequencies of the dam based on the power spectra of dam vibrations caused by water discharge, turbine operation or ambient seismic noise. The record of natural dam vibrations at Enguri dam shows that the dominant frequency on the crest of the dam is about 1 Hz; this is in good agreement with results of the analysis of accelerograms recorded during the Racha earthquake (2005, M=6) and numerical analysis of a typical dam.

Our data show that the vibration spectrum also covers other than 1 Hz, much lower frequencies. These LF vibrations were recorded by the network of precision tiltmeters (Applied Geomechanics). The frequency response of the device, shown in Fig. 5 demonstrates, that in principle we can register LF vibrations in the wide range 0.05-20 Hz. We found that the amplitudes and frequencies of the broadband power spectra respond clearly to changes in the state of the dam, which means that monitoring of LF vibrations is a promising technique for dam diagnostics.

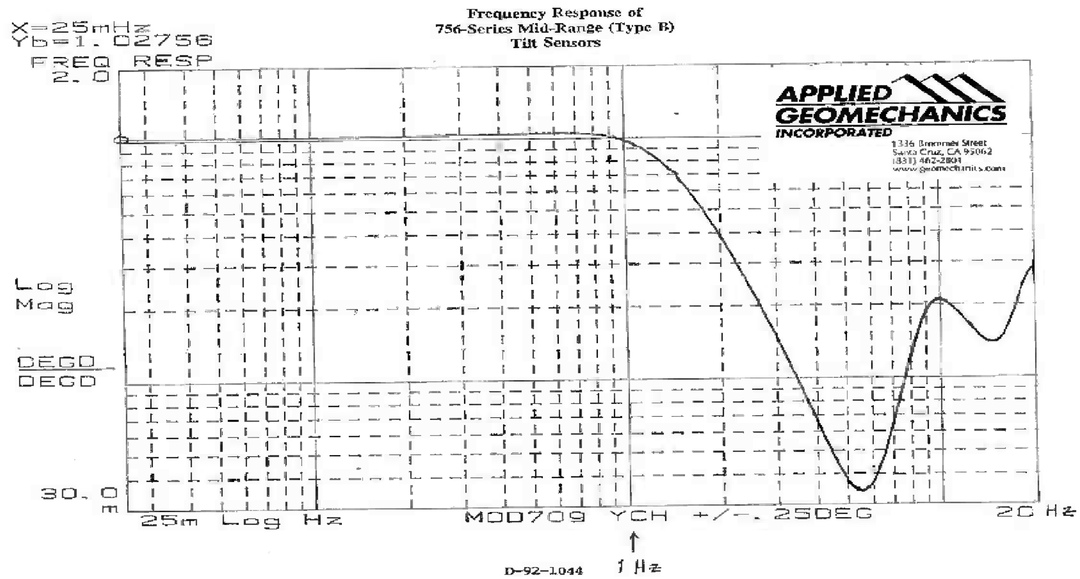

Fig.5. The frequency response of the precision tiltmeters (Applied Geomechanics).

Methods of linear and nonlinear analysis of strain and tilt time series for dam stability assessment. In order to ensure correct statistical and dynamical investigation of dam stability problem, modern methods of linear and nonlinear analysis of strain and tilt time series are used. The following time series analysis methods are used: statistical methods (moments, distribution testing), time-frequency analysis methods (power spectrum, autocorrelation function), time-frequency (wavelet transformation) and eigenvalue methods, denoising of data sets (nonlinear noise reduction), testing of memory properties of targeted process (long range correlation testing, detrended fluctuation analysis (DFA), multifractal detrended fluctuation analysis; correlation and information dimension calculation recurrence plots (RP) and recurrence quantitative analysis (RQA) (Press et al. 1996, Strogatz 2000, Marwan 2003, Matcharashvili&Chelidze 2000).

Nonlinear dynamics analysis allows revealing hidden structures (regularities) in seeming random time series. In order to test the sensitivity of selected methods and to assess effects of external influences on Earth tilt dynamics in the dam foundation, we have carried out retrospective analysis of tilt data. Namely, we considered tilt data sets of Earth crust tilt, hourly measured for 13 years of continued observation in the dam foundation (1971-1983). Tilt data sets in the following 7 time windows have been analyzed: 1) long before reservoir filling, 2) immediately before and 3) just after beginning of filling, 4) after second, 5) third and 6) fourth stage of reservoir filling and 7) long after completion of reservoir filling. Figures illustrate RQA determinism (RQA%DET) and Lempel-Ziv algorithmic complexity measure for mentioned 7 periods. Note that nonlinear dynamical properties of tilt time series after long enough regular (periodic) reservoir exploitation return to the patterns observed before the dam building and lake fill. These data confirm possibility of detection of man-made effects (i.e. diagnostics) in tilt time series.

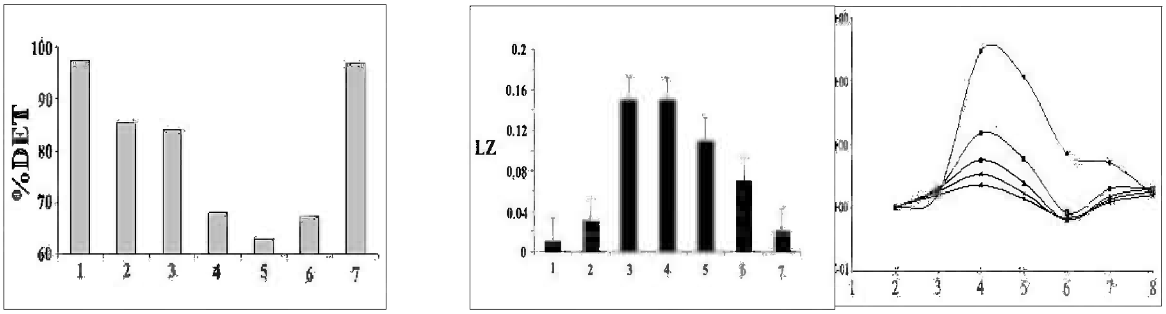

Fig.6. Left: RQA determinism measure calculated for dam foundation tilt data series for different stages of observation. Middle: Lempel-Ziv complexity measure calculated for tilt data series for different stages of observation. Right: variation of Tsallis entropy calculated for Earth tilt data series for different stages of observation. Curves from top to down correspondent to different q values from 1 to 5. Numbers on abscissa correspond to periods of observation (see text).

Reservoir induced synchronization of seismicity. Nonlinear dynamics analysis of seismic time series in the Enguri reservoir area and water level in the lake reveals strong increase of order in earthquake occurrence during quasi-periodic load-unload regime of the lake. It is well known, that large reservoirs located in the seismically active zones are often considered as a factor, quantitatively and qualitatively influencing earthquakes generation. During impoundment or after it both the number and magnitude of earthquakes around reservoir significantly increases. After several years these changes in earthquake generation, named as reservoir induced seismicity (RIS) essentially decreases down to the level, when lesser earthquakes occur with lower magnitudes. To explain this decrease, we propose the model of phase synchronization of local seismic activity by the periodic variation of the water level - reservoir induced synchronization of seismicity (RISS). Data, presented in Fig. 7 evidence that increase of order in dynamics of daily earthquake occurrence, earthquakes temporal and energy distribution took place around Enguri high dam water reservoir (Western Georgia) during the periodic variation of the water level (WL) in the lake. Here the upper plot shows the WL time series – it became quasi-periodic after the day 4000 after beginning tiltmeter observations. The middle plot RQA %DET of daily number of earthquakes calculatedfor consecutive non overlapping 1-year sliding windows(*circles*). Averaged results of RQA %DET for 20 shuffled (*asterisks*)and phase-randomized (*triangles*) surrogates of daily numberof earthquakes in consecutive 1-year sliding windows. The lowest plot shows RQA %DET of magnitude (*black columns*) and waiting time(*grey columns*) sequences: (1) before impoundment, (2) duringflooding and reservoir filling, and (3) periodic change of waterlevel in reservoir.

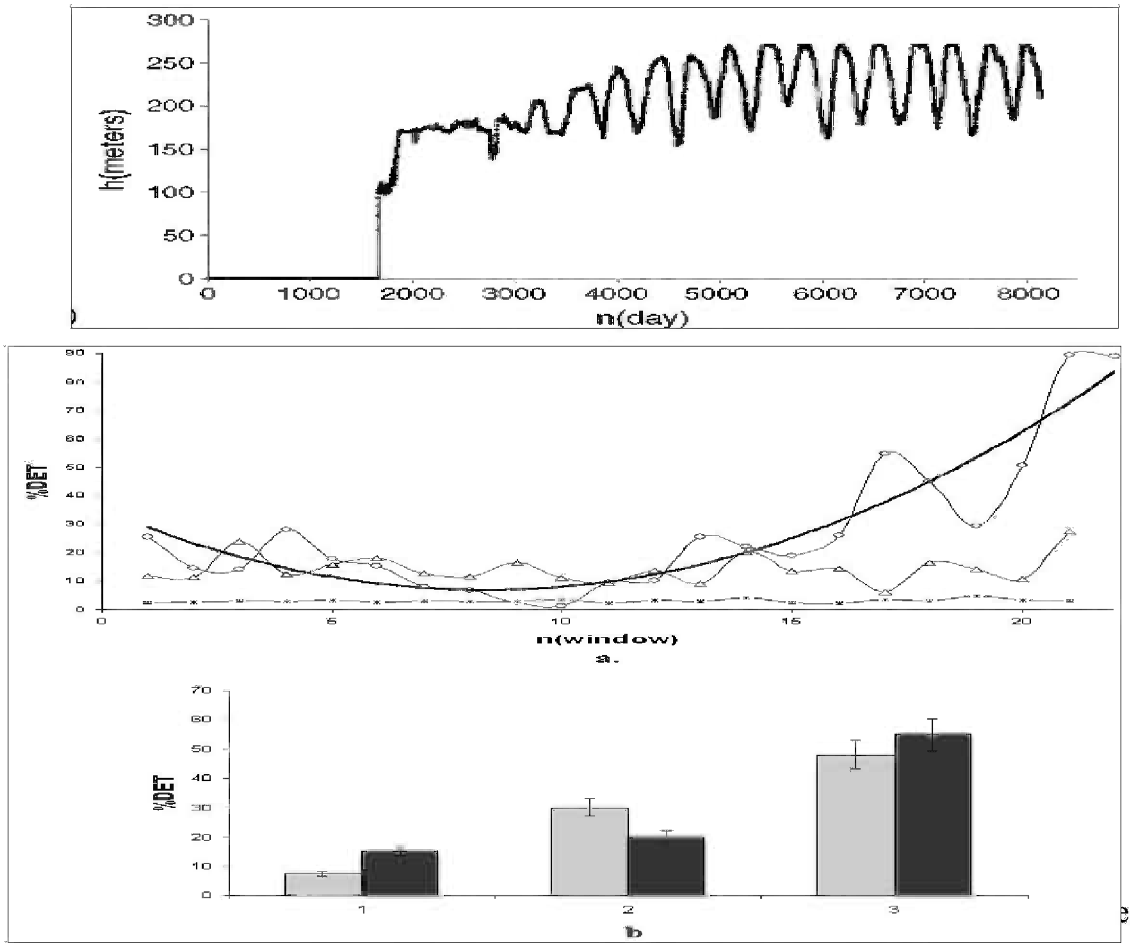

Fig. 7. The upper plot shows the WL time series – it became quasi-periodic after the day 4000 after beginning tiltmeter observations. The middle plot RQA %DET of daily number of earthquakes and its randomized version.The lowest plot shows RQA %DET of magnitude (*black columns*) and waiting time(*grey columns*) sequences for three intervals of lake exploitation. See text for details.

Based on the above analysis carried outexperimental time series, we conclude that the order in dynamics of earthquakes' daily occurrence, as well as in temporal and energy distributions increases significantly when water level variations became quasi-periodic.

*DAMTOOL- a package for operative control of engineering constructions.*DAMTOOL is a program intended for visual estimate, processing and analyzing the data of large engineering constructions' (dams, bridges etc) tilt measurements. It can be used also for analysis of any monitoring time series (strains, stresses, tilts etc). The program has 5 tabs (Data import, Data preview, Fluctuation analysis, Recurrent analysis, Tsallis Entropy).

Fig. 8 demonstrates the potential of nonlinear dynamics approach to analysis of tilt time series from April 2010 to June 2010. The upper plot shows tilt time series from April to June 2010 for one of stations of our network. The lower plot shows results of processing of the tilt record by DAMTOOL package: namely it presents RQA percent of determinism or RQA %DET (Marwan, 2003). The deviations from the normal behavior in the mid-May and June are evident even visually, but the usage of DAMTOOL allows assessing these deviations quantitatively. Note high values of and %DET during regular regime in April and first decade of May (which points to stability of monitoring data) and strong deviations in DET% due to geotechnical impact – addition of high frequency component during intensive discharge of water through dam outlet in 12.05-22.05.2010 and 01.06-11.06.2010 time intervals.

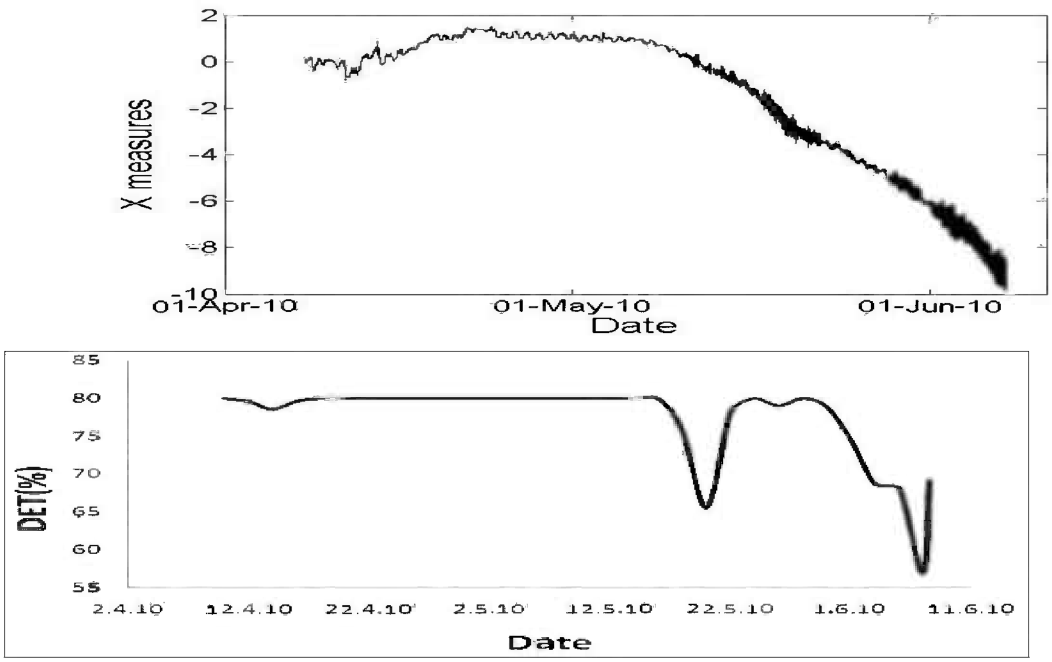

Fig. 8. The potential of nonlinear dynamics approach to analysis of tilt time series. Upper plot-original tilt time series; lower plot - RQA (% of determinism). Note high values DET during regular regime and strong deviations due to geotechnical impact (see text)

The data obtained already show very interesting long-term and short-term patterns of tilts' dynamics in the dam body, including tilt hysteresis during annual loading-unloading cycle, low-frequency dam oscillations etc, which can be used for dam diagnostics using packages DAMWATCH and DAMTOOL. The possible interpretation of hysteresis phenomena in by mesoelasticity (nonlinear elasticity) approach is suggested. It is shown that the main contribution to annual tilts hysteresis comes from the dam body tilts, thus these data are appropriate for dam damage diagnostics.The tiltmeter recordings with one minute resolution reveal many interesting details of dam behavior, which expand the spectrum of dam vibrations to low frequencies and give new diagnostic tools. Analysis of retrospective tilt data show that used methods are appropriate to detect and quantify dynamical changes in dam body behavior caused by different external and internal causes, though mechanism of some observed effects still need to be studied in detail.

3. Flood risk assessment for different scenarios of Enguri High Dam damage.

This work is the first step for Flood risk assessment in Georgia for Enguri High Dam, located on the Enguri River in western Georgia near the point at which the river leaves the Caucasus Mountains on its way to the Black Sea. For the modeling of flooding in case of Enguri Dam breaking has been used an important tool for simulating flood events in complex terrain a 2D flood propagation modeling program "SOBEK", which offers possibilities to quantify the dynamics of a flood event and to run different scenarios to evaluate the consequences of certain actions.

Using SOBEK the calculation of water depths and velocities, max water deep etc in case of a dam breakhas been done. The animation shows the simulation results of a dam break. The results may be used for dam breaking analysis, disaster management, evacuation planning, flood damage assessment, risk analysis and landscape, infrastructure, and urban planning.SOBEK-1D and 2D instrument for flood forecasting, like other flood modeling programs, is based on the Navier-Stokes equations.ILWIS (Integrated Land and Water Information System) a GIS / Remote sensing software also were used for modeling Enguri Dam break and flood scenario: Fig. 9shows only one small part of results.

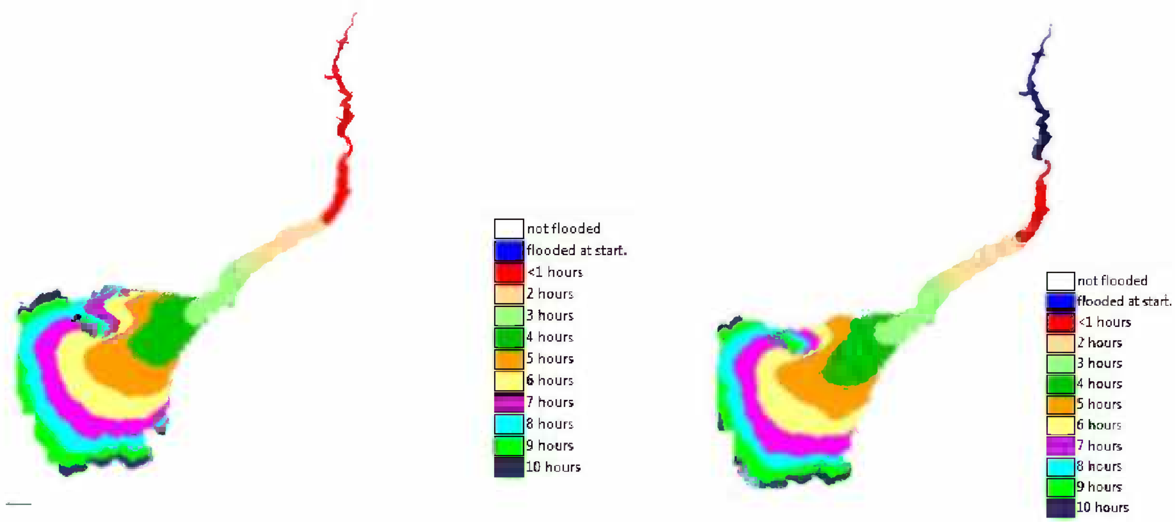

Fig. 9. Dynamics of flooding due to Enguri Dam damage for two different scenarios.

Results of calculations show that in case of dam brake the $1.1*10^9$ m^3 water would flow out downstream.The maximum velocity of the water body should be 44.0 m/s and the minimum 1.5 m/s (at 54 km from the dam). The area affected by flooding will be 1840km^2.The scenario of dam break influence on the speed velocity and propagation of the water, but difference is not large. More then 7 cities and villages in the area of the water propagation would be completely destroyed.

4. Climate Change; statistical and nonlinear dynamics predictions of regional effects

The greenhouse effect (global warming) is one of the main hazards facing the whole planet. The climate forcing is due to rising concentration of greenhouse gases (CO_2, methane, water vapor): according to different assessments, the temperature will rise by 1.4-5.8^{0}C at the end of 21-th century. This can cause a lot of devastating effects and many of them will be impossible to prevent, which means that the humankind should find some way to adapt itself to global warming.

Georgia as a whole Caucasus is prone to many negative effects, connected with climate change: the mountain glaciers can melt and partially disappear, the sea level can rise, the vast areas of land can became deserts, water resources can be seriously affected.

Despite some earlier efforts, devoted to assessment of climate change in Georgia, the results are still ambiguous. In particular, the research carried out shows that during last decades the mean temperature in the Eastern Georgia is rising and in Western Georgia it is decreasing. These conclusions are debated and there is a need to re-consider them using new data and new methods of mathematical analysis of meteorological time series. For reliable assessments new modern methods of obtaining and analysis of climate data in the past, present and future is necessary to use.

Another problem is to ascertain whether this warming is exclusively the man-made effect or it is the result of natural cyclicity in the earth climate.

Specific objective is assessment of persistence and memory characteristics of regional air temperature variation in Georgia in the light of global climate change. For this purpose longest available temperature time series of Tbilisi meteorological station (since 1890) are analyzed. Similar time series on shorter time scales of five stations in the West and East Georgia will also be used as well as monthly mean temperature time series of five stations (1906-1995) in the West and East Georgia. Both mono- and multivariate reconstruction procedures of climate change dynamics are implemented. Additionally, temporally and spatially averaged daily and monthly mean air temperature time series are analyzed. Extent of persistence in mentioned time series is evaluated.

The existing instrumental temperature data are from 1850 in Tbilisi and from 1880 in 12 meteorological stations in Georgia. These data were used in analysis of trends and for climate forecast. The detail (daily) digital data bases covering the whole observation period (1850-2010) are absent.The spatial distribution of warming (ΔT) in Georgia for 1906-1995 has been calculated in the frame of "Georgia's initial national communication under the United Nations Framework Convention on Climate Change" (1999). This study reveals the striking difference in the climate change trend between West and East Georgia.

The simplest prediction can be done by just extrapolation of time series: for example let us consider the extrapolation of 156 year Tbilisi temperature data (Fig. 6), which are best fitted by second order polynomial. The extrapolation display for the period 1850-2055 the increment $\Delta T = 2.4^0C$ with the most part of ΔT is in the last hundred years, from 1950 to 2050 and for the longer period 1850-2105, the increment $\Delta T = 4.4^0C$ with the most part of ΔT is in the last hundred fifty years, from 1950 to 2105.

It is interesting to note that this simplest extrapolation gives the assessment of temperature increment comparable with the predictions of the complicated mathematical models

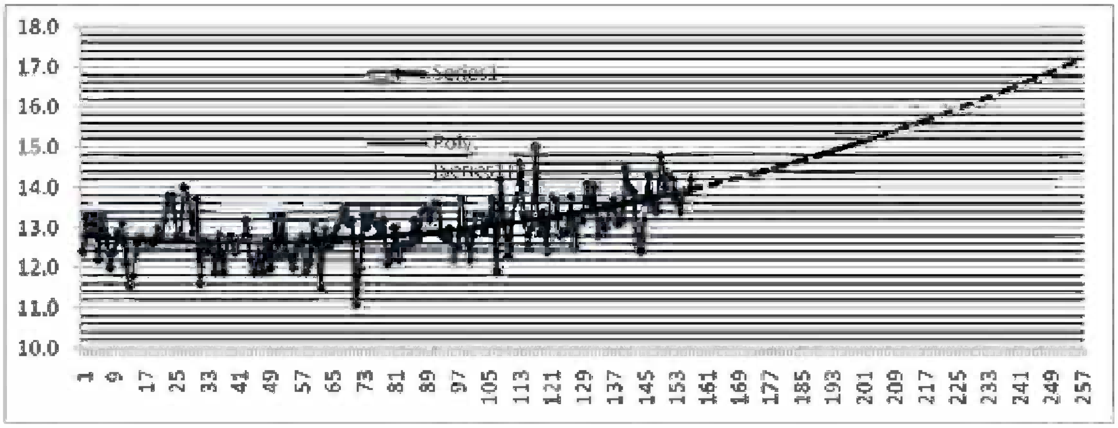

Fig. 10. Simple second order polynomial extrapolation of 156 year Tbilisi temperature data to the year 2105.

We also performed (linear) statistical assessments of future trends in climate in Tbilisi (Fig. 11) and 12 locations in Georgia, using modern methods of statistical assessments: autocorrelation, correlation fields, revealing periodicities, analysis of residuals etc.

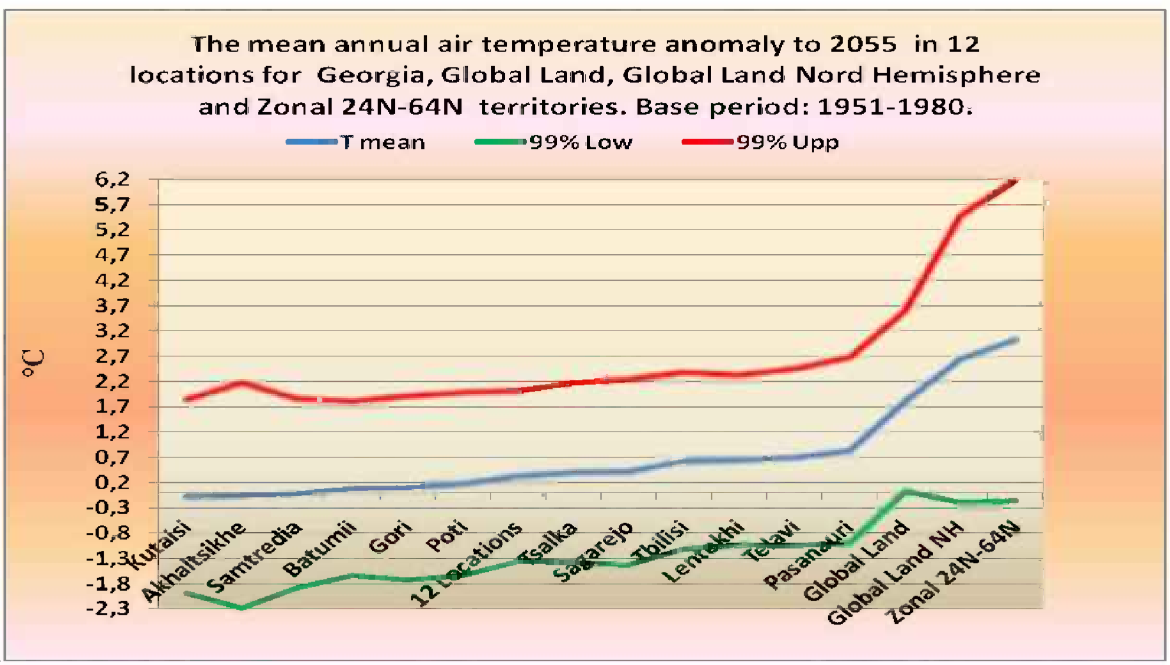

Fig.11. The mean annual air temperature change prediction for 2055 in 12 locations for Georgia, Global Land, Global Land Nord Hemisphere and Zonal 24N-64N territories

Common statistical analysis indicates to weak auto-correlation and at the same time reveals several periodicities both in original and detrended time series (Fig. 12).Extrapolation of the observed temperature trends by statistical methods predict mainly continuation of warming in the East Georgia and cooling or negligible change in the West with predominant warming in the cool periods.

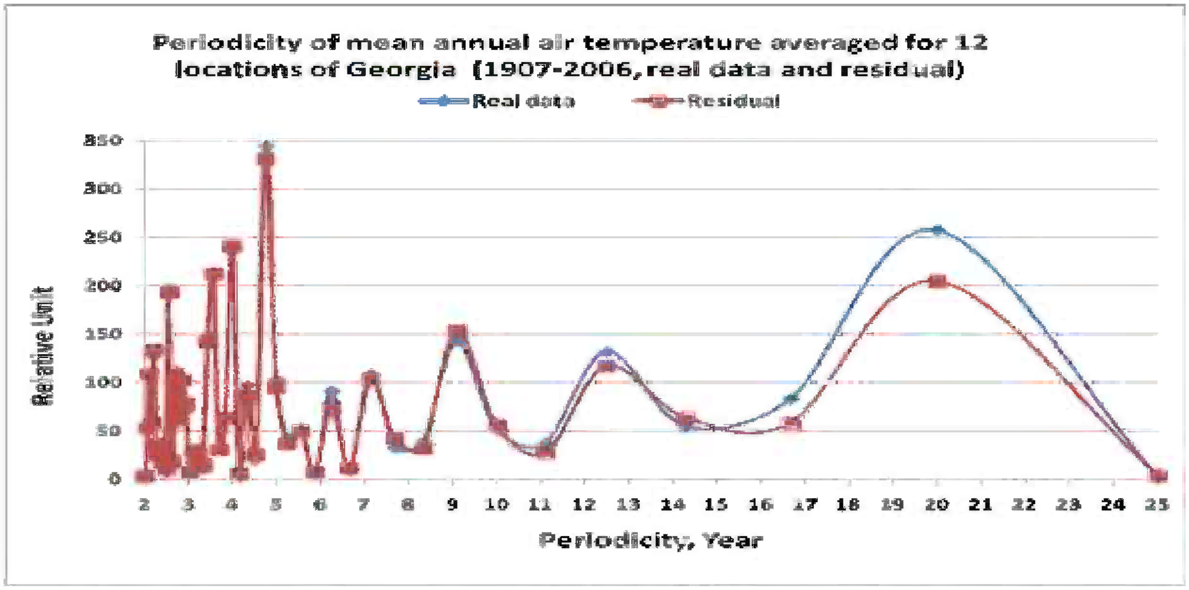

Fig. 12. Periodicities of mean annual air temperature averaged for 12 stations of Georgia (real data and residual)

Besides linear statistical methods we apply the nonlinear dynamics tool to temperature time series. Our nonlinear analysis, namely Detrended Fluctuation Analysis (DFA) shows that time series exhibit several time scales with different dynamical characteristics.

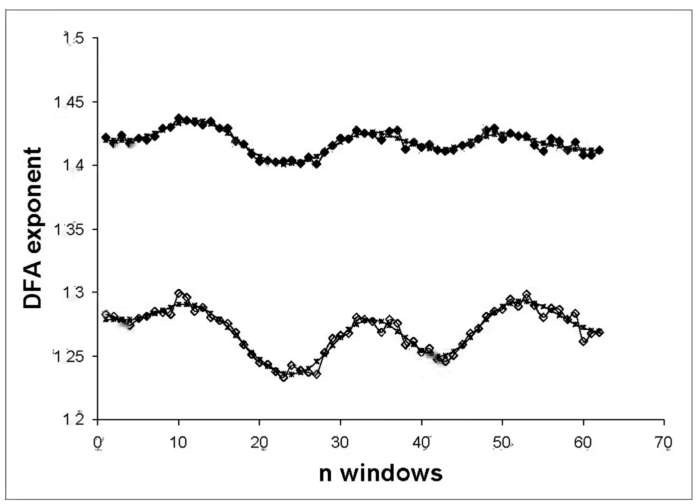

Fig.13. Smoothed by Savitzky Golay filtering DFA scaling exponents for Tbilisi (top) and Kutaisi(bottom) mean daily temperature data, 1936-2006, One year time scale. Asterisks correspond to smoothed data.

Taking into consideration that value of DFA exponent close to 1 means that investigated process is similar to white noise, it can be assumed, that daily temperature variation in Tbilisi is more regular comparing to Kutaisi for all considered time scales.The variations of DFA exponents' values reveal some periodic features. In order to better visualize suggested quasi-periodicity in scaling features of analyzed data we used Savitzky-Golay smoothing and filtering procedure for calculated DFA slope values for 3 different time scales – one year, one month to one year and one month (Fig. 13).

In addition to said above in methodology section RQA is a tool for qualitative and quantitative evaluation of nonlinear dynamical structure. It is sensitive and effective even for relatively short time series. Recurrence plots (Fig.14) shows much regular pattern for Tbilisi (East Georgia) in comparison to Kutaisi. These differences in the degree of regularity are definitely of local origin.

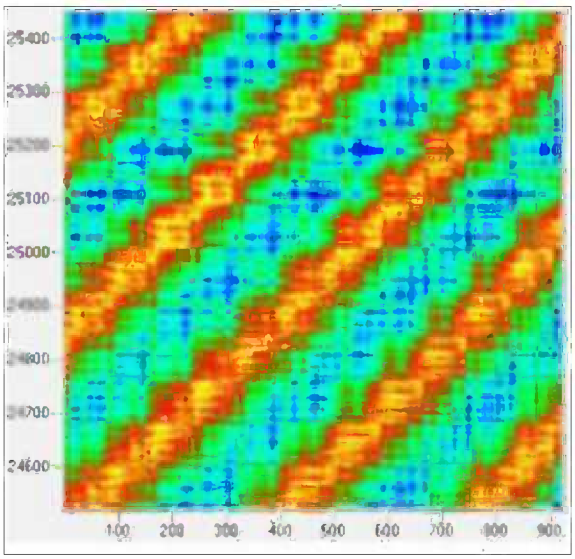

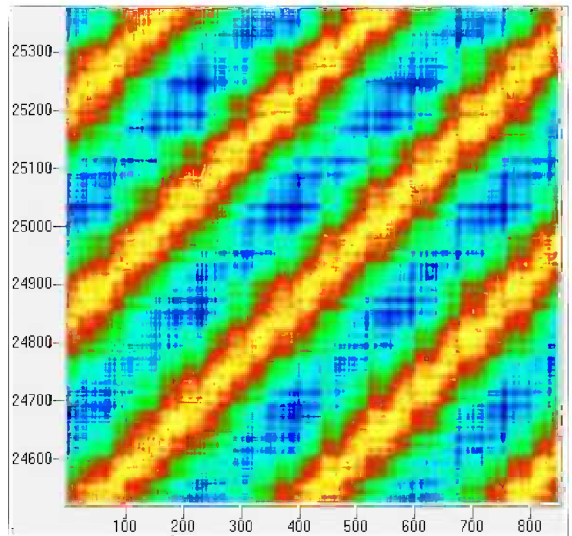

Fig. 14. Recurrence plots of Kutaisi (left figure) and Tbilisi (right figure) daily mean temperatures data, 1936-2006.

The ordering strength of temperature time series vary in time revealing existence of low-dimensional processes close enough to multi-scale quasi-periodicity (Fig. 15).The physical mechanism of such time-dependence is not clear: some of them can be connected with North Atlantic, Pacific Decadal or El Nino (NAO, PDO or ENSO) cycles.

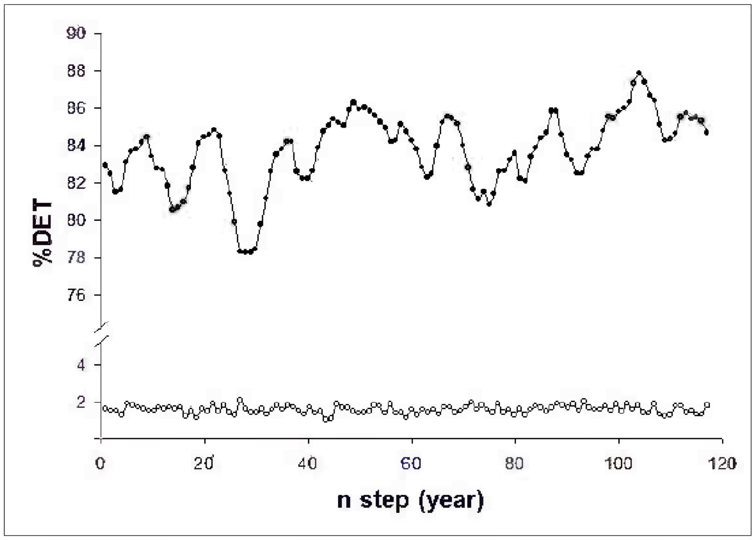

Fig. 15. Recurrence quantification analysis of daily mean temperature data Tbilisi 1981-2006, calculated for consecutive 5 year windows by one year step. Lower curve shows randomized time series.

We suppose that besides local peculiarities leading to different levels of ordering in the West and East Georgia there are some global factors leading to similar type of time-dependent dynamics in the both parts of country.For time scales larger than one year process always looks as strongly antipersistent, i.e. at this time scales stability of observed trends is questionable and inversion of observed trends is a typical feature of dynamical process.

Using nonlinear methods a small increase of temperature can be predicted in both parts of Georgia for the next 10 years and this process is not affected by different noises contained in existing data sets (Fig. 16 a).

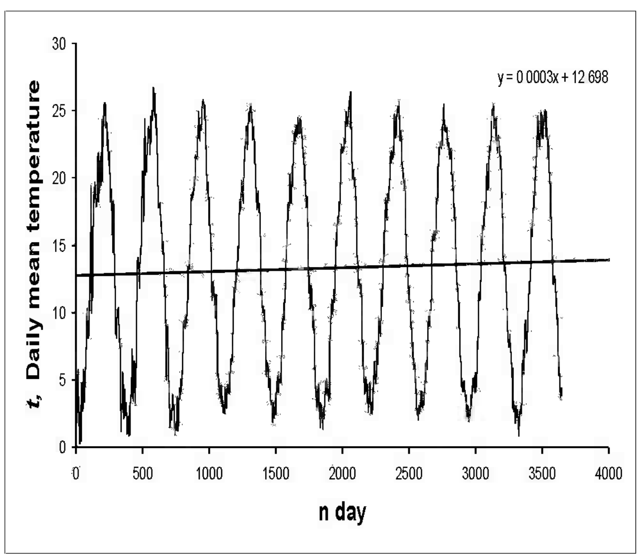

Fig. 16 a. Weak positive trend in the forecasted for 10 year Tbilisi daily mean temperatures data sets. Forecast was made based on Tbilisi mean daily temperature time series from 1881 to 2006.

The program package Drought Assessment Package Application (DAP APP) was compiled to assess the recurrence of droughts in a given area. Program package presents easy-to use friendly toolbox working with time series. Application is designed to work with TXT or DAT files which contain for example temperature or precipitationmeasures.Input files should have only one column.This package includes different popular instruments for data analysis:

1. Recurrent Plots (RECURRENCE PLOT tab menu) and Recurrent Quantification Analysis (RQA)
2. Detrended Fluctuation Analysis (DFA tab menu);
3. Power Spectrum and Histogram (HISTOGRAM/POWER SPECTRUM tab menu);
4. Correlation calculation (CORRELATION DIM/AUTOCORRELATION tab menu);
5. Lyapunov exponent calculation (LYAPUNOV EXPONENT tab menu);
6. Stationary test (STATIONARY TEST);

Here we show only the results on the recurrence of the droughts defined as days with temperature higher then 30^0C of various durations using Tbilisi data.We took only summer month from Tmax daily series and calculated duration of droughts (in days) with max temperature (Tmax) higher than 30 C° in summer months.

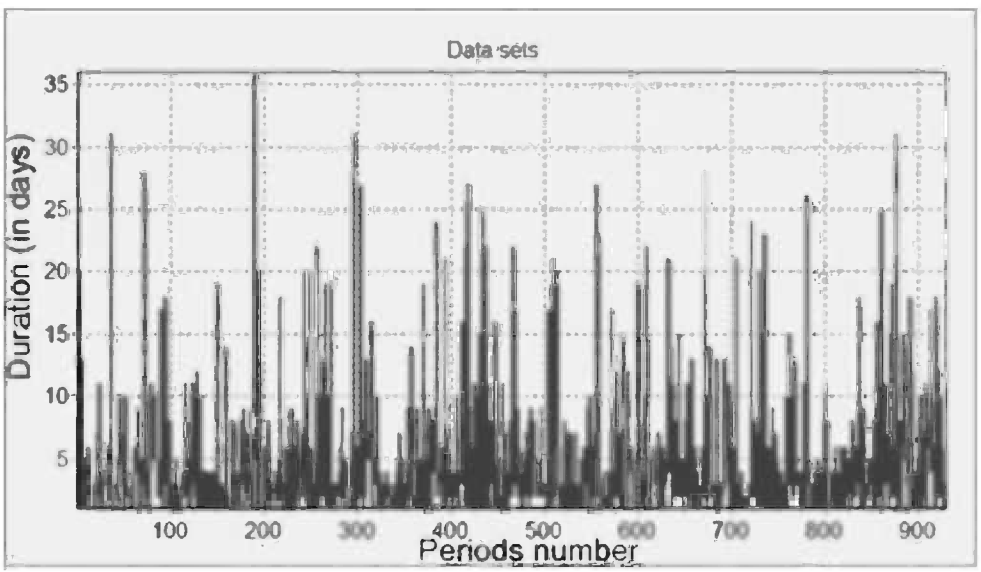

Fig.1. Duration of periods with Tmax higher 30 C° versus period number of period with Tmax higher than 30 C°, which can contain m = 2, 5,10,....35 days.

As a result we get Tmax duration series versus period number, which is depicted on the Fig.16b. Note, that the number of periods with Tmax higher than 30 C° are not uniform - so the X-axis shows only the number of high temperature period, which can contain m = 2, 5, 10,.....35. days.

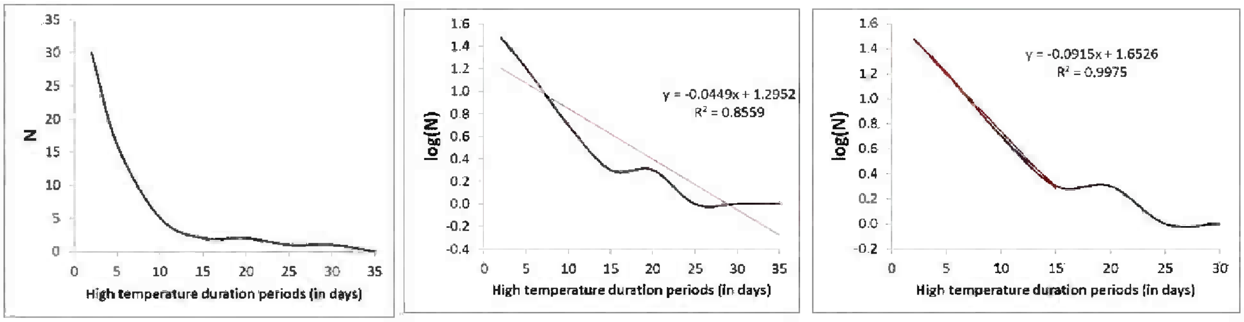

Fig. 16 b. Frequency-Intensity Estimate Plot: a) linear plot of number of droughts N in five years (i.e. drought rate) with duration more than 2days versus corresponding durations (intensity of droughts); b) the same in semilog scale - log N versus intensity with straight line approximation for all intensities; c) the same as 7b with straight line approximation for intensities from 2 to 15 days.

Frequency-Intensity Estimate Plot or plot of number N of droughts in 5 years (i.e. drought rate) with duration $m$more than 2, 5, 10, 15, 20, 25, 30, 35 days versus corresponding durations (intensity of droughts (Fig.2 a, b, c) of high-temperature periods was done on duration series (Fig. 1).It manifests the presence of heavy-tail i.e. different statistics for extreme events (long droughts) with duration larger than 15 days (Fig. 2 a). We observe that up to period length equal to 15 days, relationship between occurrence of high-temperature periods and period lengths is very well approximated by exponential function (Fig. 2 c) and recurrence time T_R can be accessed accurately for 15-days droughts. For example, 15 days drought reoccur as (antilog(log0.3))/5 (1/year) ≈ 2/5≈ 0.4 (1/year) or T_R = once per twoand a half years. The linear approximation for a whole semilog plot (Fig. 2 b) is much less accurate and for 15 days drought reoccurrence we get (antilog(log0.6))/5 (1/year) ≈ 4/5 ≈ 0.8 (1/year) or T_R ≈ once per year and for droughts with duration 35 days ((antilog(log(-0.35)))/5 (1/year) ≈0.45/5 (1/year) =0.09 /5 (1/year) ≈ 0.1 (1/year) or T_R ≈ once per ten years, which is less than observed data. According to observed data ((antilog(log(0)))/5 (1/year) ≈ 1/5 (1/year) or T_R ≈ once per five years.

5. Pan-European and nation-wide landslide/debris flow susceptibility assessment

The earth surface is not static but dynamic, and landforms change over the time as a result of weathering and surface processes (i.e., erosion, sediment transport and deposition). These changes have the potential to cause significant harm to civil engineering projects as they resulted into different hazardous processes, i.e. landslides, which are important natural geomorphic agents that shape mountainous areas and redistribute sediment]. Landslides are commonly responsible for significant losses of money and lives, and the severity of the landslide problem became worsens with increased urban development and change in land use.

In Georgia, where up to 80% of the territory is mountainous and more than 30% of settlements are located in the high mountains (above 1000 m altitude) the slope stability is recognized as the problem of high importance. Investigations, carried out in last decades, show that the negative impact of landslide activities becomes perturbing almost all over the territory of Georgia.

The goal of the project was to compile a new maps of landslide, derris-flow and rock-falls susceptibility (hazard) map following standards of Pan-European map.

The following dataset has been collected during preparation period:

1. DTM (Digital Terrain Model) – The digital elevation model of the territory of Georgia(extracted from Aster Satellite mission (ASTER: Advanced Spaceborne Thermal Emission and Reflection) (http://asterweb.jpl.nasa.gov/). From DTM data one of the main factors - the terrain's slope model was compiled (Fig. 17).

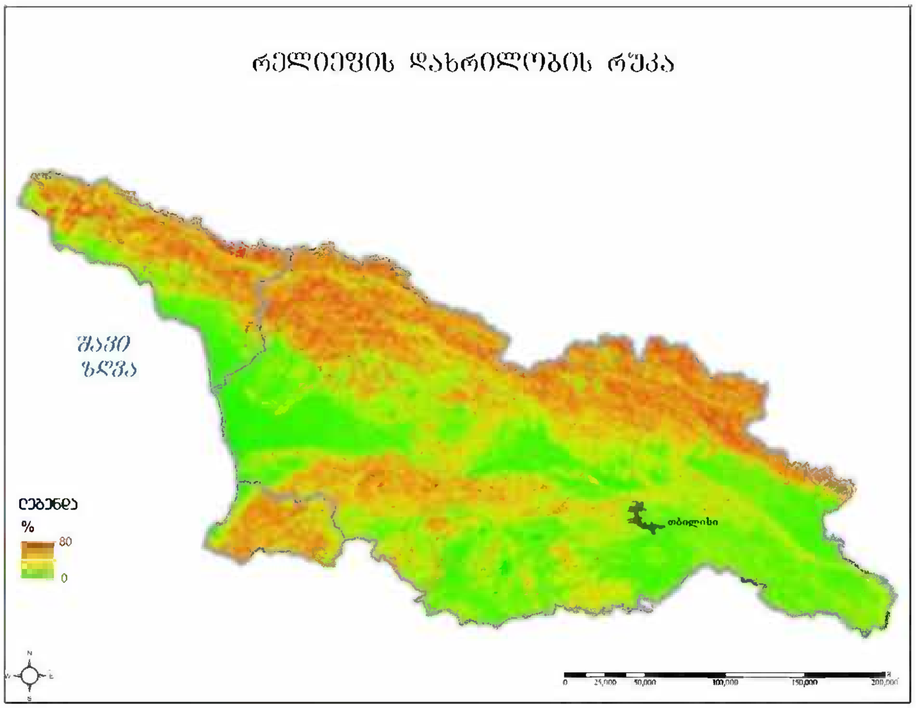

Fig. 17.The terrain's slope model of Georgia – one of the risk factors.

2. Rivers network of teritory of Georgia (the database have been extracted from 1:50 000 topographic map)
3. Engineering geological structure's map of Georgia (the database have been created based on the Engineering geological map of Georgia of 1:200 000 scale)
4. Active tectonic faults database of Georgia (created from geological map ofGeorgia 1:200 000 scale)
5. Soil types map of Georgia (1:200 000 scale database)
6. Land use database (Terra modis dataset) (http://modis.gsfc.nasa.gov/)
7. Landslide inventory databases, compiled using different sources (around 500 events).

The next step, after data colection and processing is parametrisation of the factors' maps. For this goal the analysis of different factors' maps have been carried out. For this goal the expert judgment and knowledge have been used. Each factor map was classified and for each classes the value from 0-to 100 have been graded, where 0-is absence of the class to produce mass movement and 100 is the highest value of formation which should produce mass movement.

The parameterized maps have been reworked into raster type maps with 30m resolution and methodology have been tested using all (9) parameters. The combining of the selected parametrical maps carried out usingArc-Gis. The maps have been combined using different types of weight of each parameter. In the table 2 the numbers of models are shown with parameter's weights for landslides.

Table2.Model parameterization of factors' weights for landslides(%).

		1	2	3	4	5	6	7	8	9
1	Geology	20%	20%	20%	25%	20%	20%	20%	20%	20%
2	SLOPE	18%	18%	20%	20%	20%	20%	20%	18%	18%
3	Land_Use	15%	15%	15%	10%	10%	20%	10%	15%	15%
4	Soil	12%	12%	15%	15%	15%	10%	10%	12%	17%
5	Fault	5%	5%	5%	5%	5%	5%	5%	5%	5%
6	RIVER	5%	5%	5%	5%	5%	5%	5%	5%	5%
7	Dem	10%	10%	10%	10%	10%	5%	5%	15%	10%
8	ASPECT	5%				5%	5%	5%		5%
9	Water erosion	10%	15%	10%	10%	10%	10%	20%	10%	5%
	%	100	100	100	100	100	100	100	100	100

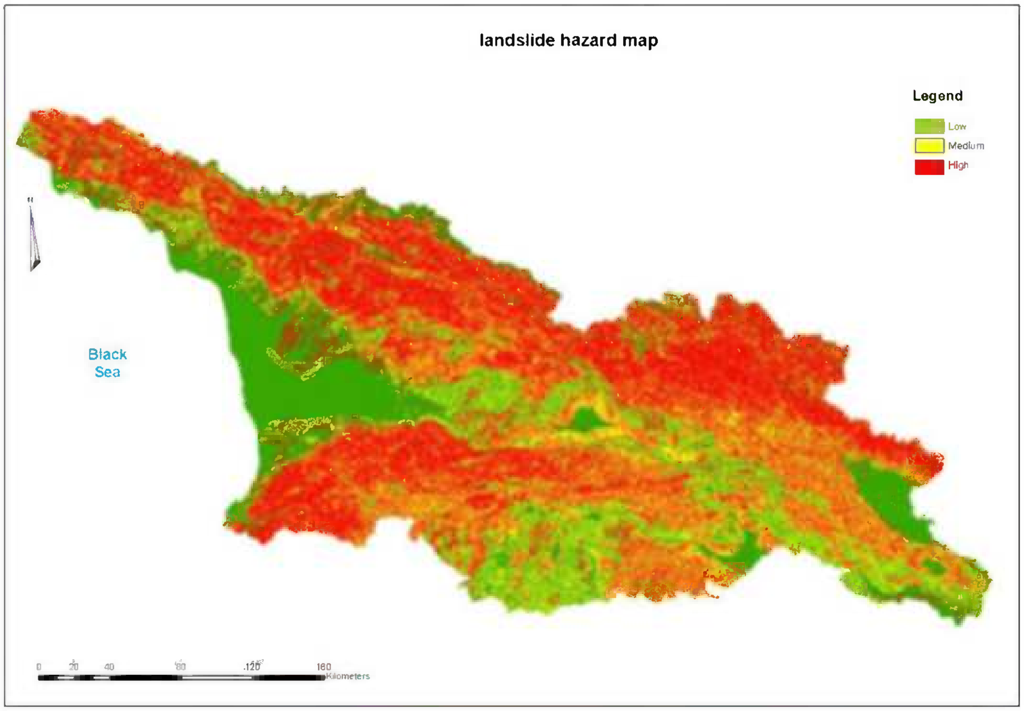

Fig. 18. Landslide susceptibility map of Georgia.

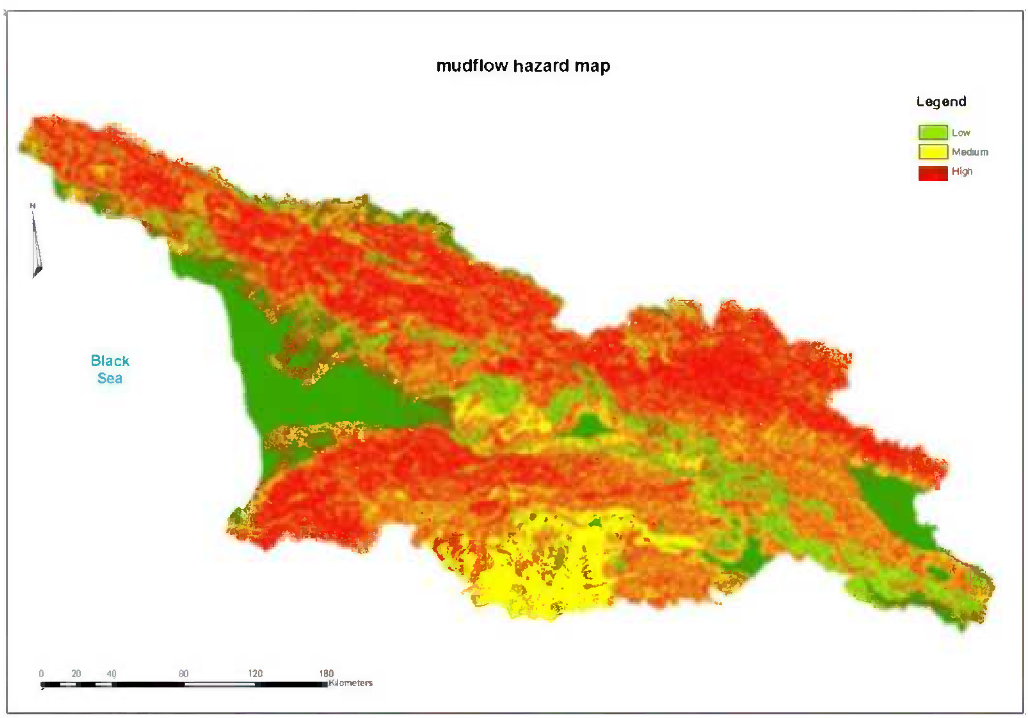

Fig. 19. Mudflow susceptibility map of Georgia.

The resulting prognostic maps 18, 19 are much more detailed than previous ones and are in good correlation with the data on occurred events (Fig. 20).

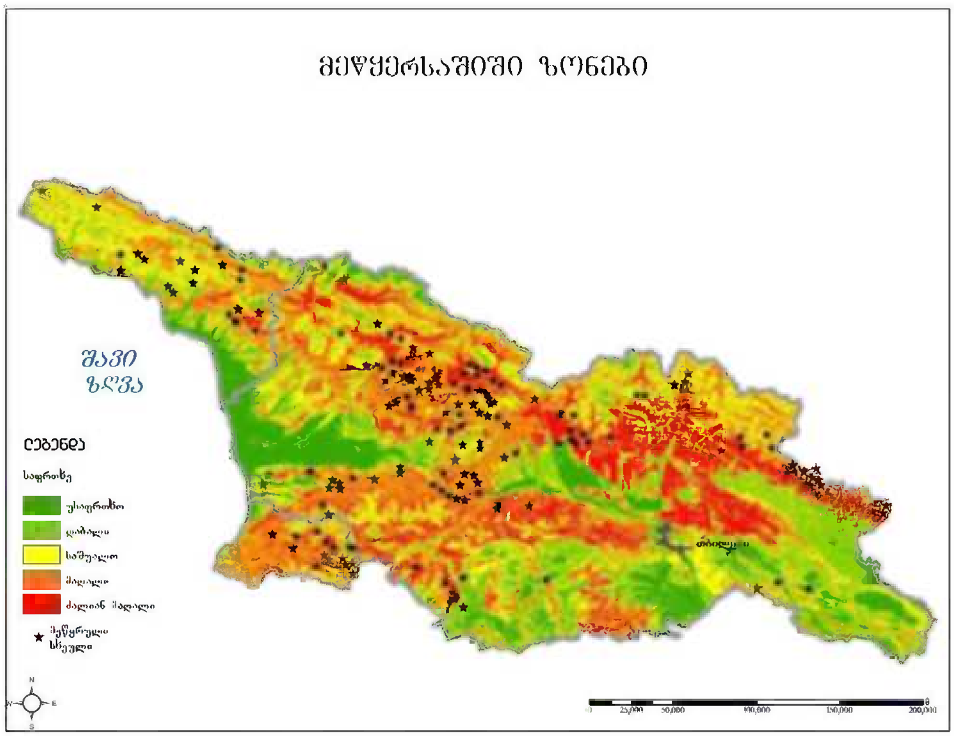

Fig. 20. Landslide susceptibility map in combination with occurred landslide events dataset.

6. *European Landslide Hazard Maps including Triggering factors: precipitation and seismic hazard (preliminary results)*

As a rule compilation of theoretical landslide/debris-flow hazard maps is founded on the analysis of several permanent factors, such as the slope of the hill, mechanical properties of geological formations etc. These factors are stationary and do not take into account impact of such important triggering agent, as precipitation. On the other hand it is well known that the occurrence of landslides/debris-flows critically depends on the precipitation, which usually is considered as one main triggering factor. The impact of triggering agent can be implemented into mass-movement stationary hazard assessment merging, for example, standard landslide hazard map with a long-term (100 years long rx5 days) rainfall data; precipitation intensity map for 100 years is practically a stationary map. Of course, it is necessary to establish some gradation rule, characterizing hazard increment with a long-term rain intensity and duration (thresholds).

Stationary Forecast for triggering factor (precipitation). This approach uses the long-term (e.g. for 100 years) local precipitation or soil wetness data as an additional quasi-stationary factor (Fig. 21), which can be added to a standard list of factors: slope, geology, etc, which are used in compilation of standard landslide/debris-flow (Fig. 18). For inclusion of precipitation triggering effects we use the map of maximum 5-day precipitation for 100 years return period in Georgia (Atlas of Natural Hazards and Risks in Georgia. 2012).

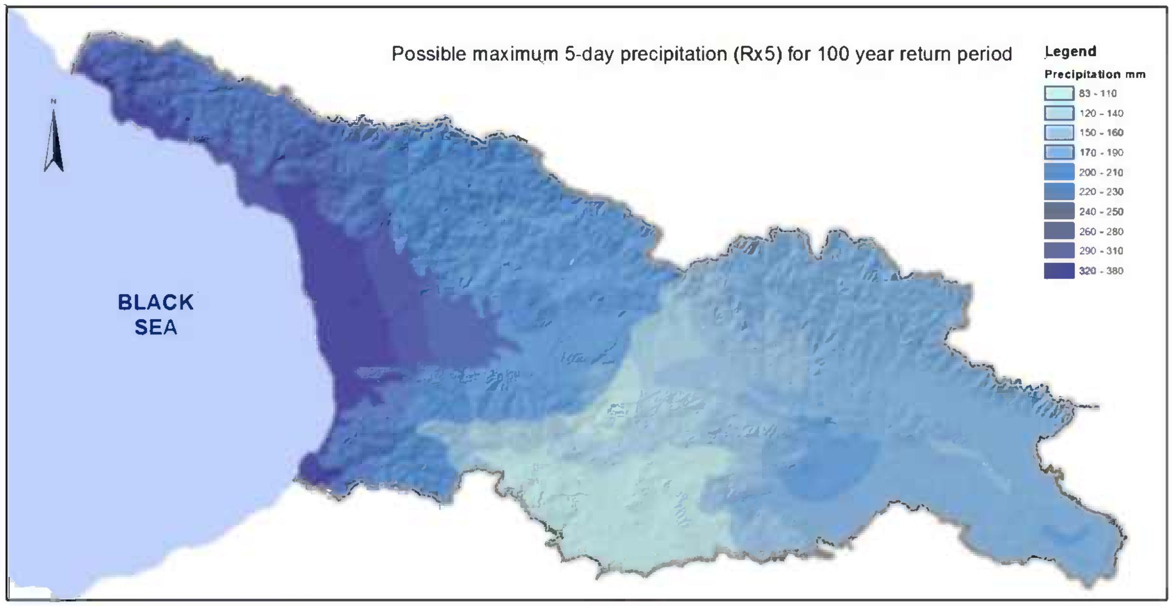

Fig. 21. Map of maximum 5-day precipitation for 100 years return period in Georgia.

Fuzzy Logic (FL) Approach. First we choose the fuzzy sets (linguistic terms)that describe the linguistic variable precipitation:low, medium, high, very high. For linguistic variable landslide let be low, medium and high.

The next step is to construct IF - THEN fuzzy rule base, where IF-part includes two variables - precipitation and landslide. They are input variables and the one output variable is hazard. The following case - IF precipitation is variable “medium” and landslide variable is “low’ - THEN hazard is low - is one example of such rule.

The above approach was first used for compilation of the stationary map of landslide hazard map of Georgia (Fig. 18) merged with the average multi-year distribution of the maximum amount for 5-day precipitation 100 years' return period maps of precipitation in Georgia, which also can be considered as a stationary map (Fig. 21). The multi-year, everyday measurement data of precipitation, obtained from the 83 meteorological stations, has been used for calculation of fuzzy logic rules for 100 years periods.

As a result of fuzzy merging stationary maps of landslide hazard and precipitation the stationary map of landslide and mudflow hazards taking into account triggering factor - precipitation - was compiled (Fig. 22).

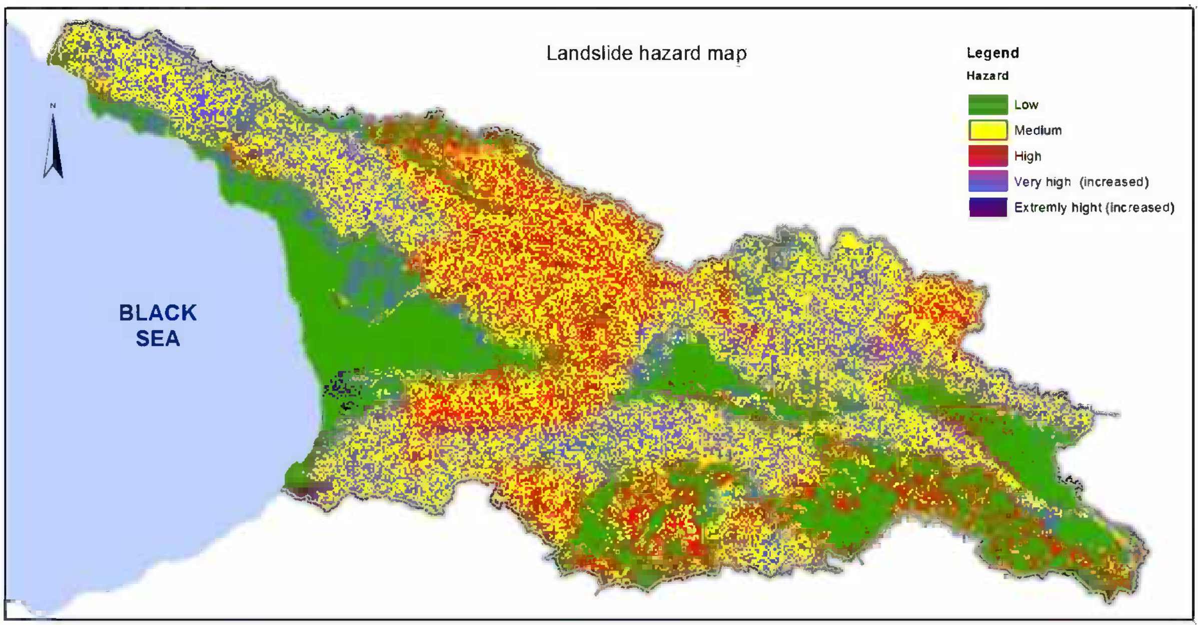

Fig. 22.Landslide hazard map of Georgia including precipitation factor (preliminary version)

It is evident that taking into account precipitation factor changes configuration of hazardous zones, namely, due to precipitation factor some hazardous zones are upgraded from $n$to $(n+1)$grade higher hazard zone (i.e. middle hazard to high hazard etc). In the landslide hazard map two more gradation –"very high" and "extreme hazard" was added, which take into account precipitation factor.

At present the center works on development of a new debris flow/landslide hazard maps, which will take into account very important factor: precipitation (intensity and duration) more exclusively as well as the seismic impact. In the former problem the space data on precipitation will be used.

7. ***Cost-effective telemetric monitoring and early warning complex systems (arrays) with high-tech elements for signaling mass-movement (preliminary results).***

The cost of precise enough monitoring/early warning system (EWS) equipment is as a rule very high (of the order of hundreds of USD) and it is practically impossible for developing countries to purchase even one system. If we take into account that the number of mass-movement dangerous sources is huge - only in Georgia there are 40000 of potential debris flow/landslide sources - the financial expenses are unaffordable. Thus, the multitude of dangerous sources, a need of covering the source area by many sensors, expensiveness of supporting personnel for a long period at potential mass-movement areas, growing number of exposed vulnerable objects and limited resources of developing countries, which are most prone to mentioned hazards, call for developing cost-effective and the same time accurate automatic monitoring/early warning telemetric systems. The network approach is important, as the mass-movement in the debris flow/landslide area is as a rule very heterogeneous and with a small number of sensors the system can miss the initiation of dangerous event.Fusion of these apparently conflicting concepts (cost-effectiveness and accuracy) became possible due to the progress of modern high-tech systems.

The main ideas in developing our EWS are: Cost-effectiveness and low power consumption; choosing informative parameters to monitor; modern sensors; micro-board for acquiring and processing information from sensors; autonomous power source; telemetric signal transmission system; analysis/decision making system.

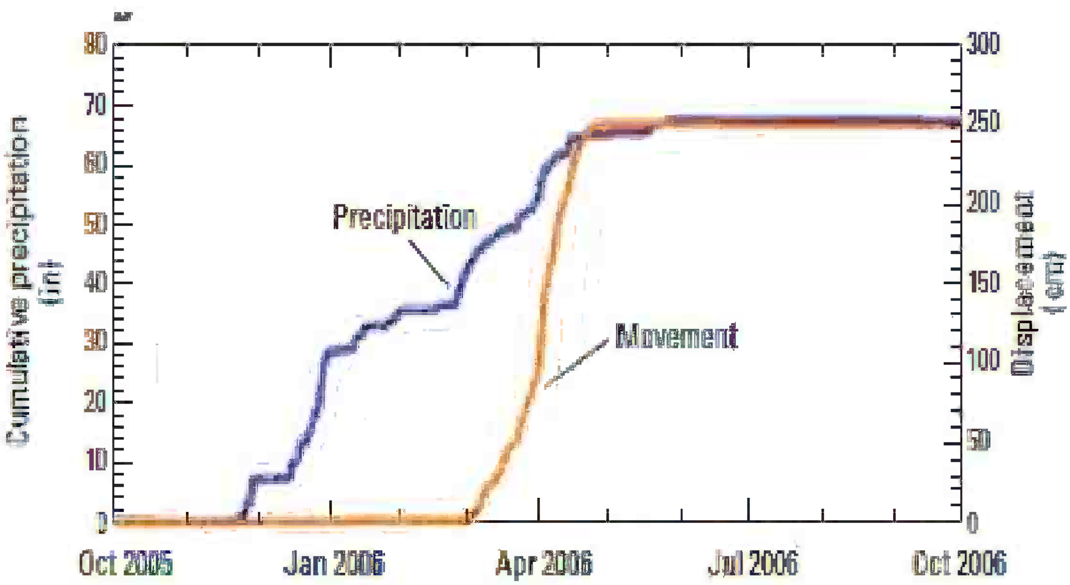

Fig. 23. The results of monitoring precipitation and mass-movement (U.S. Highway 50, California, http://landslides.usgs.gov/monitoring/hwy50/yearly.php), which show that before initiation of movement there is intensive precipitation (it can serve as long-term precursor). After exceeding threshold precipitation the mass movement is initiated.

The choice of precursory physical field is important: the precursors should be informative for diagnostics and easily measurable. The results of monitoring (U.S. Highway 50, California, http://landslides.usgs.gov/monitoring/hwy50/yearly.php), show that before initiation of movement there is intensive precipitation (it can serve as long-term precursor). After exceeding some threshold value of precipitation the mass movement is initiated (Fig.23).

Accordingly, the suggested debris flow/landslide EWS network includes monitoring of two main factors, leading to mass-movement: humidity/pore pressure/conductivity of the soil (as a relatively long-term precursor, after which will be issued long-term alarm - WATCH) and displacement/acceleration/acoustics caused by initiation of mechanical motion (as a short-term precursor, after which will be issued short-term alarm - DANGER).

Humidity sensor: The principle is to monitor the difference in ultrasonic wave amplitudes in mutually normal directions depending on the soil humidity. For this the signal from the ultra-sound wave (USW) transducer is received by two USW sensors, disposed frontally and normally to the direction of the emitted wave (Fig. 24). In water the amplitudes in both directions are the same, as the pressure is distributed uniformly in the volume. In the water-saturated soil we expect to obtain the similar behaviour in contrast to dry environment, where the amplitudes in these two directions are expected to differ significantly. The USW method was chosen because, conductivity sensors, though very sensitive, are unstable due to the electrodes' degradation/corrosion.

Mechanical motion sensors: MEMS:" Micro-electromechanical Systems (MEMS) are miniature devices comprising of integrated mechanical (levers, springs, deformable membranes, vibrating structures, etc.) and electrical (resistors, capacitors, inductors, etc.) components designed to work in concert to sense and report on the physical properties of their immediate or local environment, or, when signalled to do so, to perform some kind of controlled physical interaction with their immediate or local environment.

MEMS-based solutions yield product cost advantages for a given functionality; employing MEMS devices usually results in a reduced price for a given product, and MEMS components typically demonstrate less power consumed per a given function than do other, macro-based solutions; and the fact that MEMS device and product reliability is as good as any reliability can be." The MEMS chips, upgraded to full-scale accelerometers are shown in Fig. 24.

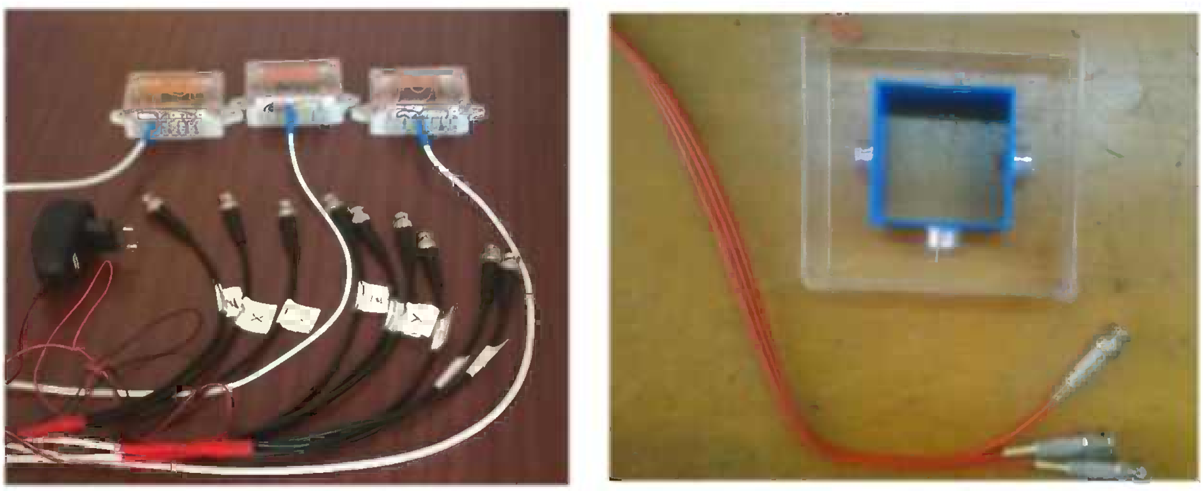

Fig. 24. Left: Array of Micro-accelerometers with MEMS sensors; right: Soil Humidity sensor: cell, USW transducer and USW receivers.

Laboratory testing of humidity sensor: Testing soil (sand) wetness using orthogonally oriented USW ratio, f=40 KHz. USW amplitudes in orthogonal directions in dry and fully saturated soil differ significantly from 1:5 for dry to1:2 for saturated state; to us, this is the state, when the long-term alarm (WATCH) should be declared (Fig. 25)

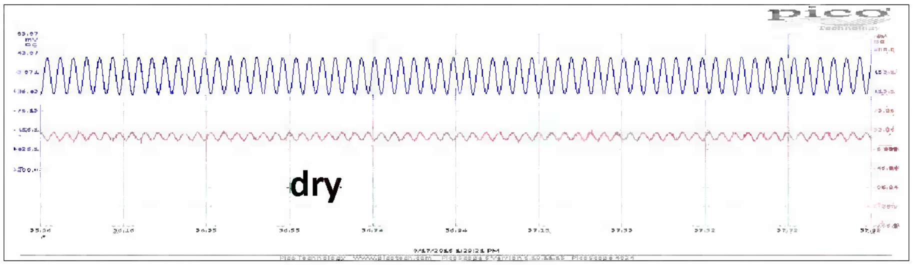

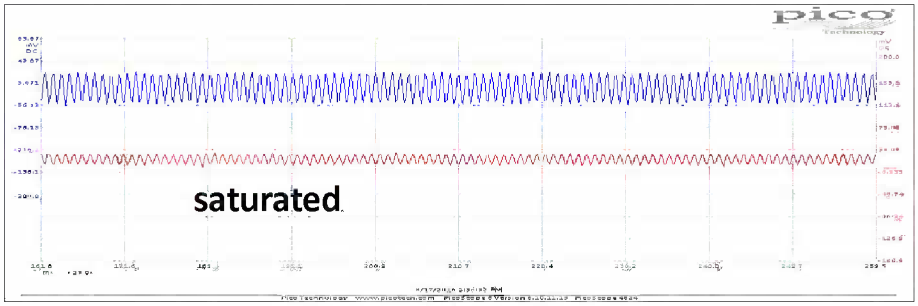

Fig. 25.USW amplitudes in orthogonal directions in dry (upperplot) and fully saturated (lower plot) soil.

Differentialaccelerometry. In complex with displacement and soil wetness measurements the method of *differential accelerometry* will allow us monitoring of landslide/debris flow motion initiation processes. For this one accelerometer is be grounded in the stable area and the other one (or the array of accelerometers) – on the potential landslide body. The differential signal between fixed and moving devices can be used for early warning on initiating disaster (Fig. 26).

Fig. 26. Left: Both accelerometers are rigidly connected during motion – no differential signal.; right: differential signal between fixed and moving sensors (maximal displacement difference between sensors - 1mm)

*Testing accelerometers and acoustic sensors on Burridge-Knopoff model:*The well known theoretical Burridge-Knopoff model of seismicity is applicable also to landslide motion. Accelerometers are fixed on the sliding blocks connected by springs (Burridge-Knopoff model) and placed on the lower fixed block. The fixed block can be horizontal or inclined to model landslide motion (Fig. 27). Fig. 28 presents the results of testing a simple Burrridge-Knopoff model on one block-horizontal system: recordings of acceleration, acoustic emission (AE) and the pulling force on the spring (see location of the sensors in Fig. 27)

Fig. 27. The array of three accelerometers fixed on the three sliding blocks connected by springs (Burridge-Knopoff model) and placed on the lower fixed inclined block. Two AE sensors are mounted on the fixed block.

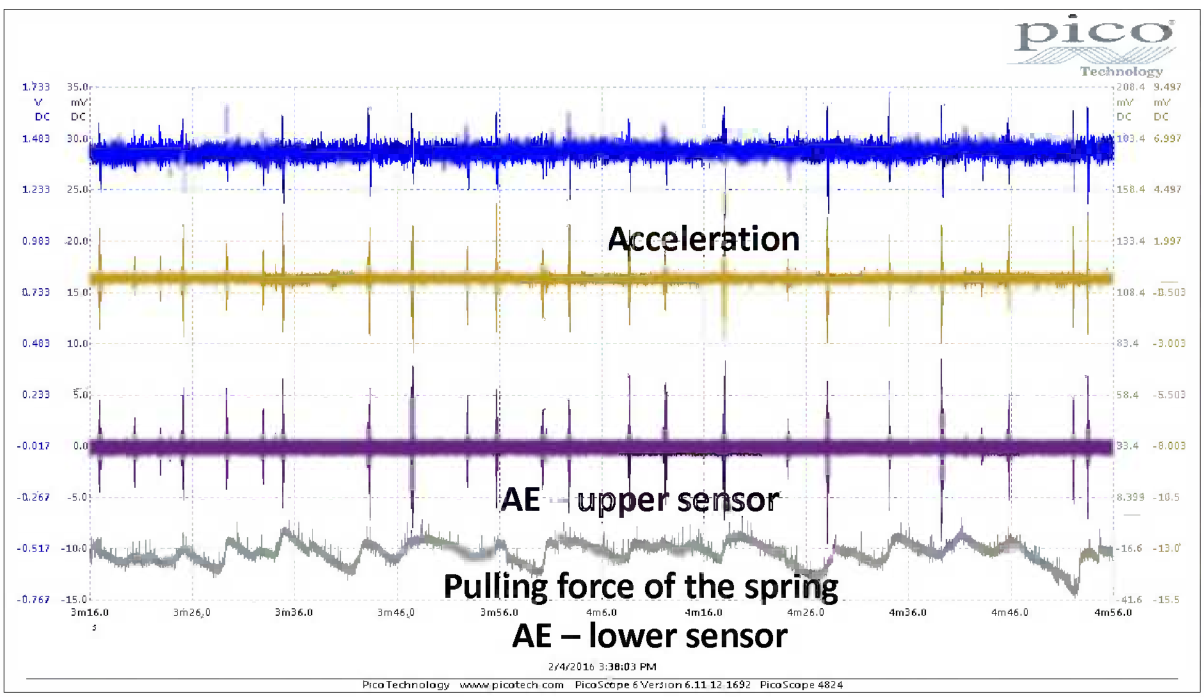

Fig. 28.Burrridge-Knopoff model–one block-horizontal system: recording of acceleration, acoustic emission(AE) and the pulling force on the spring (see location of the sensors in Fig. 27)

8. Activity related to risk culture and public safety

A supplementary textbook for Universities "Geophysical Methods in Ecology and Catastrophe Management" in Georgian was prepared and published in 2003 (author T. Chelidze).

In 2013 were edited and printedpopular brochures in Georgian: “Surviving disasters: a pocket guide for citizens” and “Basic knowledge on nuclear hazards: lessons of Chernobil and Fukusima”(Fig. 29).

Fig. 29. Title pages of popular brochures in Georgian: “Surviving disasters: a pocket guide for citizens” and “Basic knowledge on nuclear hazards”.

The brochures have been distributed to a wide audience: teachers of high schools, Universities professors, students, governmental authorities, etc.

A web-page on “Hazards and Risks of Large Dams” has been compiled and implemented into the web-site “Be Safe Net”

9. Publications of the Centre

Geodynamical Risks of High Dams. Tbilisi. 2002. Bakur Sulakauri Publ. House (In Russian)
Study of Earth’s crust tilts in the area of high Enguri dam. T. Matcharashvili, T. Chelidze, V.Abashidze.2003. Geophysical Journal (Ukraine, in Russian), v. 25, №3,153 – 158.

Investigation of dynamics of earth tilts at Enguri hydro power station high dam. T. Matcharashvili, T.Chelidze, V.Abashidze. 2004. European Geosciences Union 1st General Assembly. Nice, France, Abstract.

Influence of periodic variations in water level on regional seismic activity around a large reservoir: Field

data and laboratory model. J.Peinke, T.Matcharashvili, T. Chelidze, J.Gogiashvili, A.Nawroth, O.Lursmanashvili, Z.Javakhishvili. 2006.Physics of the Earth and Planetary Interiors. 130–142.

Increase in order in seismic process around large reservoir induced by water level periodic variation. T. Matcharashvili, T. Chelidze, 2007, Nonlinear Dynamics. DOI 10.1007/sl11071-007-9219-0.

About water regulation norm of the Enguri water reservoir. Abashidze V., Chelidze T., Kobakhidze T. 2006-2007. Journal of Georgian Geophysical Society, v.11A, 3-9.

Increase of order in local seismic energy release caused by water level variation in the Enguri high dam reservoir. Abashidze V., Javakhishvili Z., Khutsishvili T.,Meparidze E., Zhukova N., Chelidze T., Matcharashvili T. 2007.Bulletin of the Georgian National Academy of Sciences, v.1,#3, 49-51.

Influence of the periodic variation of water level in Enguri reservoir on the regional seismic activity. Chelidze T., Matcharashvili T., Javakhishvili Z., Abashidze V., Khutsishvili T.,Meparidze E., Zhukova N. 2008. Geophysical Journal (Ukraine), v. 30, 87-94. (In Russian).

Atlas of GIS-based maps of natural disaster hazards for the Southern Caucasus. T. Chelidze (Ed). Tbilisi, 2006-2007.

Influence of Large Water Reservoirs Construction and Filling on Dynamics of Earth C rust Local Tilts. T. Matcharashvili, T. Chelidze, V.Abashidze, N. Zhukova, E. Mepharidze, T. Kobakhidze. 2010. In: Hydrocomplexity: New Tools for Solving Wicked Water Problems. IAHS Publications. 338. pp. 268-269.

Changes in Dynamics of Seismic Processes Around Enguri High Dam Reservoir Induced by Periodic Variation of Water Level. T. Matcharashvili, T. Chelidze, V. Abashidze, N. Zhukova and E. Meparidze. 2010. In: Geoplanet: Earth and Planetary Sciences, Volume 1, 2010, DOI: 10.1007/978-3-642-12300-9; Synchronization and Triggering: from Fracture to Earthquake Processes. Eds.V.de Rubeis, Z. Czechowski and R. Teisseyre, pp.273-286.

Installation and utilization of Automated Data Acquisition and transmission system of the tiltmetric network in the Enguri dam. V. Abashidze, T. Chelidze, I. Jibladze, T. Tsaguria. 2010. Bulletin of the Georgian National Academy of Sciences, v.4, p.58-62.

Evidence for changes in the dynamics of Earth crust tilts caused by the large dam construction and reservoir filling at the Enguri dam international test area (Georgia). T. Matcharashvili,T. Chelidze,V. Abashidze, N. Zhukova,E. Mepharidze. 2011. Nonlinear Dynamics. DOI 10.1007/s11071-010-9930-0A.

Climate Change in Georgia; statistical and nonlinear dynamics predictions. Amiranashvili, T. Matcharashvili, T. Chelidze.2012. Journal of Georgian Geophysical Society, 15 A. 67-88.

Pitfalls and Reality in Global and Regional Hazard and Disaster Risk Assessments. T. Chelidze.2012. Journal of Georgian Geophysical Society, 15 A. 3-14.

Real time telemetric monitoring system of large dams and new methods for analysis of dam dynamics. T. Chelidze, M. Wieland, T. Matcharashvili, V. Abashidze, M. Kalabegishvili, N. Zhukova. 2012. Journal of Georgian Geophysical Society, 15 A. 49-67.

Investigating the dynamical features of the time distribution of the reservoir-induced seismicity in Enguri area (Georgia). L Telesca, T Matcharashvili, T Chelidze, N Zhukova.2013. Natural Hazards. DOI10.1007/s11069-013-0855-z.

Application of new nonlinear elasticity and nonlinear dynamics tools in real time monitoring of large engineering constructions (case of high arc Enguri dam). Chelidze T., Matcharashvili T., Abashidze V. 2013. DISASTER ADVANCES, 6(9): 84-89.

Application of the dynamic data analysis in the real time monitoring of high dam body behavior. T. Matcharashvili, T. Chelidze, N. Zhukova, Z. Tsveradze. 2016. Chaotic Modeling and Simulation (CMSIM). 3, 309-316.

ევროპის საბჭოს დიდი კატასტროფების შეთანხმების საქართველოს სპეციალიზირებული ცენტრი 20 წლისაა

რეზიუმე

თ. ჭელიძე ვ. აბაშიძე, თ. მაჭარაშვილი, თ. ცაგურია, თ. წამალაშვილი, ა. ამირანაშვილი, ნ. ჟუკოვა, ზ. ჭელიძე, ნ. ვარამაშვილი

1995 წლის ნოემბერში ევროპის საბჭოს დიდი კატასტროფების შეთანხმებაში მონაწილე ქვეყნების მუდმივი წარმომადგენლების შეკრებაზე განხილულ იქნა საქართველოს წინადადება საქართველოში “მაღლივი კაშხლების გეოდინამიკური რისკის” სპეციალიზირებული ცენტრის შექმნის თაობაზე.

წინადადება განიხილეს და მოიწონეს ევროპის საბჭოს ექსპერტებმა ფრანგმა პროფესორებმა ა.გუბემ და ჟ. ბენამ, რის შედეგად 1996 წ. დეკემბერში საქართველოს გარემოს დაცვის სამინისტროს გადაწყვეტილებით საქართველოს მეცნიერებათა აკადემიის გეოფიზიკი სინსტიტუტთან შეიქმნას პეციალიზირებული ცენტრი. ამჟამად ცენტრს აქვ სარასამთავრობო იურიდიული პირის სტატუსი.

ევროსაბჭოს დიდი კატასტროფების შეთანხმების მცირე გრანტებით შესრულდა 20-ზე მეტი პროექტი, მათ შორის აღსანიშნავია:

- შეიქმნა ენგურის მაღლივი კაშხლის საერთაშორისო პოლიგონი (Enguri Dam International Test Area – EDITA),
- შეიქმნადა 2010 წლიდან უწყვეტად მუშაობს რეალურ დროში მოქმედი დიდი საინჟინრო ობიექტების დეფორმაციების ავტომატური ტელემეტრული მონიტორინგის სისტემა ენგურჰესზე
- ქართველ, აზერბაიჯანელ და სომეხ კოლეგებთან თანამშრომლობით გამოიცა სამხრეთ კავკასიის ბუნებრივი კატასტროფების GIS ატლასი, რომელშიც მოცემულია სეისმური, მეწყრული, ღვარცოფების, ზვავების საშიშროების რუკები.
- შეფასდა გვალვების განმეორადობა და კლიმატის ცვლილება საქართველოში
- განხორციელდა ენგურის კაშხლის შესაძლო დაზიანებით გამოწვეული დატბორვის მოდელირება თანამედროვე კომპიუტერული პროგრამებით
- შედგენილ იქნა ენგურის კაშხლის რაიონის სეისმური საშიშროების, პიკური და სპექტრული აჩქარებების რუკები, შესწავლილ იქნა ენგურის რეზერვუარის შექმნითა და ექსპლუატაციით გამოწვეული ე.წ. ინდუცირებული სეისმურობა.

• საფრანგეთ-ევროპის გეომორფოლოლოგიურ ცენტრთან თანამშრომლობით შეიქმნა საქართველოს მეწყრული და ღვარცოფული საშიშროების რუკები პან-ევროპული სტანდარტით.

ГРУЗИНСКОМУ СПЕЦИАЛИЗИРОВАННОМУ ЦЕНТРУ СОГЛАШЕНИЯ ПО БОЛЬШИМ КАТАСТРОФАМ СОВЕТА ЕВРОПЫ - 20 ЛЕТ

Челидзе Т.Л., Абашидзе В.Г., Мачарашвили Т.Н., Цагурия Т.А..Цамалашвили Т.О., Амиранашвили А.Г., Жукова Н.Н., Челидзе З.Т., Варамашвили Н.Д.

Реферат

В ноябре 1995 года на собрании постоянных представителей стран-участников соглашения по большим катастрофам Совета Европы было рассмотрено предложение Грузии о создании в Грузии Специализированного центра «Геодинамический риск высоких плотин».

Предложение было рассмотрено и одобрено экспертами, французскими профессорами А. Губе и Ж. Бена, после чего в декабре 1996 года по решению Министерства Охраны окружающей среды Грузии при Институте геофизики АН Грузии был создан Специализированный центр. В данное время Центр имеет статус внегосударственного юридического лица.

По малым грантам соглашения по большим катастрофам Совета Европы выполнено свыше 20 проектов, среди которых необходимо отметить:

. создан международный полигон высокой плотины Ингури-(Enguri Dam International Test Arec – EDITA);

. на Ингури ГЭС создана и с 2010 года непрерывно работает действующая в реальном времени система автоматического телеметрического мониторинга деформаций больших инженерных объектов;

. в сотрудничестве с грузинскими, азербайджанскими и армянскими коллегами издан атлас GIS естественных катастроф Южного Кавказа, в котором представлены карты сейсмических, оползневых, селевых, лавинных опасностей;

.оценена повторяемость засух и изменения климата в Грузии;

. с помощью современных компьютерных программ осуществлено моделирование затопления, вызванного возможным повреждением плотины Ингури;

. составлены карты сейсмической опасности, пикового и спектрального ускоркений для района плотины Ингури, изучена т.н. индуцированная сейсмичность, вызванная созданием и эксплуатацией резервуара Ингури;

. в сотрудничестве с геоморфологическим центром Франции-Европа в паневропейском стандарте создана карта оползневых и селевых опасностей Грузии.

Journal of Georgian Geophysical Society,
Issue(A), Physics of Solid Earth, v.19a, 2016, pp. 35-48

Preliminary results of forced stick-slip synchronization area studies: experiments and theoretical models

Tamaz Chelidze, Teimuraz Matcharashvili, Ekaterine Mepharidze,
Dimitri Tephnadze, Natalia Zhukova
M. Nodia Institute of Geophysics, 1, Alexidze str. 0160, Tbilisi, Georgia

Abstract

Synchronization phenomena are encountered in various fields, from mechanics to biological and social processes. In the paper, the results of laboratory experiments on the mechanical and electromagnetic synchronization of mechanical instability (slip) of a slider-spring system consisting of basalt blocks are presented. Slip events were recorded as acoustic emission bursts. The data allow delineating the synchronization region in the plot of forcing intensity versus forcing frequency for both mechanical and electromagnetic synchronization. Experiments are compared with theoretical models.

Introduction

Synchronization is encountered in various fields, from mechanics to biological and economical processes (Pikovsky et al., 2003; Blekhman and Rivin, 1988). One important domain is the synchronization of seismic process and its small scale model - stick-slip by a weak external forcing (Scholz, 2003; Beeler and Lockner, 2003, Bartlow et al., 2012). As the Earth is embedded in the oscillating field of different origin with extremely wide range of frequencies, from seconds to months and years, synchronization is possible in many geophysical processes. For example there are a lot of observations that seismic activity is coupled with the action of such weak oscillating fields as Earth tides, solar activity, atmospheric pressure, electromagnetic pulses (storms), seasonal variations, and reservoir exploitation. The intensity of stress, invoked by these superimposed periodical mechanical or electromagnetic (EM) oscillations is as a rule much smaller (of the order of 0.1-1 bar) than that of the main driving force – tectonic stress (Prejean and Hill, 2009). Nevertheless, finally, this weak interaction may invoke the phenomenon of synchronization, at least, the so called phase synchronization – PS (Rosenblum et al., 1996). It is evident that these phenomena cannot be understood in the framework of traditional linear approach and that such high sensitivity to weak impact imply essentially nonlinear interactions (Kantz and Schreiber, 1997).

It should be mentioned that the papers devoted to theoretical nonlinear analysis of natural (non-forced) stick-slip equations (Becker, 2000) demonstrate beautiful phase plots with typical attractors. Similar results are obtained in theoretical studies of stick-slip under periodic forcing (Savage and Marone, 2007; Capozza et al., 2011), but the same authors also illustrate that obtaining such clear nonlinear patterns in experiments on physical models is very difficult due to a strong noise caused by the irregularity of slip surfaces of fixed and sliding blocks. In the present paper the results of laboratory experiments on the mechanical and electromagnetic (EM) synchronization of mechanical instability (slip) of a slider-spring system consisting of basalt blocks are presented and an attempt is done to find corresponding nonlinear dynamics patterns of natural and periodically forced stick-slip process, such as Arnold's tongues, Recurrence Plots etc.

Theoretical Models

The natural stick-slip can be approximated by relaxation process, where quasi-periodic sequence of slow accumulation of stress (stick phase) is followed by fast stress-drops or slips (Chelidze et al., 2010*b*) and is considered as an autonomous oscillator with a natural frequency ω_0.

The (periodically) forced stick-slip process is an example of the integrate-and fire oscillator under periodic forcing. There are many papers devoted to the problem of forced stick-slip (Beeler and Lockner, 2003, Bartlow et al., 2012; Johnson et al., 2013; Capozza et al., 2011; 2012; Savage and Marone, 2007; Guyer et al, 2013). The most general approach to a problem of forced autonomous oscillator is presented in Pikovsky et al., (2003): according to it the autonomous oscillator with natural frequency ω_0 subjected to a weak forcing of frequency ω and intensity ***I*** changes its frequency ω_0 to some different value Ω. The difference $(\omega - \omega_0)$ is called detuning: on the plot of ***I*** versus ω the area of synchronization of autonomous oscillator forms an inverse bell-shape (or triangle) area, so called Arnolds' tongue (Arnold, 1983) with a minimum at $(\omega - \omega_0) = 0$, i.e. at the point where forcing frequency is close to the natural frequency of oscillator (Fig. 1a); as the detuning increases, you need stronger forcing and at very large detuning synchronization became impossible. In many cases the phenomenon of high order synchronization can be observed at multiples of natural frequency ω_0 (Pikovsky et al., 2003; Chelidze et al., 2010*a,b*).

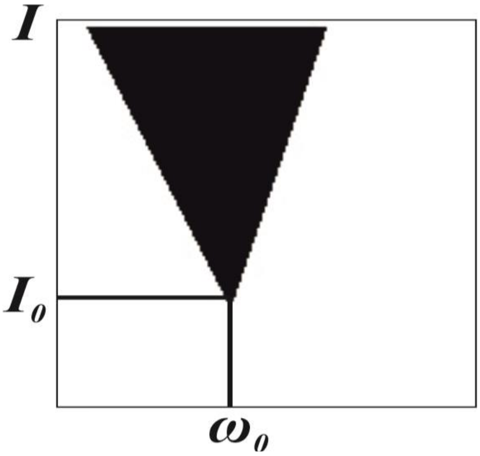

a)

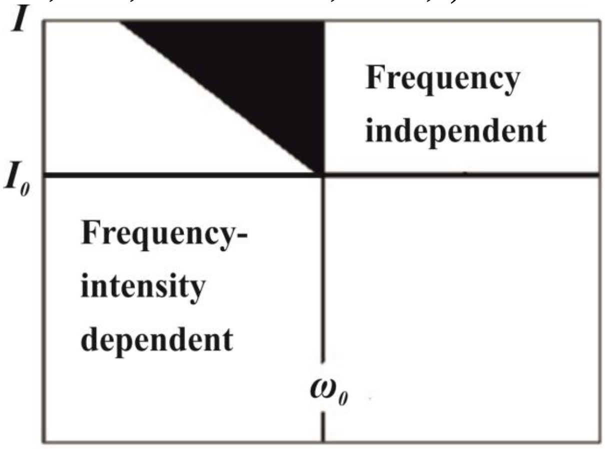

b)

Fig.1. Different models of synchronization area: (a) Arnold's tongue - the region on the plot of intensity ***I*** versus frequency ω of the external forcing, where synchronization of occurs in the presence of noise; ω_0 is the frequency of forcing when the minimal intensity I_0 is needed for synchronization (in absence of noise $\boldsymbol{I_0}$ equals zero); (b) nucleation or Scholz (2003) model - on the plot of ***I*** versus ω the correlation (synchronization) area is similar to Arnolds' tongue only at low forcing frequencies $\omega < \omega_0$ and at high frequencies the correlation of slips with forcing became frequency independent.

On the other hand in geophysical research the different (nucleation or Scholz) model of forced stick-slip is developed: according to it the plot of I versus ω (the correlation/synchronization area) is similar to symmetric Arnolds' tongue only at low forcing frequencies $\omega < \omega_0$ and at high frequencies the correlation of slips with forcing became frequency independent (Fig. 1b). For explanation of such asymmetry the concept of slip nucleation phase (time) is introduced (Scholz, 2003). According to this model if the period of forcing is greater than the slip nucleation time, nucleation does not hamper synchronization; but if the forcing period is less than nucleation time, the slips cannot follow forcing oscillations (detuning is too large), hence much higher intensity of forcing is needed to correlate slips with forcing. The above model was used to explain the lack of (or insignificant) correlation of earthquakes' occurrence with tidal stress variations (Beeler and Lockner, 2003; Scholz, 2003): according to them tides' period (hours) is too short compared to significant earthquake nucleation time (months, years).

Laboratory experiments on forced stick-slip (Beeler and Lockner, 2003; Bartlow et al., 2012; Savage and Marone, 2007) seem to confirm indeed that stick-slip synchronization area is strongly asymmetric like in Fig. 1b.

Our study is aimed to demonstrate the relevance of the presented models to laboratory experiments on the forced stick-slip.

Laboratory Experiments and Interpretation.

Experimental set up:

Experimental set up in synchronization experiments represents a system of two horizontally oriented plates of the same roughly finished basalt. The supporting and the slipping basalt blocks were saw-cut and roughly finished. The height of surface protuberances was in the range of 0.1-0.2 mm. A constant pulling force F_p of the order of 10 N was applied to the upper (sliding) plate; in addition, the same plate was subjected to periodic mechanical or electric perturbations (forcing) with variable frequency (from 10 to 120 Hz) and amplitude (from 0 to 1000 V in case of EM forcing or applying from 0 to 5 V to a mechanical vibrator in case of mechanical forcing). Mechanical pull from both these forcing were much weaker (of the order of 10^{-3}-10^{-4}) compared to the pulling force of the spring.

Slip events in synchronization experiments were registered as acoustic bursts by the sound card of PC (upper channel in Fig. 2) and the EM or mechanical forcing was recorded on the second channel (lower channel in Fig. 2).

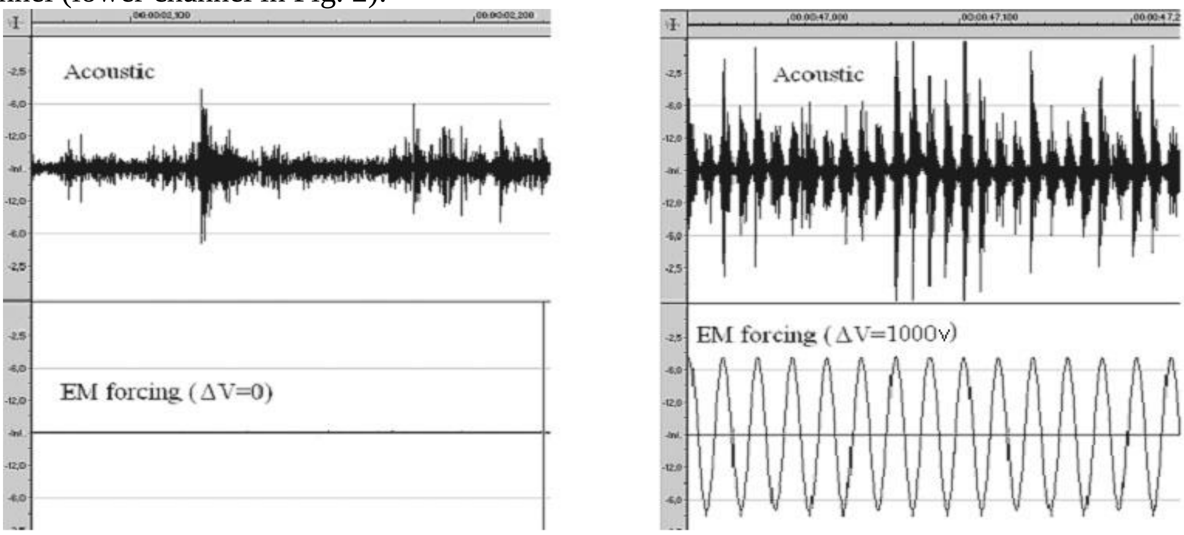

a) b)

Fig. 2. Synchronization of stick-slip by EM forcing. The upper trace is records of AE signals generated by slips; the lower channel records EM forcing; a) non synchronized (zero forcing, $\Delta V = 0$) and b) synchronized stick-slip process (forcing = 1000 V). The vertical axis shows the intensity of signal in dB and horizontal axis shows the time in msec.

Details of the setup and technique are given in (Chelidze et al., 2002; Chelidze and Lursmanashvili, 2003). In order to pick the phases of Acoustic Emission (AE) signals' relative to forcing phase onsets more precisely, a special package was developed for reducing the level of ambient noise (Zhukova et al., 2013): the result is shown in Fig.3.

Due to this methodology the weak AE signals created by microslips or precursor AE (Johnson et al., 2013) were filtered from the processing and only strong events generated by large Charaslips were selected (Fig.3).

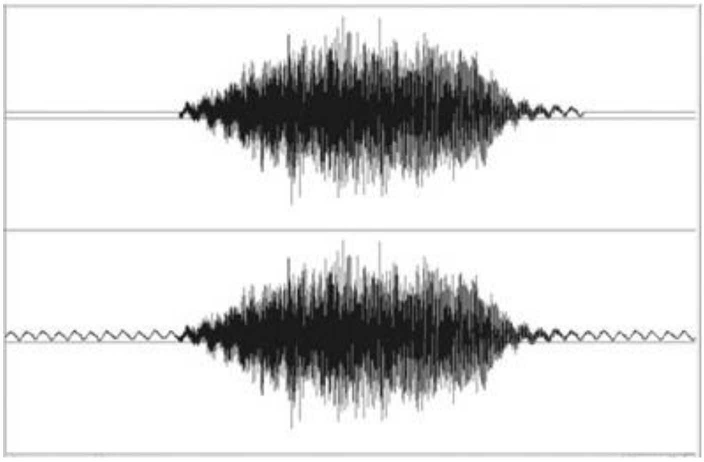

Fig. 3. Filtered (top) and original unfiltered (bottom) records of AE signal during stick-slip.

Synchronization of oscillating autonomous system of natural frequency ω_0 by forcing frequency ω results in modification of systems' natural frequency ω_0 to the so called observed frequency Ω. In our experiments the following parameters were varied: i) the frequency, ω of superimposed periodical perturbation; ii) the amplitude of the external excitation or forcing (in case of electromagnetic forcing V_a is the voltage applied to electrodes glued to contacting surfaces of fixed and pulled blocks; in case of mechanical forcing V is the voltage applied to mechanical vibrator).

Measuring synchronization strength:

Last decades several new approaches were suggested to quantify the complexity/synchronization of processes by analysis of measured time series (Blekhman, 1988; Pikovsky et al., 2003; Chelidze and Matcharashvili, 2015). The possible measures for quantification of synchronization are: generalized phase difference; mutual information; conditional probability of phases; flatness of stripes of synchrograms or stroboscopic technique; coefficients of phase diffusion (Chelidze and Matcharashvili, 2013, 2015). The other methods stem from the information theory including Shannon or Tsallis entropy, algorithmic complexity etc. It should be stressed that both laboratory stick-slip and EQ source evolution can be considered as the integrate and fire type processes, where the acoustic/seismic signals contain well-defined marked events corresponding to slips/acoustic bursts. To deal with relatively short time series new tests have been proposed such as recurrence plots (RP) and recurrence quantitative analysis (RQA). In the case of very restricted statistics (tens of events) less demanding methods, such as Shuster test (Schuster, 1897) can be used.

Synchronization at electromagnetic forcing - Arnold's tongue:

The example of synchronized and non-synchronized stick-slip at electromagnetic (EM) forcing are shown in Fig. 2. The electric field in this case was normal to the sliding plane. Synchronization was observed only at some definite sets of parameters (spring stiffness K_s, forcing frequency f, forcing intensity ΔV_a). Several methods were used for measuring synchronization strength depending on forcing parameters, which are presented in Chelidze and Matcharashvili (2013, 2015), Chelidze et al., (2002, 2003, 2005, 2010*a*,*b*).

Here we focus on the "phase diagram" for variables f and ΔV_a or so-called Arnold's tongue (see Pikovsky et al., 2003), which is presented in the Fig. 4.

The minimum forcing intensity $\Delta V_a \approx 400\,\mathrm{V}$ needed for a strong synchronization corresponds to the forcing frequencies in the range 60-80 Hz.

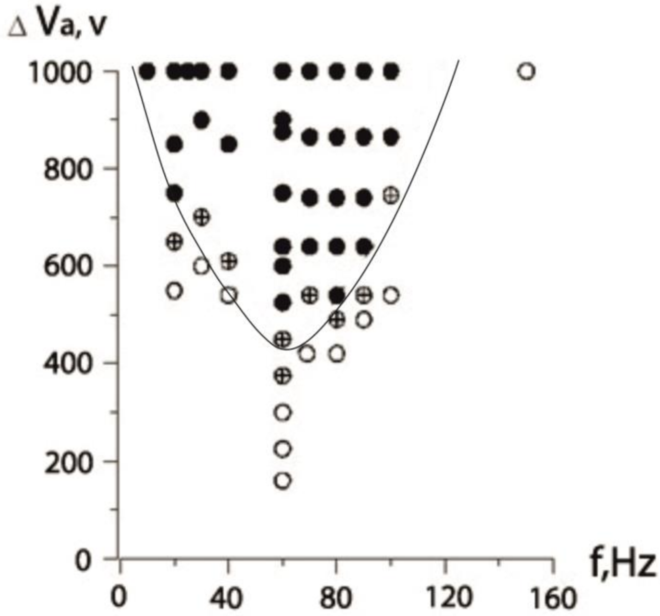

Fig. 4. Stick-slip synchronization area (Arnold's tongue) for various intensities (V_a) and frequencies (f) of the external periodic EM forcing. Filled circles – strong, circles with crosses – intermittent and empty circles – absence of synchronization (Chelidze et al., 2003, 2005, 2010a,b).

In our experiments with EM forcing besides (1:1) locking the high order synchronization (1:n) was also observed, where $n > 1$ is the number of synchronized slips generated by one forcing period (Chelidze et al., 2002, 2003, 2005, 2010 a, b, 2015).

<u>*Synchronization by mechanical forcing:*</u>

Weak mechanical periodic perturbations also imposes ordering on the slip, namely a phase synchronization. Mechanical forcing was realized by the vibrators of geophone "CB-5" or "CB-20". The intensity of mechanical vibration was regulated by the voltage V applied to the vibrator. In our experiments with mechanical forcing as a rule the high order phase synchronization (HOS) was observed, namely, the triggered slip occurred only after several tens of forcing periods. High-order synchronization means that the forcing (ω) and observed (Ω) frequencies in the system are related to each other by some winding ratio ($n \div m$) that is $n\omega = m\Omega$ (Chelidze et al., 2010*a*,*b*). The winding ratio $n \div m$ at mechanical forcing was in the range 80:1 to 200:1, depending on the experimental conditions.

The stick-slip experiments with mechanical forcing were carried out at following parameters: the stiffness of the spring, $K_s = 235.2$ N/m; the voltage applied to vibrator was 0.25V, 0.5 V, 0.75V, 1 V, 1.5 V, 2 V, 2.5V 3 V; the frequency of forcing was varied in the range 5-120 Hz and the natural frequency of the sensor was 20 Hz.

In order to assess the strength of phase synchronization phase differences between the phases of periodic forcing signal and the onsets of AE burst were picked out (in Figs. 5 a-h on X axes are shown phase differences value and on Y axes – the number of events in a bin; bin is taken equal to 1/15th of the forcing period) and the corresponding histograms were compiled; the binned distribution was approximated by parabola.

As a model for the phase distributions of events a polynomial of the second degree (parabola) was used:

$$f(x) = p_1 x^2 + p_2 x + p_3$$

The parabolic plot is considered as a proxy of probability density function (PDF) of a number of AE signals in the certain range of forcing phases y_i : the width of parabola is a proxy of

PDF width. The optimal parameters $p_1, p_2, p_3....$ of the polynomial were calculated using the least squares method for minimization of the residual between parabola and experimental values R^2:

$$R^2 = \sum_{i=1}^{n} \left[y_i - (p_1 x_i^{\ 2} + p_2 x_i + p_3) \right]^2$$

Where y_i is the number of events in the i^{th} bin, i - is a bin's current number.
The width of the parabola depends on the parameter p_1. The half-width of the parabola (a proxy of half-width of PDF) is equal to $\frac{1}{2} p_1$.

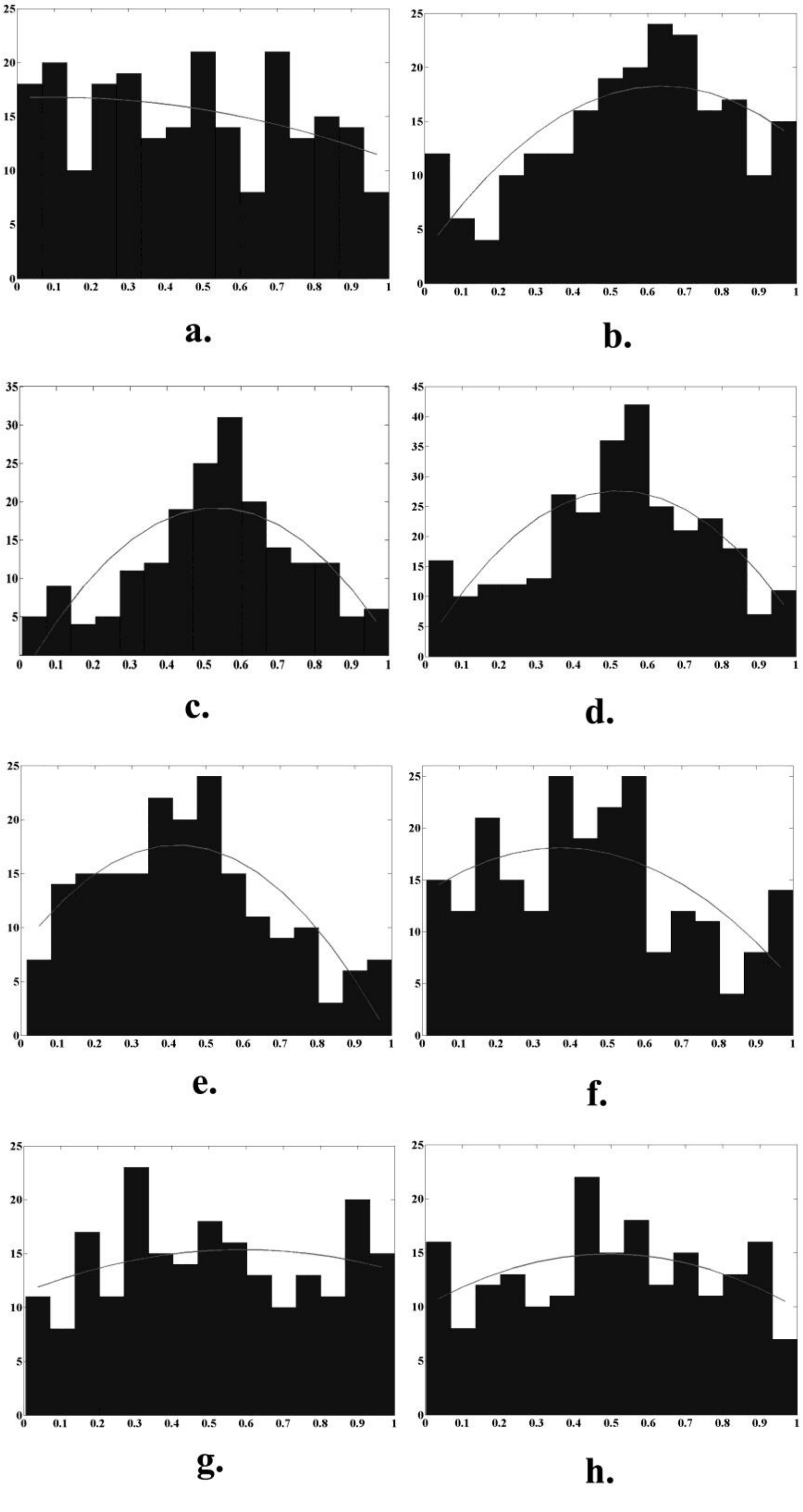

Fig. 5. PDF of number of AE signals in the certain range of forcing phases (in 1/15th bins of the forcing period) for the stiffness of the spring $K_s = 235.2$ N/m and forcing 1V (natural frequency of sensor 20 Hz). Forcing frequencies: (a) 5Hz; (b) 10Hz; (c) 20Hz; (d) 30Hz; (e) 40Hz; (f) 50Hz; (g) 80 Hz; (h) 120 Hz.

In order to assess the strength of phase synchronization and compile the Arnolds' plot phase differences between the phase of periodic forcing signal and the onset of AE burst was picked out and the plots of probability density functions (PDF) of number of AE signals at certain phases of forcing (in bins of period) were constructed (Fig. 5 a-h).

Arnold's tongue at mechanical forcing:

For randomly distributed AE signals PDF plots are almost flat and for increased strength of synchronization are bell curve like with the half-width depending on the synchronization strength.

The data obtained allow construction of phase space plot of synchronization strength dependence on intensity and frequency of forcing or Arnold's plot (Fig.6). Hollow rings mean absence, rings with crosses – moderate and filled rings – good synchronization.

The minimum forcing intensity needed for a strong mechanical synchronization corresponds to the forcing frequencies 20-40 Hz, which is not very far from the optimal forcing frequencies at EM synchronization – 60 Hz (Fig. 4). The filled dots correspond to good synchronization, hollow dots – to absence and dots with crosses – to moderate synchronization.

We guess that the similarity in optimal forcing frequencies can be related to the identity of configuration of sliding and fixed blocks of basalt as well as to closeness of other stick-slip parameters (spring stiffness, drag velocity etc) in both EM and mechanical synchronization experiments.

Obtained results confirm the inverse bell-shape configuration of the mechanically forced stick-slip synchronization area similar to EM forcing data. The minimal forcing frequency/intensity required for synchronization should provide optimal friction conditions or friction stabilization (Cochard et al., 2001; Capozza et al., 2012). Here we'd like to comment that friction stabilization by weak periodic forcing does not mean complete elimination of stick-slip: experimental data (Fig.3 in Cochard et al, 2001,) show that even at minimal friction in forced experiments there are still small scale synchronized stick-slip events; so instead of the term friction stabilization it seems better to use the term stick-slip minimization or stick-slip quantification.

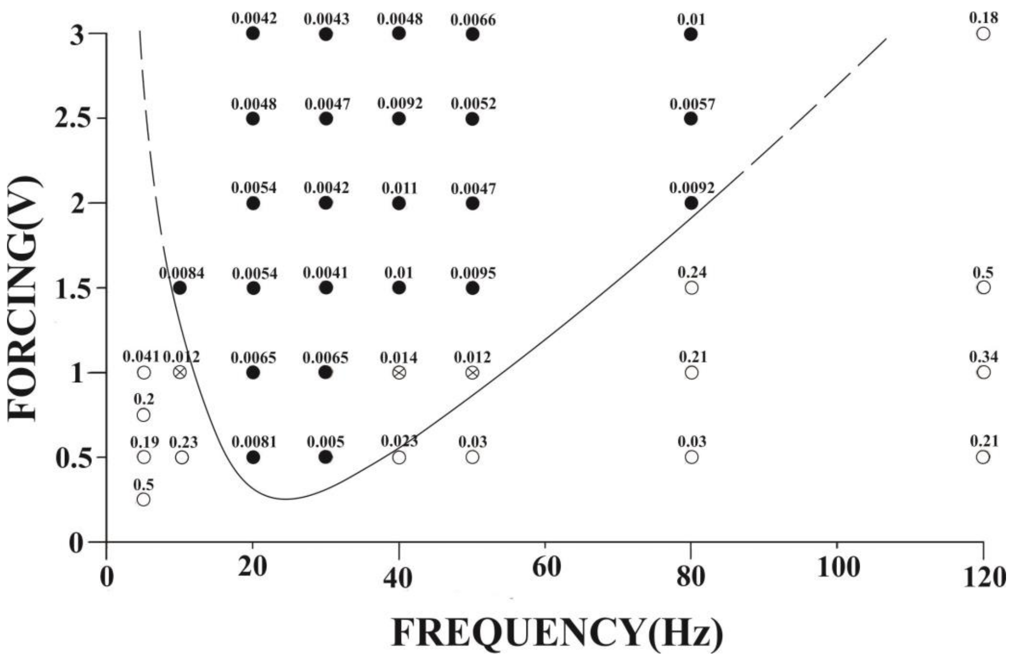

Fig.6. Phase space plot of synchronization strength (Arnold's tongue) expressed as half-widths $\frac{1}{2}p_1$ of parabola plots (proxies of PDFs) in Fig.5 a-h for the spring stiffness $K_s = 235.2$ N/m. Hollow dots mean absence (half-width $\frac{1}{2}p_1 > 0.014$), dots with crosses – moderate $0.012 \le \frac{1}{2}p_1 \le 0.014$ and filled dots – good synchronization. $\frac{1}{2}p_1 < 0.012$.

In addition to Arnold's plot some other nonlinear tests were performed, namely Recurrence Plots (RP) were composed and corresponding Recurrence Quantitative Analysis (RQA) was performed (Marwan et al, 2007; Webber, Marwan, 2015) using Visual Recurrence Analysis (VRA) tools (Kononov, 2006). RP plots for original data contain horizontal and vertical lines/clusters, which mean that during both natural and driven stick-slip some states are "laminar", i.e. they change slowly or do not change at all. We can attribute laminar states of AE waiting times to the periods, when the upper plate is stuck till strain from the spring became equal to friction force.

Recurrence Plots for various frequencies and constant forcing intensity 1.5 V show clear recurrence structures at frequencies 20-40 Hz, which are fading at higher frequencies (the plots became similar to RP of random sequence) in accordance with the Arnold's plot (Fig. 6).

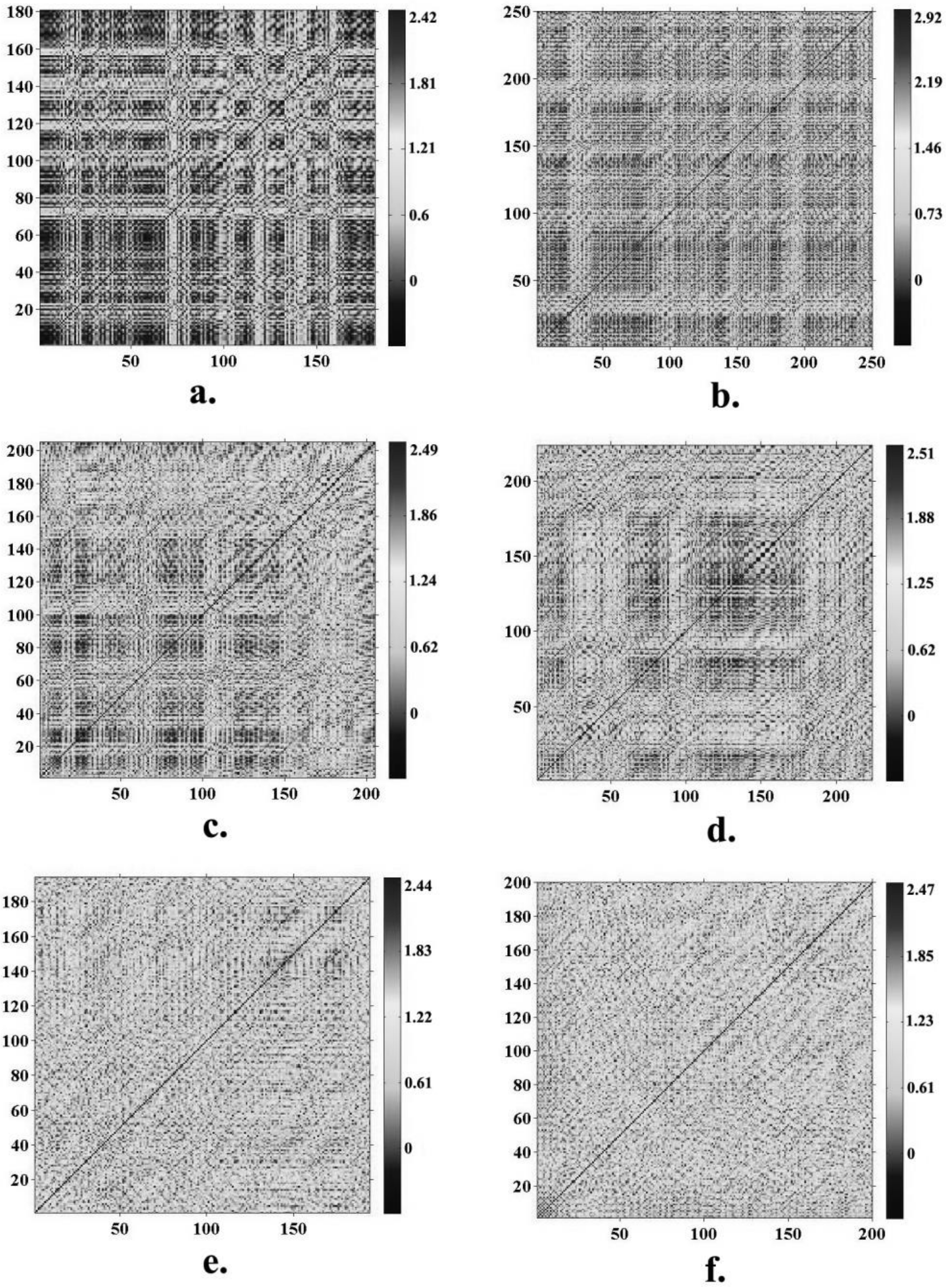

Fig. 7. Recurrence plots of slip-generated AE signals (original sequence of events) for the stiffness of the spring K_s =235.2 N/m and forcing 1.5V (natural frequency of sensor 20 Hz).

Synchronization at forcing frequencies: 20Hz (a); 30Hz (b); 40Hz (c); 50Hz (d); 80Hz (e); 120Hz (f).

Calculation of quantitative parameter (namely the percent of determinism %DET) of recurrences at various frequencies and intensities of forcing by RQA approach (Marwan et al, 2007), presented in Fig. 8, show that the %DET significantly increases in the frequency range from 20 to 60 Hz and at intensities of forcing larger than 0.5V, again in accordance with Arnold's plot (Fig.6).

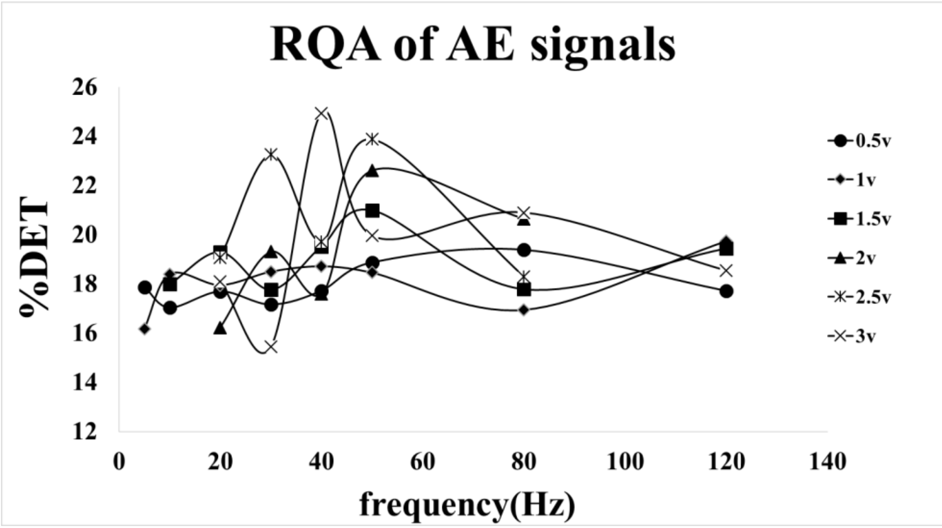

Fig.8. %DET versus the frequency of forcing at various intensities of forcing (original sequence of events).

The previous results (Figs.6-9) are related to the original sequences of AE events. It was interesting to consider also the smoothed sequences as according to general statistics terminology they correspond to a conditional rate (conditional intensity) models in the point process theory. We used the rates, obtained by Savitsky-Golay (S-G) filtering. Savitzky-Golay filter helps to resolve smoothing problem in the time domain as the magnitude of the variations in the data, i.e., the value of the local extremes, is preserved to a large extent (Press et al., 1997). The operation of smoothing performs actually a low-pass filtering of the sequence, which in turn allow revealing long-range correlations in the data. RQA calculations for the waiting times (WT) data, smoothed by Savitzky-Golay filter (Fig.9) indicate that the sequences of WT of the natural stick-slip (left plot) is less ordered than that of the periodically forced one (right plot); increase in the determinism %DET from 67% for natural process to 84% in the forced stick-slip.

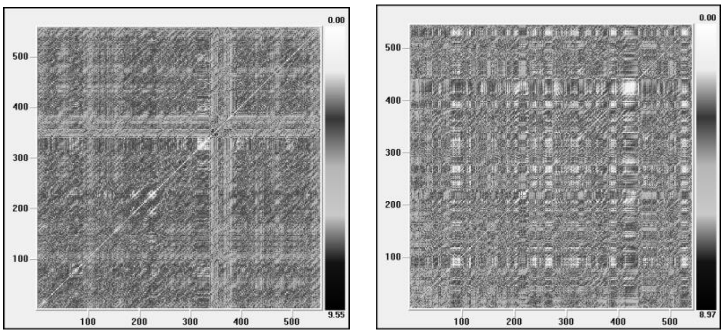

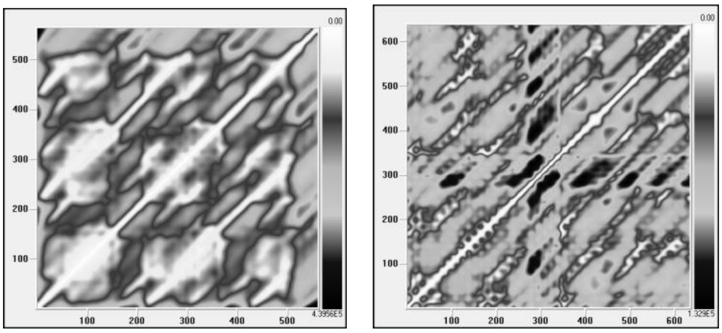

Fig.9. Visual Recurrence Analysis (VRA) plots (Kononov, 2006) of waiting times sequences of acoustic emissions (AE) smoothed by Savitzky-Golay filter: left column - RP (top) and VRA (bottom) plots for waiting times sequences of AE generated during natural stick-slip, right column - RP (up) and VRA plots of waiting times sequences of AE generated during stick-slip under periodic mechanical forcing (spring stiffness of 235 N, drag velocity 0.7 mm/s, forcing frequency 20 Hz

According to our experiments, the intensity-frequency phase space plot for forced stick-slip (Fig.7) follows inverse bell-shape pattern of Arnold model (Fig.1a), though a bit skewed at higher frequencies. We guess that the absence of the high-frequency branch declared in some studies of forced stick-slip (Beeler and Lockner, 2003; Bartlow et al., 2012; Savage and Marone, 2007) and explained in terms of Scholz model (Fig.1b) in principle can be due to some experimental restrictions (e.g. to a high inertia of the loading frame, transition from the synchronization regime to modulation mode etc). Besides, it should be noted that in some experiments of the cited authors the incipient high-frequency branch of Arnold plot seems to be present (see Figs. 5a, 7a in Beeler and Lockner, 2003 and Fig. 3a in Bartlow et al., 2012).

At the same time we cannot exclude the possibility of the strongly asymmetric pattern shown in Fig.1b: for example, simulations of frictional slip triggered by mechanical vibrations (Capozza et al., 2012) show that in some specific conditions, namely in case of very strong attractive interparticle forces the time-averaged friction coefficient $<\mu>$ at high enough forcing frequencies became frequency independent. At the same time the values of $<\mu>$ in this high frequency domain are very low, which seems to be in contradiction with nucleation model (according to it friction is very high during nucleation period).

We presume that the frictional behavior can be very different depending on many variables: rate, state, normal and pore pressure, gorge characteristics, intensity and frequency of forcing etc. This makes the response of the sliding systems to external forcing extremely variable. Mapping of Arnold tongue plot is informative for solving friction optimization/stabilization problem by application of weak external forcing. Application of nonlinear dynamics methods such as Recurrence Plots and Recurrence Quantification Analysis can be very helpful in analysis of forced stick-slip process.

Conclusions

In the paper the results of laboratory experiments on the mechanical or electromagnetic periodic forcing of mechanical instability (slip) in a slider-spring system are presented. Slip events were recorded as acoustic emission bursts. The data allow delineating approximately the synchronization regions (Arnold's tongues) in the plot of forcing intensity versus forcing frequency for both mechanical and electromagnetic synchronization.

The minimum forcing intensity needed for a strong mechanical synchronization is not very far from the optimal forcing frequencies at EM synchronization. We guess that the similarity in optimal forcing frequencies can be related to the identity of configuration of sliding and fixed blocks of basalt as well as to closeness of other stick-slip parameters (spring stiffness, drag velocity, normal stress/sliding block weight etc) in both EM and mechanical synchronization experiments.

Our experiments with both electromagnetic and mechanical periodic forcing support the general model of stick-slip synchronization area (known as Arnold's tongue), whose geometry is close to symmetric inverse bell-curve form; in this model both low- and high-frequency branches of forcing intensity vs frequency plot are frequency dependent. At the same time frictional motion depends on many variables like rate, state, normal and pore pressure, gorge characteristics, intensity and frequency of forcing etc other configurations of synchronization area cannot be excluded.

The results obtained by analysis of half-width of phase difference distribution are confirmed by other method, namely calculation of Recurrence Plots and Recurrence Quantification Analysis. The results can be important in tribology as the minimum of Arnold's tongue corresponds to optimal friction control (friction stabilization) by application of minimal external mechanical/EM forcing. Further investigations in this direction are needed to describe in detail the complexity of frictional motion.

Acknowledgements

Authors acknowledge the grant of the Shota Rustaveli National Science Foundation of Georgia (Project 31/31 - "FR/567/9-140/12").

References

Arnold, V., 1983. Notes on the perturbation theory for the problems of Matieu type, Russ. Mat. Surveys, 38, pp. 215-233.

Beeler, N. M., Lockner, D. A. 2003.Why earthquakes correlate weakly with the solid Earth tides: Effects of periodic stress on the rate and probability of earthquake occurrence. J. Geophys. Res., 108, B2391, doi:10.1029/2001JB001518,

Bartlow, N. M., Lockner, D. A., and Beeler N. M., 2012. Laboratory triggering of stick-slip events by oscillatory loading in the presence of pore fluid with implications for physics of tectonic tremor, J. Geophys. Res., 117, B11411, doi:10.1029/2012JB009452.

Becker, T., 2000. Deterministic chaos in two state-variable friction sliders and the effect 0f elastic interactions. In: "GeoComplexity and Physics of Earthquakes" (Eds. J. Rundle, D. Turcotte, W. Klein), pp. 5-27.

Blekhman, I.I. and Rivin E.I. 1988. Synchronization in Science and Technology. Asme Press Translations.

Capozza, R., Rubinstein, Sh., Barel, I., Urbakh, M.,and Fineberg, J., 2011. Stabilizing Stick-Slip Friction. Phys. Rev. Letters, v.107, 024301; DOI: 10.1103/PhysRevLett.107.024301.

Capozza R., Vezzani A., Vanossi A., Zapperi S., 2012. Triggering Frictional Slip by Mechanical Vibrations, Tribol. Lett. 48, pp. 95–102; DOI 10.1007/s11249-012-0002-0.

Chelidze, T., Varamashvili, N., Devidze, M., Tchelidze, Z., Chikhladze, V., Matcharashvili, T., 2002. Laboratory Study of Electromagnetic Initiation of Slip, Annals of Geophysics, 45, pp. 587-599.

Chelidze, T., Lursmanashvili, O., 2003. Electromagnetic and mechanical control of slip: laboratory experiments with slider system, Nonlinear Processes in Geophysics, 20, pp. 1-8.

Chelidze T., Matcharashvili, T., Gogiashvili, J., Lursmanashvili, O, Devidze, M., 2005. Phase synchronization of slip in laboratory slider system, Nonlinear Processes in Geophysics, 12, 1-8.

Chelidze, T., Lursmanashvili, O., Matcharashvili, T., Varamashvili, N., Zhukova, N., Mepharidze, E., 2010, High order synchronization of stick-slip process: experiments on spring-slider system, Nonlinear Dynamics, DOI 10.1007/s11071-009-9536-6. ***a***.

Chelidze, T., Matcharashvili, T., Lursmanashvili, O., Varamashvili, N., and Zhukova, N., Meparidze, E., 2010. Triggering and Synchronization of Stick-Slip: Experiments on Spring-Slider System. In: Geoplanet: Earth and Planetary Sciences, Volume 1, 2010, DOI:

10.1007/978-3-642-12300-9; Synchronization and Triggering: from Fracture to Earthquake Processes. Eds.V.de Rubeis, Z. Czechowski and R. Teisseyre, pp.123-164. ***b***.
Chelidze, T., and Matcharashvili, T., 2013. Triggering and Synchronization of Seismicity: Laboratory and Field Data - a Review. In: Earthquakes – Triggers, Environmental Impact and Potential Hazards. (Ed. K. Konstantinou), Nova Science Pub.
Chelidze, T., and Matcharashvili, T., 2015. Dynamical Patterns in Seismology. In: Recurrence Quantification Analysis: Theory and best practices. (Eds. C.Webber and N.Marwan). Springer Cham Heidelberg, pp. 291-335.
Cochard, A., Bureau, L., and Baumberger, T. 2001. Stabilization of frictional sliding by normal load modulation: A bifurcation analysis. Trans. ASME, J.Appl.Mech, 70, 220
Guyer, R. A., Le Bas, P-Y., Trugman, D., and Marone, C., 2013. Acoustic emission and microslip precursors to stick-slip failure in sheared granular material. Geophys. Res. Lett., 40, pp. 1–5, doi:10.1002/2013GL057848.
Johnson, P. A., Kaproth, B. M., Scuderi, M., Ferdowsi, B., Griffa, M., Carmeliet, J., Guyer, R. A., Le Bas, P-Y., Trugman, D., Marone, C., 2013. Acoustic emission and microslip precursors to stick-slip failure in sheared granular material, Geophysical Research Letters, 40, 21, pp. 5627–5631.
Kantz, H., Schreiber T., 1997. Nonlinear time series analysis, Cambridge University Press, Cambridge.
Kononov, E. 2006. Visual Recurrence Analysis. www2.netcom.com/~eugenek/page6.html.
Marwan N, Romano MC, Thiel M, Kurths J: 2007. Recurrence plots for the analysis of complex systems. Phys Rep, 438:237–329.
Pikovsky, A., Rosenblum, M. G., Kurths. J., 2003. Synchronization: Universal Concept in Nonlinear Science, Cambridge University Press, Cambridge.
Prejean, S., Hill, D., 2009. Dynamic triggering of Earthquakes. In: Encyclopedia of Complexity and Systems Science, R. A. Meyers (Ed.), Springer, pp. 2600-2621.
Press, W., Teukolsky, S. A., Vetterling, W.T., Flannery, B. P. 2007. Numerical Recipes: The Art of Scientific Computing (3rd ed.). New York: Cambridge University Press.
Rosenblum, M. G., Pikovsky, A., Kurths, J., 1996. Phase synchronization of chaotic oscillators. Phys. Rev. Lett., 76, pp. 1804-1808.
Savage, H., Marone, C., 2007. Effects of shear velocity oscillations on stick-slip behavior in laboratory experiments, J. Geophys. Res.: Solid Earth, 112B, DOI: 10.1029/2005JB004238.
Scholz, C. H., 2003. Good Tidings, Nature, 425, pp. 670-671.
Schuster, A., 1897. On lunar and solar periodicities of earthquakes. Proc. R. Soc. Lond. 61, 455–465
Webber, Ch., Marwan, N.(Eds). 2015.Recurrence Quantification Analysis, Theory and Best Practices. Springer Cham Heidelberg.
Zhukova, N., Chelidze, T., Matcharashvili, T., 2013. Automatic onset time picking of acoustic signals. Journal of Georgian Geophysical Society, Issue (A), Physics of Solid Earth, v.16a, 2013, pp.115-119.

ფორსინგის პირობებში არამდგრადი ხახუნის (სტიკ-სლიპის) სინქრონიზაციის არის შესწავლის წინასწარი შედეგები : ექსპერიმენტები და თეორიული მოდელები

თამაზ ჭელიძე, თეიმურაზ მაჭარაშვილი, ეკატერინე მეფარიძე, დიმიტრი ტეფნაძე, ნატალია ჟუკოვა

რეზიუმე

სინქრონიზაციის ფენომენი მრავალ დარგში გვხვდება, მექანიკიდან დაწყებული ბიოლოგიურ და სოციალურ პროცესებამდე. სტატიაში მოყვანილია ლაბორატორული ექსპერიმენტების შედეგები ზამბარა-მცოცის სისტემის მექანიკური არამდგრადობის და ელექტრომაგნიტური დასინქრონების (წაცოცებების) თაობაზე. წაცოცებები ფიქსირდებოდა როგორც აკუსტიკური ემისიის იმპულსები. ეს მონაცემები საშუალებას იძლევა შემოფარგლულ იქნას სინქრონიზაციის არე (მასინქრონებელი ზემოქმედების) ფორსინგის სხვადასხვა სიხშირესა და ინტენსივობის პირობებში. ექპერიმენტები შედარდა თეორიულ მოდელებს.

Предварительные результаты синхронизации неоднородного трения (Стик-Слип) при внешнем воздействии: теоритическая модель эксперимента

Тамаз Челидзе, Теймураз Мачарашвили, Екатерина Мепаридзе, Дмитрий Тепнадзе, Наталья Жукова

Резюме

Явление синхронизации наблюдается во многих направлениях, как в механическом, биологическом, так и в социальном. В статье приведены результаты синхронизации лабораторных экспериментов системы скольжения пружины при механическом и электрическом воздействии. Скольжение фиксировалось в виде импульсов акустической эмиссии. Такие данные дают возможность ограничить область синхронизации (воздействие) в условиях приложенного воздействия частот и интенсивности. Также было произведено сравнение экспериментальных данных с теоритическими моделями.

Journal of Georgian Geophysical Society,
Issue(A), Physics of Solid Earth, v.19a, 2016, pp. 49-57

Underground water level/temperatureresponse to seismic/tectonic transients: effects of poroelasticity

Tamaz Chelidze

Abstract

The problem of underground water flow is discussed in many publications. The upper crust down to approximately 20 km is a sequence of layers of porous/fractured fluid-saturated deformable rocks. When subjected to stress of various duration and mode, the excess transient pressure appears in the pore fluid, which can be observed practically as water level change/oscillations in boreholes.

In the paper are presented elementary theoretical models of underground water level/temperature response to seismic/tectonic transients taking into account effects of poroelasticity (Biot model). Besides, a direct mechanical squeezing of pore water by seismic vibrations (instantaneous flow) is considered.

The problem of underground water flow is discussed in many publications beginning from papers of Branchard and Bayerly (1935), Meinzer (1939), Jacob (1939), Biot (1941), which were followed by publications of Bredehoft (1967), Roeloffs (1988), Palciauskas and Domenico (1989), Brodsky et al (2003), Costain and Bollinger (2010).

Underground water levelresponse to seismic/tectonic transients. The upper crust down to approximately 20 km is a sequence of layers of porous/fractured fluid-saturated deformable rocks. When subjected to stress $\sigma$of various duration and mode, the excess transient pressure P_{ex} appears in the pore fluid. The fluid diffusion (or consolidation) equation defines the response of one-dimensional vertical flow to the appearance of P_{ex}(Domenico and Schwartz, 1994):

$$K_z \frac{d^2 P_{ex}}{dz^2} = \rho_w g(\Phi\beta_w + \beta_p)\frac{dP_{ex}}{dt} - \rho_w g\beta_w \frac{d\sigma}{dt} \qquad (1)$$

Here K_z is vertical hydraulic conductivity, ρ_w is density of water, g is acceleration due to gravity, Φ is porosity, $\beta_w$and β_p arecompressibilities of correspondingly water and pore space, σ is the total stress

$$\sigma = \sigma_{eff} + (P_s + P_{ex}) \qquad (2)$$

whereσ_{eff} is effective stress and P_s is the hydrostatic component of pressure. The coefficient $\rho_w g(\Phi\beta_w + \beta_p)$ is defined as a specific storage S_s and $\rho_w g\beta_p$ is a contribution to S_s, produced by pore compression.

Equation (1) states that the time rate of stress change defines the response of system to a given impact. There are two limiting cases: for stress rate much less than the characteristic time of diffusion of pore fluid, the excess pressure can exist only at small times; it dissipates quickly and the fluid is most of the time under constant pressure. As dissipation of excess pressure results from the rapid redistribution of fluid in the media of high permeability, this behavior is defined as a drained (relaxed) one. At fast loading, pore fluid has no time to escape; the mass of fluid in a given volume remains constant. This response is defined as undrained (unrelaxed). The undrained porous system is much stiffer as the part of load is supported by the uncompressible liquid. Accordingly, the fluid flow term in (1) d^2P_{ex}/dz^2 can be neglected.

Of course, elastic moduli of porous media differ considerably under drained and undrained conditions; in drained mode the porous system is more deformable.

If we convert the diffusion equation into a dimensionless form, a useful parameter, defining response mode of the aquifer can be obtained, i.e. the Fourier number N_{Fo}:

$$N_{Fo} = \frac{S_s L^2 / K}{t_e} = \frac{T^*}{t_e} \qquad (3)$$

Here $T^* = S_sL^2/K$ is the time constant of a given aquifer and t_e is the characteristic time of a transient (or observation time), L^2 is some characteristic length, in this case aquifer thickness.

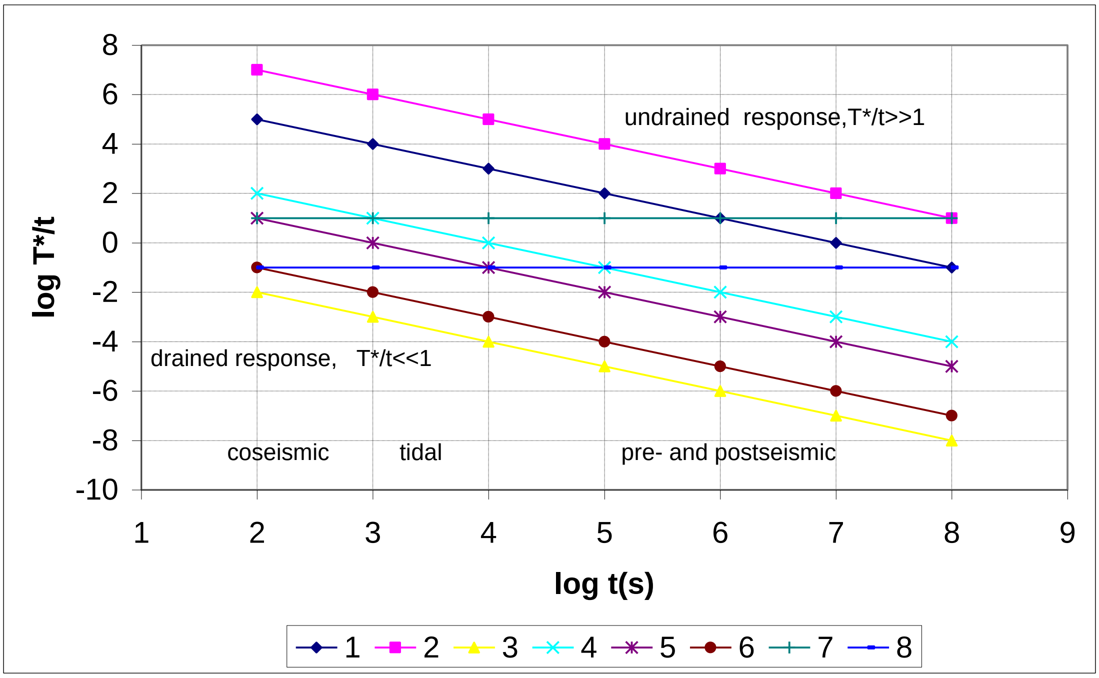

Fig.1. *Hydrodynamic Fourier number* $N_{Fo} = (S_sL^2/K)/t_e = T^*/t_e$ *versus characteristic time of transient (or observation interval)* t_e *for various* S_sL^2/K *ratios:*
1- $K = 10^{-8}$ *m/s;* $L^2S_s = 10^{-1}$*m; 2 -* $K = 10^{-10}$ *m/s;* $L^2S_s = 10^{-1}$*m; 3 -* $K = 10^{-8}$ *m/s;* $L^2S_s = 10^{-4}$*m;*
4 - $K = 10^{-4}$ *m/s;* $L^2S_s = 10^{-1}$*m; 5 -* $K = 10^{-2}$ *m/s;* $L^2S_s = 10^{-1}$*m; 6 -* $K = 10^{-4}$ *m/s;* $L^2S_s = 10^{-4}$*m;*

Large Fourier numbers N_{Fo} correspond to the undrained response; that means that all transients with $T^*>10t_e$ can be recorded. At small Fourier numbers $N_{Fo}<0.1$ or $T^*<10t_e$ the respond is drained, which means that transients, generated by fluid flow will be observable in a drained mode. So, depending on (local) aquifer properties the well can be selectively sensitive to co-seismic (t_e from 10 to 1000 s), tidal (t_e from 10^3 to 10^6 s), air pressure or pre- and post-seismic transient strain signals (t_e from 10^6 to 10^9 s and more).

The plot of "thermal" Fourier number N_{FoT} is identical with N_{Fo} at the condition $S_{sT}/c = S_s$.

All transients with t_e much less than T^* can be recorded by monitoring, but if the characteristic time of a basin T^* is much less than t_e, than the transient will not be observable, because the medium relaxes very fast.

It is evident that on the conceptual level time-dependence of hydraulic and microtemperature responses can be explained by the above theory. Therefore, a different response to coseismic (minutes), tidal (hours and days) or pre- and post-seismic (months and years) processes can be expected.

The plot of N_{Fo} versus characteristic time t_e for various values of S_sL^2, that is, for various time constants of a basin is shown in Fig. 1. The plot allows to predict the probable mode of response of a given aquifer to the impacts of various duration (Fig. 1). For highly permeable rocks ($K < 10^{-2}$ m/s), the coseismic impact (t_e of order of 10^2-10^3 s) N_{Fo} is very small, if the basin parameter S_sL^2 is of the order of 10^{-4}-10^{-5} m (which corresponds to L = 10 m, S_s= 10^{-6} m). Because $N_{Fo}$is small we have to expect drained response in hydraulics and microtemperature, i.e. the coseismic signal will not be steadily observable.

The same can be said on the tidal impact (t_e of order of 10^{-5} s), as well as on pre- and post-seismic signals (t_e = 10^{-6}-10^{-7} s).

In rocks of a permeability of K = 10^{-8} m/s, coseismic and tidal transients will be steadily observable, whereas slow pre- and post-seismic processes are observable in drained mode.

Only in tight rocks (K = 10^{-10} m/s) all three effects are steadily observable in unrelaxed mode for S_sL^2 = 10^{-4}-10^{-5} m.

If we consider an aquifer with basin parameters of S_sL^2 = 10^{-1} m (e.g. L =100 m, S_s = 10^{-5}m) the highly permeable rocks of K = 10^{-2} m/s again seem to be unfavorable for observation of all three transients in undrained mode, but at K = 10^{-8} m/s all of them are observable.

Values of hydraulic conductivity, favoring undrained response, seem to be too high, but in these calculations the porous formation was presumed as homogeneous. Real aquifer can be composed by layers of various hydraulic conductivity, or the porous space can be fractal (Sahimi, 1994); in these cases the channels of lowest permeability may limit the rate of (vertical) fluid flow.

It should be stressed that even in drained regimes the long pulse-like excitation can be observed at initial stage of response before pore fluid attains its drained equilibrium state.

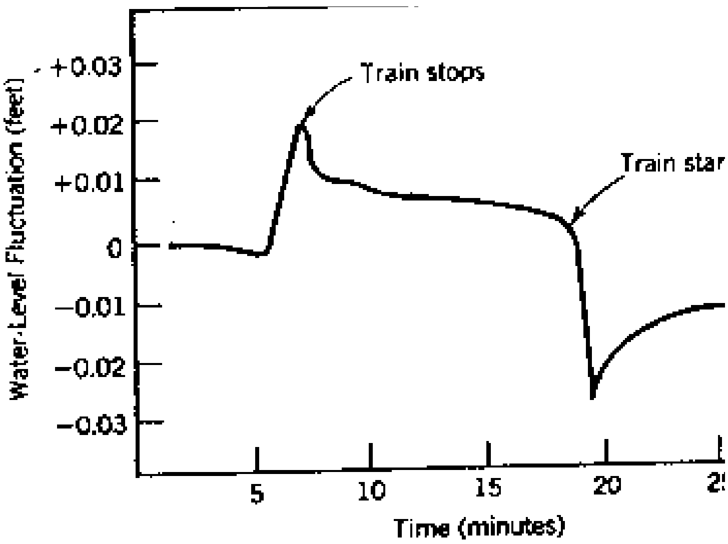

Fig. 2. Water level response to train passing close to a well

The spikes in water level immediately after arrival and departure of a train are transient undrained contributions to the response; the transients decay soon, giving way to the dominant drained contribution.

In the above analysis it was supposed that the deformation is reversible and the impact is transient, which means that the system regains its undrained elastic moduliafter distortion. If the mechanical impact lasts long enough like tectonic strain, even in reversible systems the largest portion of response reflects drained modules, which equals that the resulting “drained” strain should be maximal. Thus, in principle, the response to tectonic strain should be stronger than for short-living perturbation. In real systems, the strain time history can be more complicated(Fig.2); this can be connected with additional factors (saturation state, gas component, nonlinear response, etc.).

Underground water temperatureresponse to seismic/tectonic transients. The above analysis was related mainly to the hydraulic response. Therefore the question arises whether it is directly applicable to the thermal one? In relation to the atmospheric pressure the responses are very similar: both microtemperatures and water level are in a negative correlation with atmospheric pressure. Thus, the above analysis seems to be applicable at least qualitatively, to microtemperatures. A quantitative analysis should be founded on the solution of the heat conduction Equation with mass transfer, which is in the one-dimensional form:

$$\frac{k_e}{\rho' c'}\frac{\partial^2 T}{\partial z^2} - v_z \frac{\Phi \rho_w c_w}{\rho' c'}\frac{\partial T}{\partial z} = \frac{\partial T}{\partial t} \qquad (4)$$

wherek_e is the effective thermal conductivity for porous system with moving water

$k_e = \Phi k_w + (1-\Phi)k_s + c v_z$

k_w and $k_s$are water and solid thermal conductivities, $\rho' c'$ is the effective heat capacity for the unit volume

$\rho' c' = n\rho_w c_w + (1-\Phi)\, \rho_s c_s$

c_w and$c_s$are water and solid specific heat capacities respectively, and v_z is the mean ground water velocity in z direction, c is proportionality factor. A simplest, linear dependence of k_e on v_z is assumed. As a rule, quantity v_z in Equ. (14) is considered as Darcy velocity (Domenico, Schwartz, 1994); combination of Darcy Equation with Equation (14) allows to model a thermal transient, which is connected with tectonic/seismic perturbations. It has to be noted that regional flow is a slow carrier of thermal perturbation; its velocity is 10^{-4}-10^{-5} m/s or less. It follows that this approach can be successfully applied to the modelling of the decay phase of co-, pre and post-seismic phase in the earthquake source area when the forced convection, generated by elastic pulse, comes to an end. The build-up (coseismic) phase of signals themselves call for another explanation, because their velocity is not less than 0.2 km/s. Presumably, the build-up phase of strain-related thermal signal results from some of elastic perturbation of medium by an elastic pulse, such as seismic wave, dislocation, plastic or deformation wave, Biot's slow wave, etc. The pulse disturbs the hydraulic and thermal stability of the borehole liquid through mixing of fluids with different temperatures. The analysis of this case can be founded on the solution of the heat equation when the source moves with velocity v_z much larger than the Darcy velocity of regional flow (forced convection).

A further model of fast heat transfer is based on analysis of losses caused by the friction on the solid-liquid interface in porous rocks. Friction generates heat during passing of seismic waves through the borehole area.

In both models the thermal anomaly appears "instantly" after the earthquake or generally after elastic displacement, but relaxation to the stable state will be slow, as the system is driven by conduction and slow convection only.

Dimensionless Eq.(14) reveals, like in the case of hydraulics, some controlling parameters of thermal process, i.e. the Peclet number

$$N_{pe} = (\Phi \rho_w c_w v_z L)/\kappa_e \qquad (5)$$

(process is dominated by convection at $N_{Pe} >> 1$), and Fourier number for heat diffusion

$$N_{FoT} = (L^2 \rho' c' / \kappa_e)/t_e = (L^2 S_{sT}/k_e)/t_e = T_t{}^*/t_e \qquad (6)$$

where$S_{sT} = \rho' c'$ can be defined as a "thermal specific storage". The effective thermal conductivity includes also the effect of fluid motion and in this case it is dominated by the convective term.

Plots, similar to Fig.3 can be drawn, using typical values of $\rho' c'$ for rocks. The hydraulic and thermal time response coincide at $S_{sT}/c = S_{sT}$.
Using this formalism we calculate N_{FoT} for various values of governing parameters c, v_z and L (Fig. 3), assuming typical values of thermal parameters of rock components:
$c_w = 1$ cal/g °C; $\rho_w = 1$g/cm^2; $c_s = 0.2$ cal/g °C; $\rho_s = 2.5$ g/cm^3 ; $n = 0.1$.

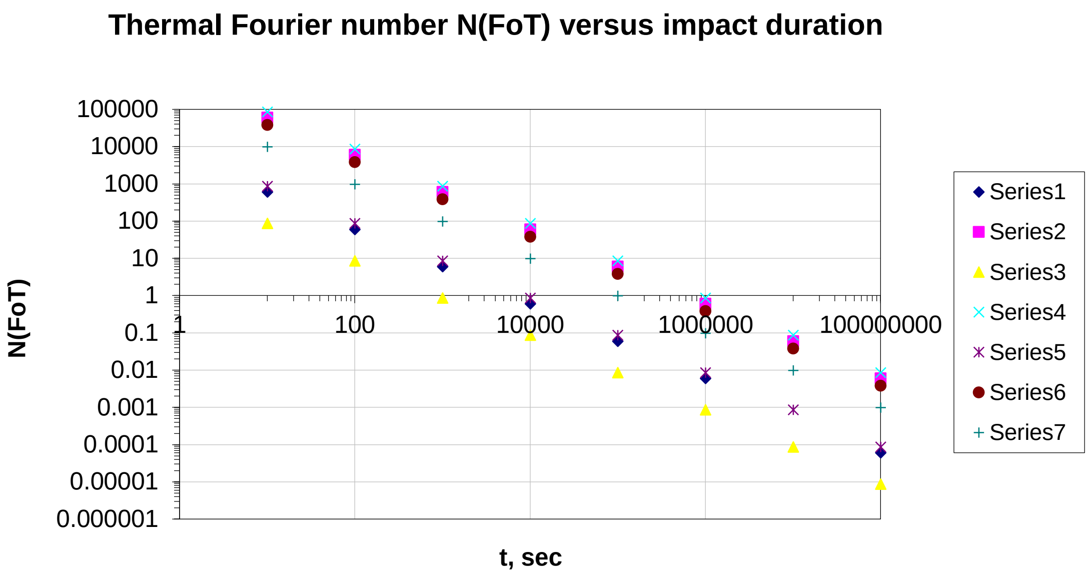

Fig. 3. Thermal Fourier number for heat transfer N_{FoT} versus characteristic time of thermal transient t_e :
1 – c = 10 cal/cm^2, v_z = 1 cm/s, L = 10^3 cm, λ = 170;
2 – c = 10 cal/cm^2, v_z = 1 cm/s, L = 10^4 cm, λ = 170;
3 – c = 10^{3}cal/cm^2, v_z = 1 cm/s, L = 10^3 cm, λ = 1164;
4 - c = 10^{3}cal/cm^2, v_z = 1 cm/s, L = 10^4 cm, λ = 1164;
5 - c = 10^{3}cal/cm^2, v_z = 10^{-3} cm/s, L = 10^4 cm, λ = 1164;
6 –c = 1.0 cal/cm^2, v = 100 cm/s, L = 10^4 cm, λ = 38 000;
7 – c = 1.0 cal/cm^2, v = 100 cm/s, L = 10^{3}cm, λ = 98.

The ratio $k_e/\rho' c'$ in (6) of units L^2/T is referred to as the thermal dispersivityλ ; it includes influence of moving fluid, which is so important in strain-related microthermometry. Thermal dispersivity reduces to thermal diffusivity, if the fluid is resting. Thermal Fourier number, like its hydraulic analogue, allows understanding the response of the formation to thermal transients. The conclusion can be drawn that thermal transients with $L^2/\lambda \ll 1$ are not observable; in other words, observation ofshort thermal transients is favored by large thickness of aquifer and large velocity of moving water.

It seems that in principle hydraulic and thermal decay phases can differ significantly due to inertia of thermal perturbation. If in the build-up phase the thermal relaxation time of the system is governed by thermal dispersion, in the decay phase, at $v_z = 0$, the heat is dissipated by thermal diffusion. Thus, thermal anomaly can persist even when the pressure transient has gone.

Hydro-seismic response to tides and wave-trains of remote strong earthquakes. The tidal response of water level (WL) in boreholesis well known; its intensity depends mainly on the aquifer properties. The strain-sensitivity of a given well is calculated as ratio of WL change to tidal impact, expressed in units of displacements or stresses (Table 1).

Generally, the reaction of the underground water (Wang et al, 2009; Zhang, Huang, 2011; Wang, Manga, 2010), WL responds to the EQ wave trains' impact depends on the distance of the well to the ruptured fault: i. Very close to the fault intensive shaking may increase opening of fractures, i.e. it cause rock dilatation and consequently, WL dropdown; ii. Outside this zone, but still very close to the fault shaking can consolidate loose sediments causing sudden upraise of WL; iii. In the intermediate field both positive and negative signs of sustained WL change are observed, which are explained by permeability changes; iv. Lastly, in the far field (which is our case) mainly correlated with seismic wave oscillations of WL are observed (hydroseismograms), sometimes accompanied with sustained WL change. As the seismic impact is close to instantaneous, it is expected that pore water has no time to displace, which in turn means that the WL response is undrained (Wang, Manga, 2010).

Below we present the observation data on hydro-seismic response to tidal strains and wave-trains of remote strong earthquakes recorded by the hydrogeodynamic network of deep wells of the M. Nodia Institute of Geophysics.

Table. 1. Reactions to tidal strain on the water level WL the various boreholes of network.

Name	water level (kPa)	tidal (kPa)	Response (%)	Date
Axalakalki			no	
Ajameti	0.66841	3.6247	18.4	22.01.2016
Kobuleti	0.47743	3.4204	14.0	06.02.2016
Lagodexi	0.46481	3.9388	11.8	11.01.2016
Marneuli	0.71401	3.9549	18.1	11.01.2016
Oni			no	
Gori	0.30677	3.9228	7.8	11.01.2016
Nakalakevi	0.51188	3.9223	13.1	11.01.2016
Borjomi70	1.5125	3.6395	41.6	19.08.2013
BorjomiPark	0.1962	3.3492	5.9	22.08.2013
Borjomi47	1.1473	3.5874	32.0	29.05.2014

Responseis calculated as a ratio of WL stress (KPa) to the theoretical value of the tidal stress (KPa) in percents. “no”means absence of tidal reaction. The ratio is time dependent, so the calculated values are characteristic for corresponding dates.

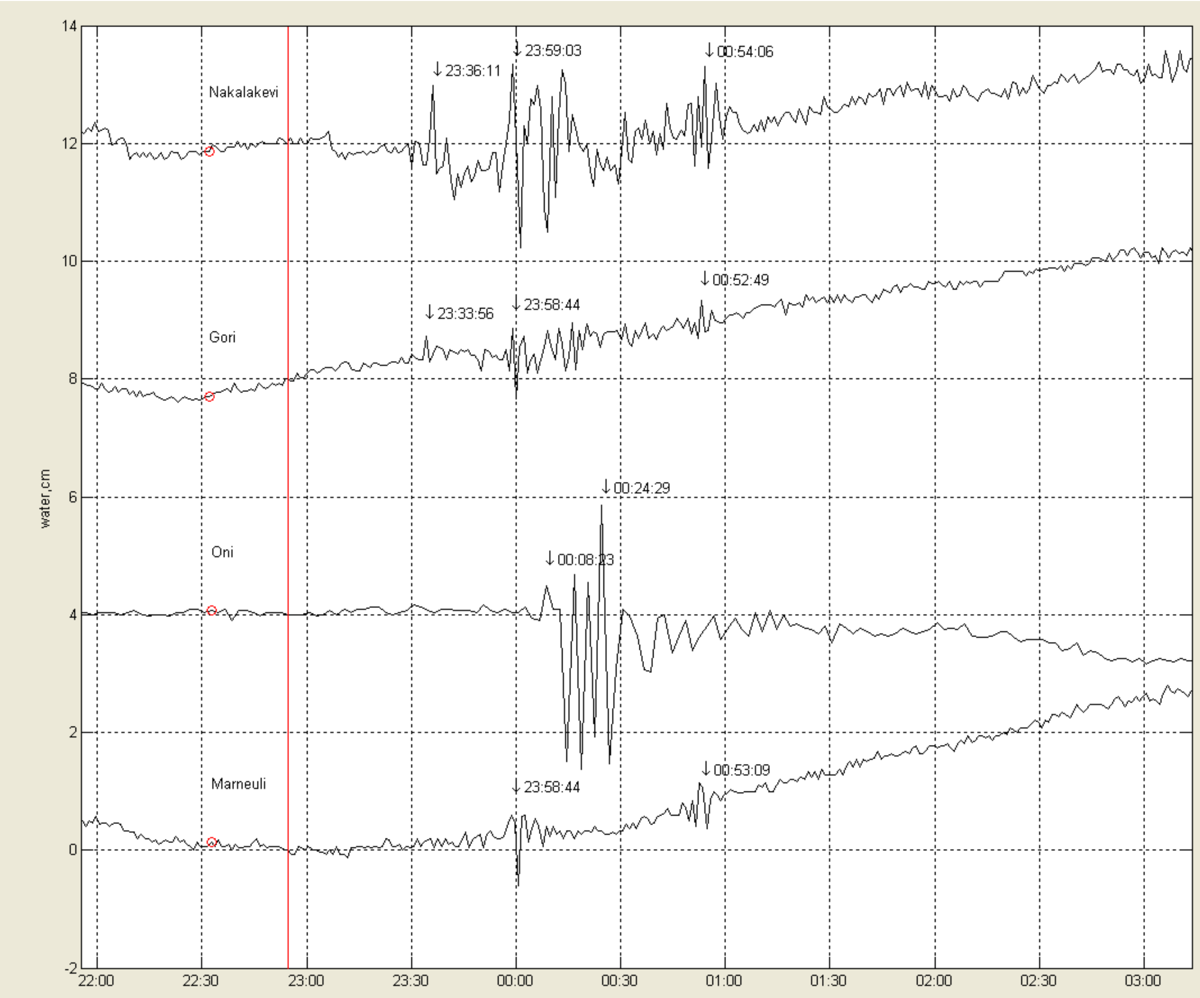

Fig. 4. WL oscillations due to passage of wave-trains of the Chile earthquake 16-09-2015,time:22:54,M8.3.Reactions successively from top to bottom in: Nakalakevi, Gori, Oni,Marneuli.

Fig. 4 shows that WL in the network of wells responses to the passage of seismic waves (here – mainly to direct and multiple Rayleigh waves). This seems to contradict the common knowledge that due to relatively short duration of seismic oscillation the groundwater regime should be undrained, i.e. the WL in the borehole should not change during seismic wave passage: the data of Fig.4 testify against this model. The explanation of synchronous oscillation of WL with fast seismic vibrations should take into consideration, that even in the undrained regime small-scale water displacement in the wellis observed (Fig.4). This effectis connected not with a pore water diffusion in the aquifer (slow flow, Eq.1), but with direct mechanical squeezing of fluid from the porous media, surrounding the well,by the passing seismic wave (Dvorkin, Nur, 1993): this we can call instantaneous flow. In this case again *p*-waves, though compressive, are less effective in generation of WL oscillations. It seems that the most effective impact on the WL manifest Raileigh waves; then follow Love and *s*-waves. Thus, in the instantaneous flow also should be some time constant of the order of dozens of sec for mechanical vibrations to be effective generators of WL oscillations.

Conclusions

We considered theoretical models of underground water level/temperatureresponse to seismic/tectonic transients taking into account effects of poroelasticity (Biot model): we show that the response intensity depends on the Hydrodynamic Fourier number in case of water level change and on the Thermal Fourier number in case of temperature response. Calculations manifest that response depends strongly on the characteristic time of hydraulic/thermal transient.

Besides, a direct mechanical squeezing of pore water by seismic vibrations (instantaneous flow) is considered.

References.

Biot, M. A. 1962. Mechanics of deformation and acoustic propagation in porous media, *J. Appl. Phys*., 33, 1482 – 1498.

Blanchard, P. and Byerly P. (1935). A study of well gage as a seismograph. Bull. Seismol.Soc. Amer., 25, 313-321.

Bredehoeft (1967). Response of well-aquifer system to Earth tides. J.Geophys. Res.72, 3075-3087.

Brodsky, E., Roeloffs, E., Woodcock, D., Gall, I., & Manga, M. 2003. A mechanism for sustained groundwater pressure changes induced by distant earthquakes. *J. Geophys. Res.* 108, B8, 2390, doi:10.1029/2002JB002321,

Costain, J. &Bollinger, J. 2010. Review: Research results in Hydroseismicity from 1987 to 2009. *Bull. Seismol. Soc. Am*. 100, 1841-1858, doi: 10.1785/0120090288.

Domenico P. and Schwartz F. (1990), Physical and Chemical Hydrogeology.
J. Wiley&Sons.

Dvorkin, J., Nur, A. 1993. Dynamic poroelasticity: a unified model with the squirt and the Biotmechanisms. *Geophysics*, 58, 524-533.

Wang, C.-Y., Chia, Y, Wang, P-L., &Dreger, D. 2009. Role of S waves and Love waves in coseismic permeability enhancement. *Geophys. Res. Lett.* 36, L09404, doi:10.1029/2009GL037330.

Wang, C.-Y., &Manga, M. 2010. *Earthquakes and Water*. Springer-Verlag Berlin, Heidelberg.

Zhang, Y. &Huang, F. 2011. Mechanism of Different Coseismic Water-Level Changes in Wells with similar Epicentral Distances in Intermediate Field. *Bull. Seis. Soc. America*, 101, 1

Blanchard, P. and Byerly P. (1935). A study of well gage as a seismograph. Bull. Seismol.Soc. Amer., 25, 313-321.

Bredehoeft (1967). Response of well-aquifer system to Earth tides. J.Geophys. Res.72, 3075-3087.

Meinzer, O. (1939). Groundwater in United States: US Geol. Survey, Water Supply Papers, 628C, pp. 94-144.

Jakob C.E. (1939) Fluctuations in artesian pressure produced by passing railroad trains as shown in a water level on Long Island, New York. Trans. Amer. Geophys. Union, 20, 666-674.

Palciauskas, V. and Domenico, P. (1989). Fluid pressures in deforming porous rocks. Water Res. Research, 25, 203-213.

Roeloffs E. (1988). Hydrologic precursors to earthquakes: a review. Pure and Appl. Geophys. 126, 177-206.

მიწისქვეშა წყლების დონის/ტემპერატურის რეაქცია სეისმურ და ტექტონიკურ გარდამავალ ზემოქმედებაზე: ფოროელასტიურობის ეფექტები.

თამაზ ჭელიძე

რეზიუმე

ზედა ქერქი დაახლოებით 20 კმ სიღრმემდე წარმნოადგენს ფოროვან ან დაბზარულ ფლუიდით გაჯერებულ დეფორმადი ფენების მიმდევრობას. სხვადასხვა ხანდრძლივობის და ინტენსივობის გარდამავალი დაძაბულობები იწვევს ამ სისტემაში

ფლუიდის ჭარბ ასევე გარდამავალ ფოროვან წნევას, რაც პრაქტიკულად დაიკვირტვება ჭაბურღილებში წყლის დონის ცვლილებასა და ოსცილაციებში. სტატიაში მოცემულია მიწიქვეშა წყლების სეისმურ/ტექტონიკურ გარდამავალ ზემოქმედებებზე რეაქციის ელემენტარული თეორიული მოდელი ფოროელასტიურობის ეფექტების გათვალისწინებით (ბიო-ს მოდელი). გარადა ამისა, განხილულია ფოროვანი სითხის პირდაპირი მექანიკური გამოდევნება სეისმური ვიბრაციებით (წამიერი დინება).

РЕАКЦИЯ УРОВНЯ ПОДЗЕМНЫХ ВОД /ТЕМПЕРАТУРЫ НА ПЕРЕХОДНЫЕ СЕЙСМИЧЕСКИЕ И ТЕКТОНИЧЕСКИЕ ВОЗДЕЙСТВИЯ: ПОРОУПРУГИЕ ЭФФЕКТЫ

ЧЕЛИДЗЕ Т.Л.

Реферат

Верхняя кора приблизительно до глубины 20 км представляет собою последовательность пористых или трещиноватых, подвергнутых деформации пород, насыщенных флюидом. Переходные напряженности разной длительности и интенсивности в этой системе вызывают избыточное, также переходное, поровое давление флюида, что, пректически, наблюдается в скважинах, как изменение уровня воды и ее осциляциях. В статье дана элементарная теоретическая модель реакции на сейсмические/ тектонические переходные воздействия на состояние подземных вод с учетом эффекта пороупругости (Модель Био). Кроме того, рассмотрено прямое механическое выжатие пористой жидкости сейсмическими выбрациями (Мгновенное течение).

Journal of Georgian Geophysical Society,
Issue(A), Physics of Solid Earth, v.19a, 2016, pp. 58-65

Laboratory modeling of landslide and seismic processes triggering

Nodar Varamashvili, Tamaz Chelidze, Dimitri Amilakhvari, Levan Dvali

Abstract

The modern concept of seismic and landslide processes relays mainly on the model of frictional instability. Simple models of mass movement and seismic processes are important for understanding the mechanisms for their observed behavior. In the present paper, we analyze the dynamics of a single-block and Burridge-Knopoff model on horizontal and inclined slope. We investigated stick-slip process: triggering of instabilities by recording acoustic emission, accompanying the slip events. Also acceleration was recorded on each sliding plate using attached accelerometer. In the case of the inclined slope experimental model, a seismic vibrator, which produces low frequency impact (forcing) was attached to the sliding or/and immovable plate. We can impose an external periodical mechanical loading to sliding plate and at several points of fixed plate individually or together. Simple landslide model triggering effect is depend on inclination angle, numbers of vibrators, distribution and triggering signal amplitude

Introduction

In the last years it has been shown that the triggering of dynamic events by weak external forcing is ubiquitous and is observed in biological systems, lasers, electronic networks, etc. The aim of the study was modeling landslides and landslides' triggering processes. For many countries around the world landslides are one the most severe of all natural disasters, with large humanitarian and economic losses. The earth surface is not static, but dynamic system and landforms change over time as a result of weathering and surface processes (i.e., erosion, sediment transport and deposition). The fast mass-movement has a potential to cause significant harm to population and civil engineering projects. Large-scale experiments and field observations show that the landslide may reveal stick-slip motion [Helmstetter et al., 2004; Fabio Vittorio De Blasio, 2011]. Analysis of the experimental data, obtained by investigating of spring-slider system motion has lead to empirical law, named rate- and state-dependent friction law [Dieterich 1979, Ruina 1983].

To study the stick-slip process, a mathematical model, proposed by Burridge-Knopoff is also used [Burridge R. and Knopoff L. 1967; Erickson et al., 2010, Matsukawa, H., Saito, T., 2007] (Fig.1). Plates are arranged on a massive platform and pulled by the upper platform. The upper plate moves with a constant loading velocity *v*. The blocks of mass *m* are connected to the upper plate by linear springs with spring constant k_p. The blocks are also connected to each other by linear springs with springs of natural length *a* and the constant k_c. Frictional force acts between the lower plate and each block.

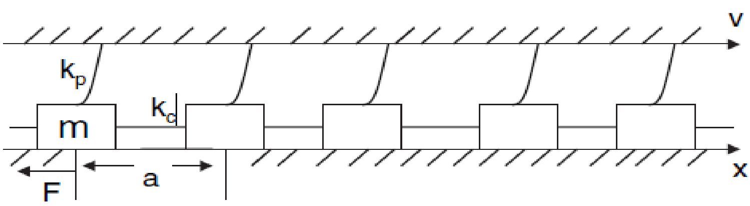

Fig.1. The schematic presentation of Burridge-Knopoff model

The Burridge-Knopoff model is convenient, as it allows us to simulate many scenarios of rupture without being too expensive in regard to computing time. Thus we have the ability to explore the parameter space of the system more broadly and observe the emergent dynamics introduced by the friction law.

Experimental setup

Experiments were conducted on a Burridge-Knopoff laboratory device for the models consisting of one, two or three basalt plates (Fig.2). Registration was made with the help of accelerometers and piezo sensors. In one plate model three accelerometers were attached on the sliding plate, which recorded x, y and z components. Plates were pulled via the upper platform. The experiments were also conducted for the model of the three plates. To each plate was attached one accelerometer, which measures the x component of the acceleration. Was also recorded the pulling force, using fabricated in our laboratory sensor (dynamometer). Accelerations, acoustic emissions and pulling force recording are presented in Figure 3. Mass of the each sliding plate $\approx 335\, g$, spring constants $k_c \approx 360 \frac{N}{m}$ and $k_p \approx 155 \frac{N}{m}$. Dragging velocity was $v \approx 1\, mm/s$.

Fig.2. The Burridge-Knopoff experiments with accelerations, acoustic emissions and pulling force registration (with clean surfaces of plates and with a layer of sand between the plates)

Burridge-Knopoff stick-slip experiments were conducted for the horizontal position of fixed and sliding plates with clean surfaces and with a layer of sand between the sliding plates (Figure 3 b, c). The information was recorded on a 8-channel PicoScope 4824.

a)

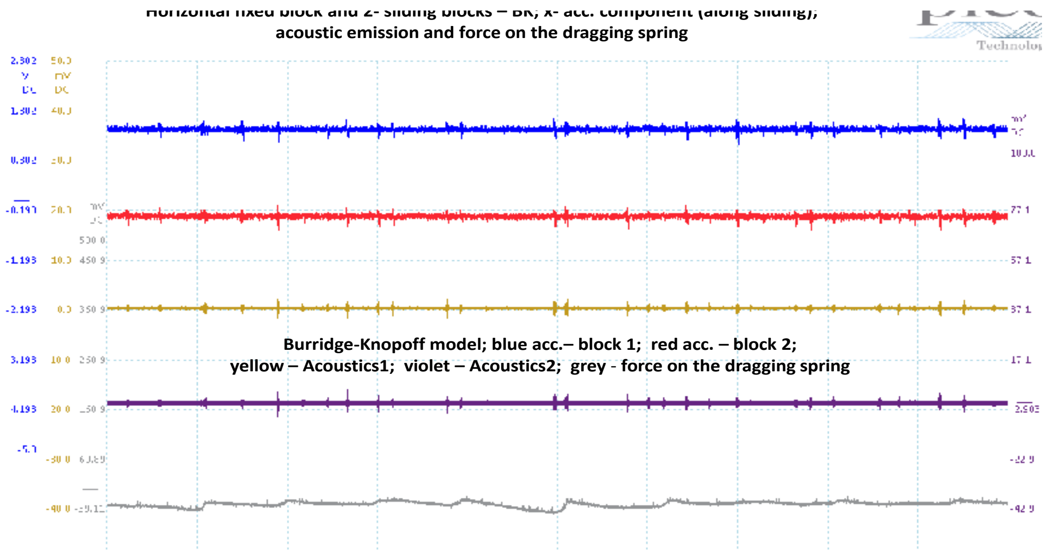

b)

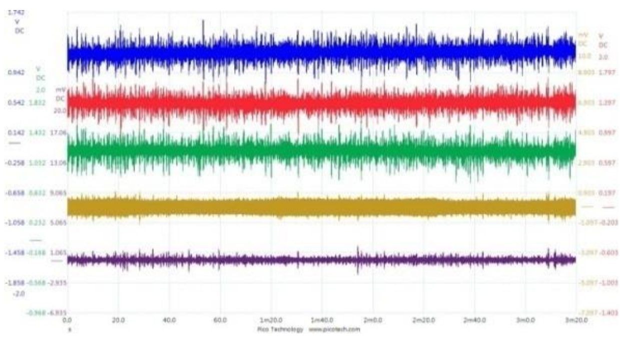

c)

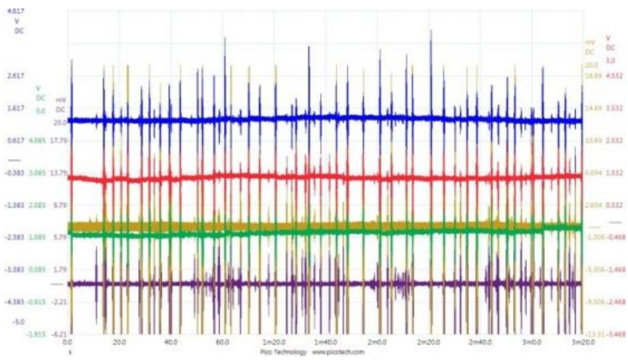

Fig.3. The Burridge-Knopoff experiments accelerometers, acoustic emission and pulling force data recordings: blue and red curve – acceleration, yellow and violet acoustic emission and grey – pulling force.

To study the phenomena of stick-slip and triggering of Burridge-Knopoff model under the influence of gravitational forces we collected laboratory equipment with an inclined and horizontal plane (Figure 6). These settings may help to learn the process of landslide stick-slip motion triggering under different conditions on the sliding surface between basalt plates and under the influence of gravitational forces. The acoustic emission and acceleration arising during sliding of upper plate was recorded. To this goal piezo sensors were attached to the upper and lower corners of the large (fixed) plate and accelerometer were attached to the sliding plate. At the critical angle of inclination of the system triggering forcing was applied by a seismic vibrator attached to the sliding or on the fixed (immovable) plate. On the fixed plate we have 8 seismic vibrator attached. Seismic vibrators can have any configuration. The information was recorded on a 8-channel PicoScope. In experiments the inclination slope of boards was measured.

Fig. 4. Laboratory model for series of Burridge-Knopoff experiments under the influence of gravitational forces. Middle figure shows the seismic vibrator attached to the sliding plate.

Experimental results for one- and three plate models under the influence of gravitational force are presented in Fig.7. The critical angle of slip is different for one- and three plate models. Triggering of sliding close to the critical slope, but still stable, is triggered by a seismic vibrator. Namely, the system was left close to the critical angle for 45 minutes. Then, to the attached seismic vibrator a forcing of 20 Hz frequency and 1.6 V intensity was applied. The information was recorded on a 8-channel PicoScope. As can be seen from Fig.7 during the experiment several intermediate slips took place. The beginning of sliding of system of plates was caused by influence of the seismic vibrator. The seismic vibrator played the role of a trigger in slip.

a)

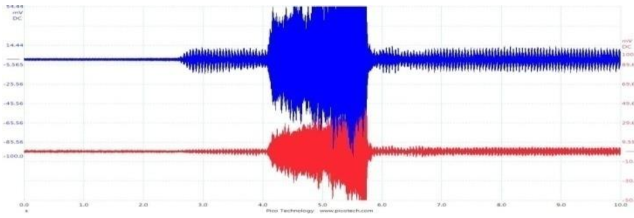

b)

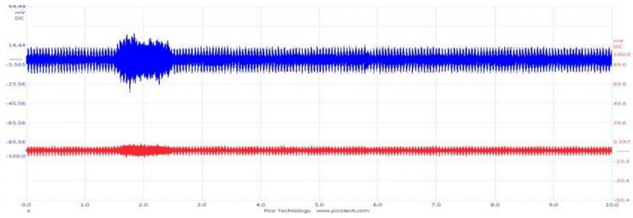

c)

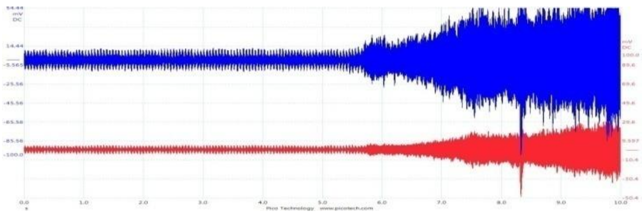

d)

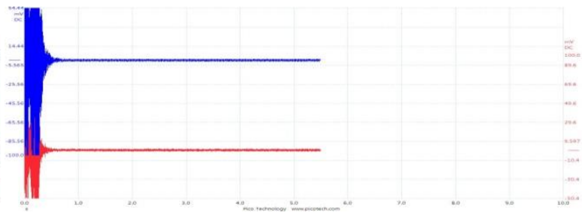

Fig.5. a) The record the acoustic emission occurred on the one-plate model, b), c), d) record the acoustic emission, when sliding occurred on three-plate model.

We carried out experiments on the inclined plane. Periodic external impact is applied to fixed (immovable) plate. Forcing performs seismic vibrators. For the external influence we arrange 6 different points on the external surface and 2 points on the rear surface of the fixed plate. We carried out experiments on the impact, applied at different points of the fixed plate and also in the some cases, on the standby time at the critical angle of the sliding.

a) b) c)

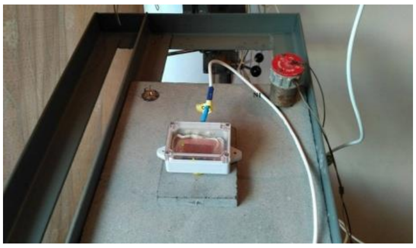

d) e) f)



g) h)


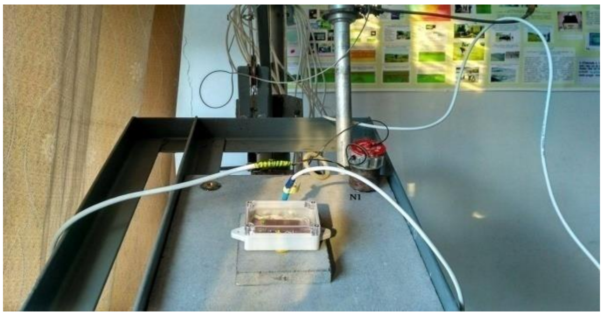

Fig.6. Triggering experiments on the inclined model. a.b.c.d.e.f.g.- seismic vibrator attached at different points. h. experiments by the other critical slip angle.

Experiments, presented in Fig.6 a., b., c., d., e., f., were carried out by attaching seismic vibrators on a upper surface of fixed plate at 6 different points. In all the experiments we changed frequency on seismic sensor in 1,2,3,4,5 Hz range. Maximal voltage ~8V.

In a), b), c), d) experiments the upper plate starts slipping at the frequency of 5 Hz, from1 to 2 minutes after the switching seismic vibrator on. The longer is kept the upper plate, the longer must operate a vibrator to start sliding. The tilt angle was 26.65°.

In e), f) experimentis seismic vibrator is placed far enough from the sliding plate position, therefore triggering period increased noticeably (5-10 minute range).

In g) experiments seismic vibrator attached to the back surface of the fixed plate could not trigger plate even after a few tens of minutes in some experiments. When we switch the vibrator to the c) or d) position slipping begins after 1-2 minutes.

a) b)

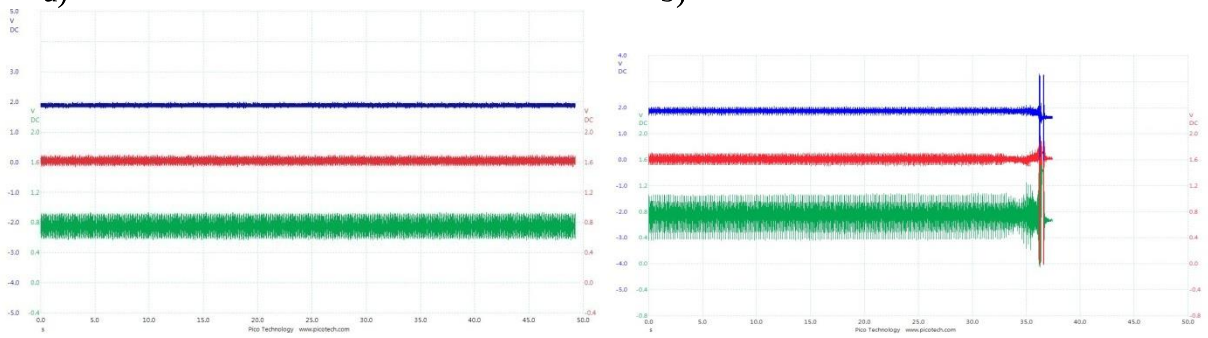

Fig. 7. Recordings of the accelerometer: a) seismic vibrator is placed on the outer surface of the fixed plate according to “d” condition; b) the seismic vibrator is placed on the rear surface of the fixed plate.

Figure 7 shows that when the vibrator is applied on the top and back surface of the fixed plate, different perturbation amplitude reach the accelerometer attached to the moving plate. As can be seen, high values disturbance causes in one case triggering sliding, in another case triggering is absent.

h) A few days later, when it the environment humidity and accordingly, the plate surface moisture was changed (increased), slip critical angle increased from 26.65° to 28.90°. Experiments results were fundamentally the same, but slipping critical angle, probably, due to the additional force of water surface tension between surface water on the fixed and sliding blocks, increased appreciably.

Conclusions

For each experiment we have files of large volume with records of accelerations and acoustic data. Data recording in a digital form was made at the sampling rate 2 kHz. First gravitational experiments taking into account a parking phase (prior to the impact of the seismic vibrator) proceeded about 50 minutes. In gravitational experiments duration of the parking phase under the external periodical influence depends on the location of the seismic vibrators, the frequency and amplitude of the periodic signal, sliding plate delay time, moisture of the sliding surfaces. The greater the distance from the vibrator to a sliding plate, the more activation time is needed for triggering slip. Along with the growth of the sliding plate delay time increases triggering time. By attaching seismic vibrator to the fixed plate rear surface triggering event does not occur at all. We guess, that by attaching seismic vibrator on the upper surface, we arise surface waves, which (as in the case of an earthquake) cause a sliding plate perturbation and triggering (slipping). By attaching seismic vibrator to the rear surface of the fixed plate, to the small plate reaches only weak perturbation (Fig 7), which can not cause slip triggering. Thus, more powerful impact (forcing) and relevant experiments are needed.

Acknowledgement: This work was supported by Shota Rustaveli National Science Foundation grant, FR/258/9-160/13, 2014

References

[1] Boettcher, M. S., and C. Marone, Effects of normal stress variation on the strength and stability of creeping faults,. J. Geophys. Res., 109, B03406, doi:10.1029/2003JB002824, 2004

[2] Fabio Vittorio De Blasio, Introduction to the Physics of Landslides, Springer, 2011

[3] A. Helmstetter, D. Sornette, J.-R. Grasso, J. V. Andersen, S. Gluzman, and V. Pisarenko, Slider block friction model for landslides: Application to Vaiont and La Clapie`re landslides, Journal of Geophysical Research, 109, 2004

[4] Dieterich, J.H. (1979), Modeling of rock friction 1. Experimental results and constitutive equations. Journal of Geophysical Research, **84, B5,** 2161-2168.
[5] Burridge R. and Knopoff L. 1967. Model and theoretical seismicity. Bulletin of the Seismological Society of America, 57(3): 341-371,
[6] Ruina A. 1983. Slip instability and state variable friction laws. Journal of Geophysical Research, 88, 10359-10370
[7] Chelidze T., N. Varamashvili, M. Devidze, Z. Chelidze, V. Chikhladze and T. Matcharashvili (2002), Laboratory study of electromagnetic initiation of slip. Annals of Geophysics, **45,** 587- 599
[8] Chelidze T., Gvelesiani A., Varamashvili N., Devidze M., Chikchladze V., Chelidze Z., and Elashvili M. 2004. Electrmagnetic initiation of slip: laboratory model. Acta Geophysica Polonica, 52, 49-62
[9] Chelidze T., Matcharashvili T., Gogiashvili J., Lursmanashvili O., and Devidze M. 2005. Phase synchronization of slip in laboratory slider system. Nonlinear Processes in Geophysics, 12, 163 – 170.
[10] Chelidze T., Lursmanashvili O. Matcharashvili T. Devidze M. 2006. Triggering and synchronization of stick slip: waiting times and frequency-energy distribution. Tectonophysics, 424, 139-155
[11] Nasuno S., Kudrolli A., Bak A., and Gollub J. P. 1998, Time-resolved studies of stick-slip friction in sheared granular layers. Phys. Rev. E 58, 2161–2171
[12] Matsukawa, H., Saito, T., Friction, Stick-Slip Motion and Earthquake, Lect. Notes Phys. 705, 169–189, 2007.
[13] Erickson B., Birnir B., Lavallee D., Periodicity, Chaos and Localization in a Burridge-Knopoff Model of an Earthquake with Dieterich-Ruina Friction, Center for Complex and Nonlinear Science, UC Santa Barbara, 2010, http://escholarship.org/uc/item/3r5811tp

მეწყრის და სეისმური პროცესის ტრიგერირების ლაბორატორიული მოდელირება

ნოდარ ვარამაშვილი, თამაზ ჭელიძე, დიმიტრი ამილახვარი, ლევან დვალი

რეზიუმე

სეისმური და მეწყრული პროცესების თანამედროვე კონცეფცია ძირითადად დაფუძნებულია არასტაბილური ხახუნის მოდელზე. მასების მოძრაობის და სეისმური პროცესების მარტივი მოდელები მნიშვნელოვან როლს თამაშობენ მათი მექანიზმების შესასწავლად. წარმოდგენილ სტატიაში ჩვენ ვაანალიზებთ, ჰორიზონტალურ და დახრილ სიბრტყეზე ზამბარა-ბლოკის და ბურიჯ-კნოპოვის მოდელის დინამიკას. ჩვენს ვიკვლევდით სტიკ-სლიპის პროცესს, არამდგრადობების ტრიგერირებას, სრიალის თანმხლები აკუსტიკური ემისიის ჩაწერის საშუალებით. ასევე ხდებოდა თითოეული მოსრიალე ბლოკის აჩქარების ჩაწერა აქსელერომეტრების საშუალებით. დახრილი ექსპერიმენტული მოდელის შემთხვევაში სეისმური ვიბრატორები, რომლებიც იძლევიან მცირე სიხშირის ზემოქმედების საშუალებას, მიმაგრებული იყო მოსრიალე და უძრავ ფილებზე. ჩვენ შეგვიძლია მოვდოთ გარეშე პერიოდული მექანიკური დატვირთვა მოსრიალე ფილაზე და/ან უძრავი ფილის რამდენიმე წერტილში ცალ-ცალკე ან ერთად. მეწყრის მარტივი მოდელის ტრიგერირების ეფექტი

დამოკიდებულია დახრის კუთხეზე, ვიბრატორების რაოდენობაზე, მათ განალაგებაზე და ტრიგერირების სიგნალის ამპლიტუდაზე.

Лабораторное моделирование тригерирования оползневых и сейсмических процессов

Нодар Варамашвили, Тамаз Челидзе, Димитри Амилахвари, Леван Двали

Резюме

Современная концепция сейсмических и оползневых процессов в основном связана с моделью нестабильного трения. Простые модели движения масс и сейсмических процессов имеют важное значение для понимания механизмов их наблюдаемого поведения. В настоящей работе мы анализируем динамику моделей пружина-блок и Бурриджа-Кнопова на горизонтальной и наклонной плоскости. Мы исследовали процесс стик-слип, тригерирование неустойчивостей путем записи акустической эмиссии, сопровождающие события скольжения. Также записывали ускорение каждой скользящей плиты с помощью прикрепленного к плите акселерометра. В случае наклонной экспериментальной модели сейсмические вибраторы, которые производят низкочастотное воздействие, были прикреплены к подвижному и неподвижному плитам. Мы можем наложить внешнюю периодическую механическую нагрузку, на подвижную и/или неподвижную плитам, в нескольких точках по отдельности или вместе. Эффект тригерирования простой модели оползня зависит от угла наклона, числа вибраторов, их распределения и амплитуды сигнала тригерирования.

Journal of Georgian Geophysical Society,
Issue (A), Physics of Solid Earth, v.19a, 2016б pp. 66-74

Seismic catalog for Georgia

N. Tsereteli[1], O. Varazanashvili[1], M. Kupradze[1], N. Kvavadze[1], Z. Gogoladze[1]
[1]M. Nodia Institute of geophysics of I. Javakhishvili Tbilisi State University

A homogeneous reliable earthquake catalog is very important in seismic hazard assessment. The accuracy of earthquake location calculation, also accuracy of magnitude estimation influence on delineation and parameterization of seismic sources. In this work, we summarize all our attempt to obtain modern earthquake catalog for Georgia

In this work, there are two main goals: 1) Drafting a new catalog of historical earthquakes of Georgia and 2) Compilation of new instrumental seismic catalog of Georgia. In the process of compiling the level of the magnitude completeness was limited to: $M_S \geq 2.9$ or $M_W \geq 4.0$.

Catalog of historical earthquakes

The methods of interpretation of macro seismic data about historical earthquakes include:

- Collection and systematization of the whole available information concerning each historical earthquake.
- Parameterization of historical earthquakes on the basis of equalizing the macroseismic field
- Restoration of historical earthquakes with pure macroseismic data by using isoseist models of earthquakes with different magnitudes, built for the territory of Georgia.
- Complex analysis of macroseismic, archeological, seismotectonic and other kinds of data

More detail information about this work are presented in Varazanashvili et al. (2011) [1]. Here we just mentioned that about 47 historical earthquakes were studied. After investigation of data, three earthquakes had to be excluded from consideration because of the uncertain input data. This directory improves the accuracy of determining the basic parameters of historical earthquakes.

The final parametric catalog for 44 historical earthquakes includes the date and the location of the epicenter, magnitude and depth of focus, intensity epicenter (Fig. 1).

Instrumental seismic catalog

The second main task of this work is to refine the catalogue of instrumental earthquakes from 1900 to the present (Fig. 2).

In the Caucasus instrumental seismological observations started in the beginning of XX century. The lack of the instrumental data, particularly for the first half of the last century requires systematic recalculation of magnitude and location of earthquakes from the beginning of instrumental period since 1900 till 1962. The revision of macroseismic data and creation of reliable macroseismic databases is one of the important tools to achieve succeed in this work.

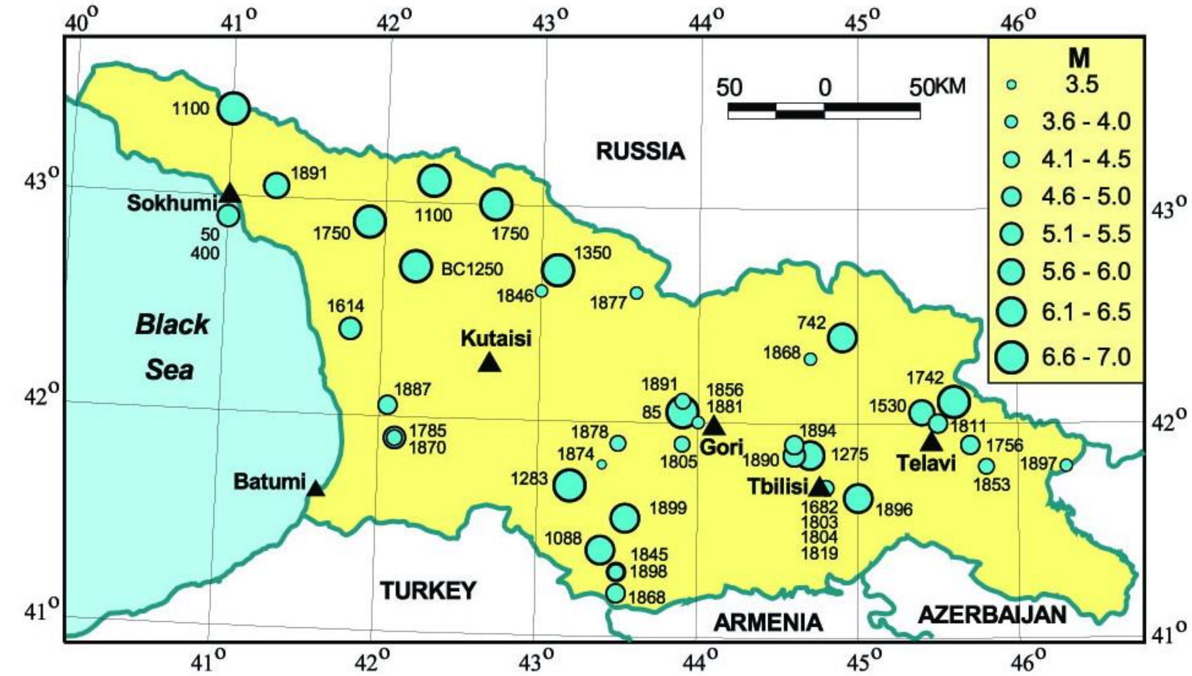

Fig. 1. Map of historical earthquakes (pre-1900) in Georgia.

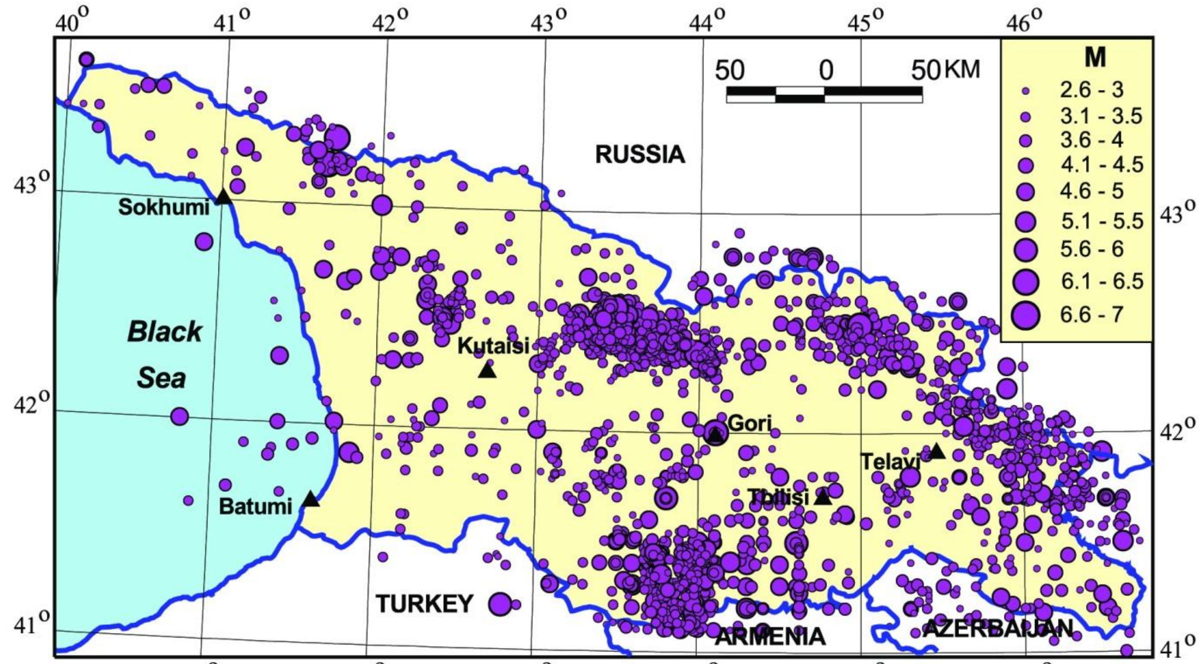

Fig.2. Map of instrumental earthquakes (1900-2009) in Georgia.

After 1962 the seismic network in the Caucasus and in Georgia began to improve, but inaccurate velocity models do not give good results. To reveal the best velocity model the hypocenter parameters of the earthquake were calculated, using the HYPO-71 program [2] for all existing velocity models of the Caucasus region, which were obtained by various geophysical methods [3, 4, 5, 6, 7]. The model obtained by the interpretation of the surface wave group velocity dispersion curves [8] gave a much higher accuracy in determining the hypocenters of earthquakes than the others. To be surer in our decision all velocity models were tested for explosions for which we directly know both the epicenter and the depth. Model [8] gives for explosions depth less than 2 kilometers, while others give depth more than 5 kilometers. The scatter of epicenter also was not high for this model. Thus we assume that the optimal crustal model consists of four layers (Table 1).

Table 1. Velocity model [8]

Layer thickness (km)	Vp (km/s)	Vp/Vs
0.0	4.2	1.71
4.0	5.5	
20.0	6.2	
30.0	6.9	
49.0	8.2	

During the period 1963-2002 for the territory of Georgia parameters of about 250 earthquakes were re-calculated. The difference between obtained and existing locations of individual earthquakes was sometimes more than 20 km (see Fig. 3, 4, 5).

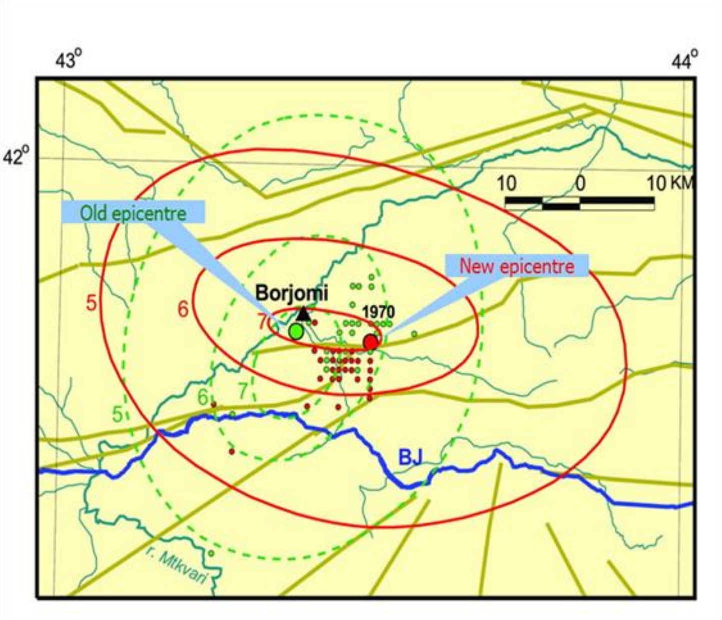

Fig. 3. Re-location of Borjomi earthquake, 1970.

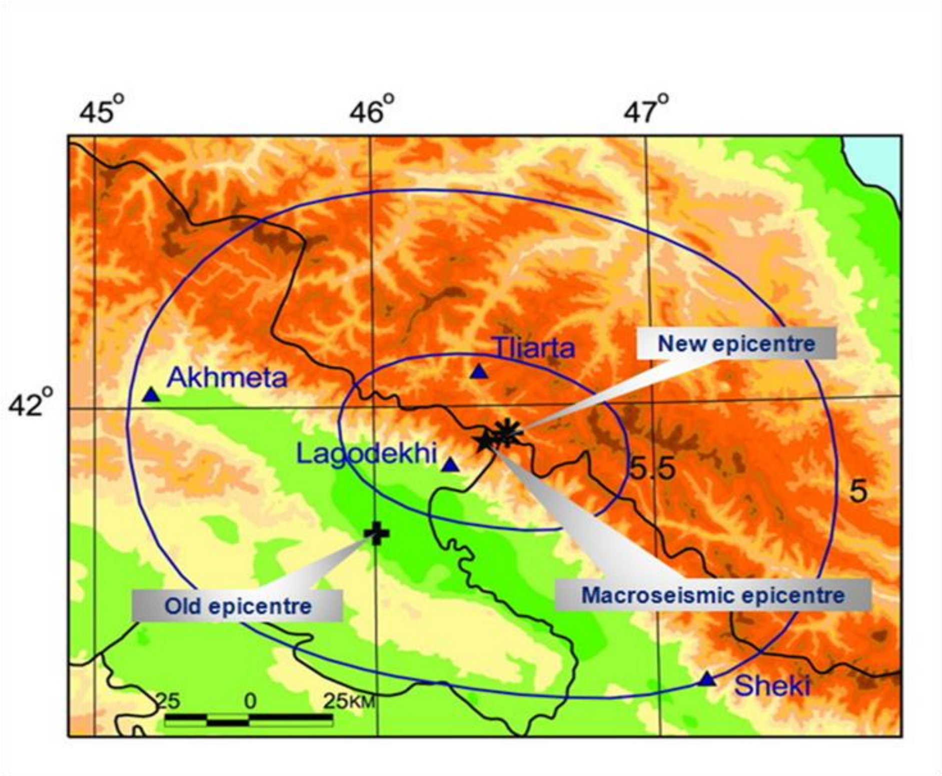

Fig. 4. Re-location of Tliarta earthquake, 1978.

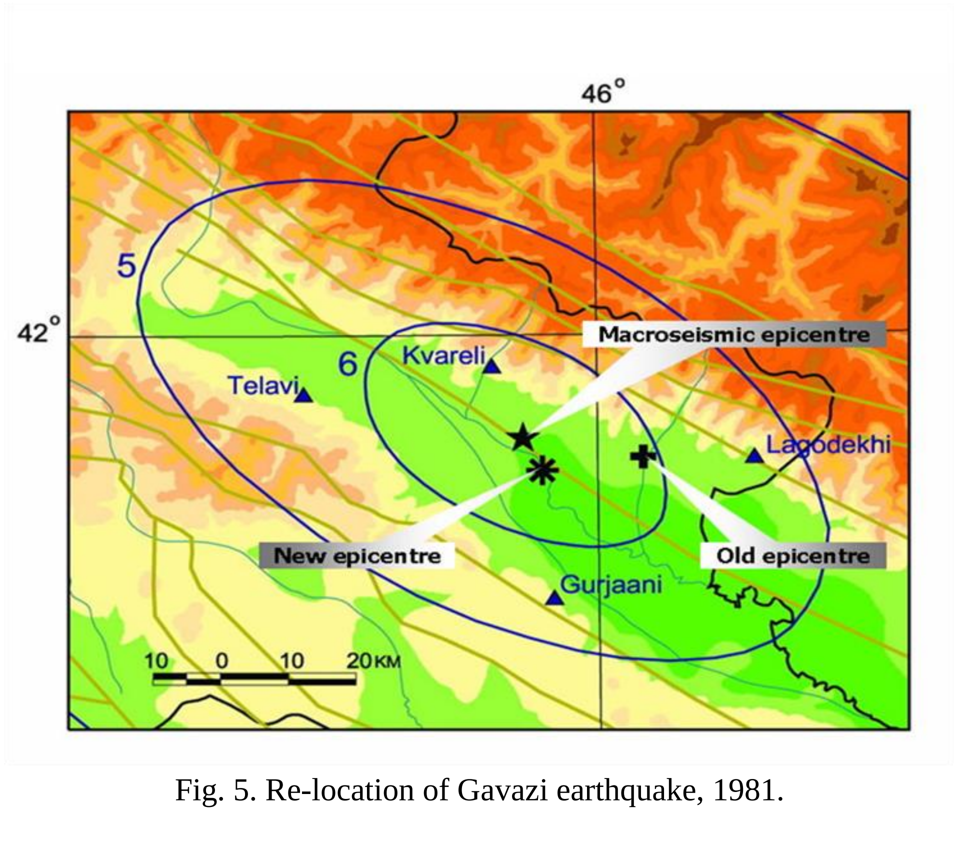

Fig. 5. Re-location of Gavazi earthquake, 1981.

In addition, it should be noted that in the catalog of earthquakes of Georgia magnitudes were categorized by surface waves (M_S). Since 1962 the accepted technique was to determine the energy class (K) of earthquakes, so in cases when the direct determination of the magnitude M_S was impossible, it was estimated mainly by the correlative dependence [9]:

$$K=1.8M_S+4$$

and sometimes following [10] we accept that $M_S \approx M_C$, where Mc is the magnitude estimated from the coda waves.

Since 2004, as a consequence of the reorganization of the network of seismic observation of Georgia, basically only local magnitude M_l was estimated for earthquakes and rarely magnitude M_d and M_b. In this case, the transition to the magnitude M_S was carried out by the correlation dependence given in Zare et al. (2014) [11].

Thus, after the determination or specification of the basic parameters of earthquakes, we present a new catalog of historical earthquakes (pre-1900) of Georgia and the refined instrumental earthquake catalog (1900-2015) of Georgia, complete for $M_S \geq 2.9$ or $M_W \geq 4.0$, in format (Fig. 6).

Year	Month	Day	Hour	Minute	Second	Lat	Long	Author	Depth	Engdahl	Mw	Author	Ms	Author
BC 1250	00	00	00	00	00	42.70	42.20	EDIG	15	362	6.9	EDIG	6.9	EDIG
0050	00	00	00	00	00	42.90	41.00	NC	10	360	5.8	EDIG	5.5	NC
0085	00	00	00	00	00	42.05	43.90	EDIG	15	362	7.0	EDIG	7.0	EDIG
0400	00	00	00	00	00	42.90	41.00	NC	10	360	5.8	EDIG	5.5	NC
0742	00	00	00	00	00	42.40	44.90	ShT	18	362	6.4	EDIG	6.4	NC
1088	04	22	00	00	00	41.40	43.40	EDIG	15	367	6.5	EDIG	6.5	EDIG
1100	00	00	00	00	00	43.10	42.30	EDIG	15	362	7.0	EDIG	7.0	EDIG
1275	04	14	00	00	00	41.85	44.70	EDIG	15	362	6.5	EDIG	6.5	EDIG
1283	00	00	00	00	00	41.70	43.20	EDIG	15	367	7.0	EDIG	7.0	EDIG
1350	00	00	00	00	00	42.70	43.10	EDIG	15	362	7.0	EDIG	7.0	EDIG
1530	00	00	00	00	00	42.05	45.40	EDIG	15	337	5.9	EDIG	5.7	EDIG
1600	00	00	00	00	00	43.40	41.00	EDIG	15	362	7.0	EDIG	7.0	EDIG
1614	00	00	00	00	00	42.40	41.80	EDIG	10	362	6.1	EDIG	6.0	EDIG
1682	06	13	22	30	00	41.70	44.80	EDIG	07	362	4.9	EDIG	4.2	EDIG
1742	08	05	00	00	00	42.10	45.60	EDIG	20	337	7.0	EDIG	7.0	EDIG
1750	00	00	00	00	00	42.90	41.90	EDIG	15	362	7.0	EDIG	7.0	EDIG
1750	00	00	00	00	00	43.00	42.70	EDIG	15	362	6.9	EDIG	6.9	EDIG
1756	00	00	00	00	00	41.90	45.70	EDIG	10	337	5.2	EDIG	4.7	EDIG
1785	05	00	00	00	00	41.90	42.10	EDIG	10	367	5.8	EDIG	5.5	EDIG
1803	10	29	00	00	00	41.70	44.80	EDIG	07	362	4.6	EDIG	3.8	EDIG
1804	10	11	17	00	00	41.70	44.80	EDIG	07	362	4.4	EDIG	3.5	EDIG
1805	02	21	19	00	00	41.90	43.90	NC	10	367	5.0	EDIG	4.4	NC
1811	01	01	05	00	00	42.00	45.50	EDIG	10	337	5.4	EDIG	5.0	EDIG
1819	02	28	00	00	00	41.70	44.80	EDIG	07	362	5.1	EDIG	4.5	EDIG
1845	05	24	01	00	00	41.30	43.50	EDIG	08	367	5.2	EDIG	4.6	EDIG
1846	04	23	21	00	00	42.60	43.00	EDIG	06	362	4.5	EDIG	3.7	EDIG
1853	03	18	00	30	00	41.80	45.80	EDIG	10	337	4.9	EDIG	4.2	EDIG
1856	02	13	04	00	00	42.00	44.00	EDIG	10	367	4.4	EDIG	3.5	EDIG
1868	02	18	17	00	00	41.20	43.50	EDIG	15	367	5.4	EDIG	4.9	EDIG
1868	12	09	16	30	00	42.30	44.70	EDIG	25	362	4.8	EDIG	4.0	EDIG
1870	07	19	14	30	00	41.90	42.10	EDIG	10	367	4.9	EDIG	4.2	EDIG
1874	02	25	19	30	00	41.80	43.40	EDIG	12	367	4.4	EDIG	3.5	EDIG
1877	08	08	06	30	00	42.60	43.60	EDIG	05	362	4.6	EDIG	3.8	EDIG
1878	11	26	23	00	00	41.90	43.50	NC	15	367	5.0	EDIG	4.3	NC
1881	08	24	20	00	00	42.00	44.00	EDIG	17	362	4.8	EDIG	4.0	EDIG
1887	07	16	17	45	00	42.05	42.05	EDIG	12	362	5.4	EDIG	4.9	EDIG
1890	10	28	19	00	00	41.85	44.60	EDIG	20	362	5.6	EDIG	5.2	EDIG
1891	00	00	00	00	00	43.05	41.30	EDIG	15	362	6.1	EDIG	6.0	EDIG
1891	03	27	18	30	00	42.10	43.90	NC	22	362	5.1	EDIG	4.5	NC
1894	11	29	10	30	00	41.90	44.60	EDIG	24	362	5.4	EDIG	5.0	EDIG
1896	09	22	03	53	00	41.65	45.00	EDIG	25	362	6.3	EDIG	6.3	EDIG
1897	02	03	02	00	00	41.80	46.30	EDIG	10	337	4.6	EDIG	3.8	EDIG
1898	08	13	00	00	00	41.30	43.50	EDIG	10	367	4.9	EDIG	4.2	EDIG
1899	12	31	10	50	00	41.55	43.55	EDIG	08	367	6.2	EDIG	6.1	EDIG
1900	01	01	19	00	00	41.60	43.50	EDIG	08	367	4.1	EDIG	3.0	EDIG
1900	04	17	02	25	00	42.20	45.10	NC	35	337	5.2	EDIG	4.6	NC
1902	02	21	03	06	00	41.70	46.60	NC	10	337	4.5	EDIG	3.6	NC
1902	03	20	06	10	26	42.60	43.40	NC	05	362	5.1	EDIG	4.5	NC
1902	06	18	23	53	10	43.00	42.00	NC	30	362	5.6	EDIG	5.2	NC
1902	07	03	00	00	00	42.80	44.20	NC	10	362	5.2	EDIG	4.7	NC
1902	07	06	19	33	00	42.80	44.20	NC	10	362	4.8	EDIG	4.0	NC
1902	08	19	02	26	00	42.60	43.40	NC	05	362	4.2	EDIG	3.2	NC
1902	10	03	23	05	43	41.80	45.60	NC	06	337	5.0	EDIG	4.4	NC
1902	10	04	01	46	00	41.90	45.60	NC	10	337	4.6	EDIG	3.8	NC
1902	10	17	07	21	00	42.10	45.80	NC	07	337	5.1	EDIG	4.5	NC

Fig. 8. New catalog of historical earthquakes (pre-1900) and the refined instrumental earthquake catalog (1900-2015) of Georgia, complete for $M_S \geq 2.9$ or $M_W \geq 4.0$.

Technique for declustering an earthquake catalog

Decluster process means to remove dependents events from seismic process and obtained independent events. This means to remove from earthquake catalog foreshocks, aftershocks and swarms. There are several declustering algorithms that applied by most users up to now [12, 13, 14, 15, 16]. However when we applied these methods for our catalog various number of earthquakes left (Table 2).

Table 2. Number of earthquakes in catalogue from various decluster methods

Reasenberg	Uhrhammer	Grünthal	Gardner and Knopoff
754	1433	674	929

As it is shown the number of independent events are very different that influence very much on seismic parameter estimations such as seismic rate and b value. That on his side influence very much on seismic hazard estimation. Moreover if obtained catalogs involve just independent events, they should follow stationary Poisson process. To be sure for it we calculated coefficient of scattering measure *R* that show us the nature of obtained process.

$$\mathrm{R} = \frac{\sigma_{\overline{\mathrm{N}}}}{\sqrt{\overline{\mathrm{N}}}} \; (1)\;; \text{ where } \overline{N} = \frac{\sqrt{N_i}}{n}\,,\; \sigma_{\overline{N}} = \sqrt{\frac{\sum (N_i - \overline{N})^2}{n}}$$

n is the number of observed year, N_i is earthquake with *I* magnitude. When *R* equal 1 means events follow Poisson process. In table 3 are presented obtained results for R.

Table 3. Results for R obtained by various declustering methods

M	R Reasenberg	R **Uhrhammer**	R **Grünthal**	R **Gardner and Knopoff**	R **Tsereteli-Butikashvili**
3.5	2.28	2.87	1.67	1.56	1.38
4.0	1.06	1.26	1.03	1.11	1.0
4.5	1.25	1.25	1.25	1.25	1.0
5.0	1.0	1.11	0.8	1.0	0.9
3.5 – 7. 0	2.25	2.42	1.34	1.12	1.36

During investigation of clustering methods we pay attention on behavior of Racha earthquake on of 1991. This earthquake had unusual high number of aftershocks that continue during the very long period. We plotted the number of earthquakes for Racha region 10 years earlier and after events Fig. 9 (blue diamond). In the same figure we plot the Spitac earthquake of 1988 (brown dots). As we see Raca region was very active during the several years after strong earthquake, while the Spitac region was active during the one year. From the same picture we can see that seismic activity remain higher after Racha earthquake up to now, while Spitac region became calm. This gave us idea that strong earthquake should be consider individually during the clustering process. Based on this consideration we develop new methodology for declustering catalog. We consider earthquake with magnitude M_S more than 6 individually.

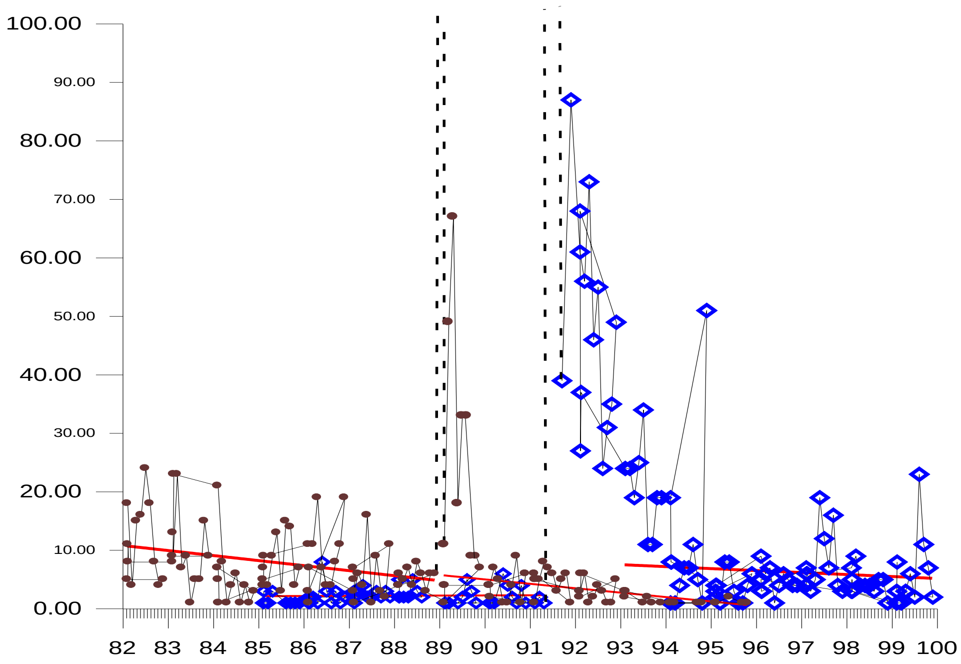

Fig. 9. The number of earthquakes for Racha earthquake of 1989 10 years earlier and after events (blue diamond). The number of earthquakes for Spitac earthquake of 1988 (brown dots). Redlines indicate the seismic level before and after earthquakes.

For the earthquake area [17] we investigate the number of earthquake before and after events during the 5 years. The average seismic level for each period is estimated. Comparison of these levels allow us estimate relaxation time period for this event. The earthquake source zone is divided by cells. The average numbers of earthquakes with various magnitudes are estimated for each cell by the seismic level that stabilized after strong earthquake. The same numbers with the same magnitude are left for each cell during the relaxation period. These increase numbers of earthquake during the relaxation period thought process anyway stay Poisson. Following this methodology total number of earthquake in decluster catalog is 2565. This is more then previous results show in table 2. The results of R are presented in table 3 as $R_{Tsereteli\text{-}Butikashvili}$.

For earthquake with magnitude less than 6 we use decluster methods described in [17] and in [18].

References:

[1] Varazanashvili, O., Tsereteli, N., Tsereteli, E. 2011. Historical earthquakes in Georgia (up to 1900): source analysis and catalogue compilation. Monograph, Pub. Hause MVP, Tbilisi, 81p.

[2] Lee, W., Larh, S., 1975. HYPO-71 (Revised), a computer program for determining hypocenter, magnitude and first motion patting of local earthquakes. U.S. Geological Survey Open File. Report 75-311.

[3] Tvaltvadze, G., 1960**.** Construction of the Earth crust of Georgia and building of the theoretical hodograph systems. Publ. Georgian Academy of Sciences, Tbilisi, pp. 60-62.

[4] Murusidze., G. 1987. Velocity model of the upper mantle in Caucasus and adjacent region. Mecniereba Publ. House, Tbilisi, 133 pp.

[5] Adamia, Sh., 1985. Peculiarity of Caucasus Earth crust and upper mantle construction and its relation with moderate structure. In: Balavadze, B. (Ed.), Geophysical fields and construction of Transcaucasia Earth crust. Nauka Publ. House, Moscow, pp.151 – 168.

[6] Adamia, Sh., Alecsidze, M., Balavadze, B., Gvantseladze, T., Gugunava, G., Diasamidze, Sh., Ioseliani, M., Ismailzade, T., Kartvelishvili, K., Kuloshvili, S., Mindeli, P., Hazaretian, S., Oganesian, Sh., Radjabov, M., Sikharulidze, D., Chelidze, T., Shengelaia, G., 1991. Complex Geophysical Investigation Of the Lithosphere of Caucasus. In: Belousov, V., Pavlenkova, N., Kviatsovskaia, G. (Eds.), Deep construction of the territory of USSR. Nauka Publ. House, Moscow, pp 41- 55.
[7] Tea Godoladze, Larry Hutchings, Bill Foxal T et al., 2005. Structural 2D modeling problem of seismic tomography . J. of the Georgian Geophys. Society 10A, pp 83-86
[8] Sikharulidze, D., Tutberidze, N., Diasamidze, Sh., Bochorishvili, S., 2004. The structure Of the Earth’s crust and the upper mantle in Georgia and the adjacent territories. J. of the Georgian Geophys. Society 9A, pp12-19.
[9] Rautian, T. G. (1964). About the determination of the energy of earthquakes at distances up to 3000 km. Akademiya Nauk SSSR, Trudy Instituta Fiziki Zemli, no. 32, pp. 88-93. (in Russian)
[10] Rautian, T.G., V.I. Khalturin, I.S. Shengelia, (1979), The coda envelopes and the determination of the magnitudes of Caucasus earthquakes, The Physics of the Earth, Acad. Sci. USSR, N6 22-29 (English translation of Russian original).
[11] Mehdi Zare , Hamideh Amini, Pouye Yazdi, Karin Sesetyan, Mine Betul Demircioglu, Dogan Kalafat, Mustafa Erdik, Domenico Giardini , M. Asif Khan , Nino Tsereteli 2014. Recent developments of the Middle East catalog. Journal of Seismology. Volume 18, N4, pp.749-772 , July. DOI 10.1007/s10950-014-9444-1 http://link.springer.com/article/10.1007%2Fs10950-014-9444-1
[12] Gardner, J. K., and L. Knopo_ (1974), Is the sequence of earthquakes in Southern California, with aftershocks removed, Poissonian?, Bull. Seis. Soc. Am., 64(5), pp. 1363-1367.
[13] Reasenberg, P. (1985), Second-order moment of central California seismicity, 1969-82, J. Geophys. Res., 90, pp. 5479 - 5495.
[14] Grünthal, G. and GSHAP Region 3 Working Group, 1999. Seismic hazard assessment for central, north and northwest Europe:GSHAP Region 3. Annali di Geofisicia 42, pp. 999-1011.
[15] Grünthal, G., Wahlström, R. and Stromeyer, D., 2009. The unified catalogue of earthquakes in central, northern, and north-western Europe (CENEC) - updated and expanded to the last millennium. Journal of Seismology, 13, pp. 517-541.
[16] Uhrhammer, R. (1986), Characteristics of Northern and Central California Seismicity, Earthquake Notes, 57(1), 21.
[17] Yurii V. Riznichenko 2013. Problems of Seismology: Selected Papers. p. 17-20.
[18] E. Jibladze, N. ButicaSvili, N. Tsereteli. 1995. Seismic regime, seismic hazard and seismotectonic deformation in the Caucasus. Tbilisi, Institute of Geophysics of the Academy of Sciences of Georgia,. p.125 (in Russian).

საქართველოს სეიმური კატალოგი

ნ. წერეთელი, ო. ვარაზანაშვილი, მ. კუპრაძე, ნ. ყვავაძე, ზ. გოგოლაძე

რეზიუმე

მიწისძვრების კატალოგების ერთგვაროვნებას და სიზუსტეს დიდი მნიშვნელობა აქვს სეიმური საშიშროების ამოცანების გადაწყვეტაში. მიწისძვრის ეპიცენტრიისა და მაგნიტუდის განსაზღვრისა და მათი ცდომილების შეფასების გარეშე შეუძლებელია მიწისძვრების სტატისტიკური კვლევა, სეისმური კერების ზონების გამოყოფა და პარამეტრიზაცია, გრუნტის მოძრაობის პროგნოზული განტოლებების შედგენა. ეს ყველაფერი თავის მხრივ გავლენას ახდენს სეისმური საშიშროების ალბათურ და დეტერმინისტულ გათვლებზე. აქ წარმოდგენილია მიწისძვრის პარამეტრების განსაზღვრის შეფასებები, როგორც ისტორიული, ასევე ინსტრუმენტული პერიოდის მიწისძვრებისთვის. ასევე განხილულია მიწისძვრის კატალოგების ფორ- და აფტერშოკებისაგან, გუნდებისაგან გაწმენდის სხვადსახვა მეთოდები, რომლებიც ფართოდ გამოიყენება სეისმოლოგიაში და შედარებულია ჩვენს მიერ შემოთავაზებულ მეთოდთან. ნაჩვენებია ამ უკანასკნელის უპირატესობა.

Сейсмический каталог Грузии

Н. Церетели, О. Варазанашвили, М. Купрадзе, Н. Квавдзе, З. Гоголадзе

Резюме

При решении задач сейсмической опасности очень важно однородность и точность каталогов землетрясений. Без определения эпицентра и магнитуды землетрясения и оценки их ошибок не возможно статистическое исследование землетрясений, выделение зон сейсмических очагов и их параметризация, составление прогнозстических уравнений двыжении грунта. Все это в свою очередь влияет на расчет вероятностной и детерминистической сейсмической опасности. Здесь представлены оценки определения параметров землетрясений, как для исторического, так и инструментального периода. Также обсуждаются различные методы очистки каталогов землетрясений от фор- и афтершоков, роев, которые широко используются в сейсмологии и они сравниваються с предложенным нами методом. Показан преимущество последнего.

Journal of Georgian Geophysical Society,
Issue (A), Physics of Solid Earth, v.19a, 2016, pp.75-83

Remote Sensing Neotectonic Research on Oil and Gas Perspective Structures on the Example of the Dnieper-Donets Basin

Zinaida M. Tovstyuk, Tatyana A. Yefimenko, Olga V. Titarenko, Mihail O. Svideniuk

State institution "Scientific Centre for Aerospace Research of the Earth Institute of Geological Science National Academy of Sciences of Ukraine" (CASRE IGS NASU), 55b Olesya Gonchara, Kyiv, Ukraine, 01601,
casre@casre.kiev.ua

Abstract

Different methods of structural and geomorphological analysis to solve problems of oil and gas searching at different stages of the work (from regional to detailed) are observed. There are the most acceptable for the Dnieper-Donets Basin are: hypsometric terrain analysis (construction of the morphotectonic structural contours maps); analysis of relief differentiation (degree of horizontal and vertical relief differentiation); morphographic techniques. A priori structural and geomorphological information in the software product ArcGIS, as well as satellite images Sich-2, Landsat–7 ETM+, Landsat–8 OLI, shuttle radar topography mission - SRTM and structural contours scheme based on SRTM data are used.
The result of this comprehensive research is the Scheme of the relative neotectonic activity of the Dnieper-Donets Basin.

Key words: oil and gas structure, remote sensing, structural and geomorphological analysis, morfotektoizogips, neotectonic scheme.

The Neogene-Quaternary period of the Earth’s crust formation is of high importance in the oil and gas deposits location and hydrocarbon migration. The ancient faults are updated, new faults laid and activation of foundation's block movements' are occurred during the Neogene-Quaternary period. The local structural forms growth and rearrange occur in the sedimentary cover. The neotectonic activity of the Dnieper-Donets Basin deep structures was contributed to the formation of the relief and its structure peculiarities and this activity can be interpreted using satellite imagery.

There are different methods of structural and geomorphological analysis used for different areas for the solving problems connected with finding oil and gas structures at the different stages of the research works (from regional to detail). The most appropriate methods for the Dnieper-Donets Basin are as follows:

- hypsometric analysis of relief (construction of the morphotectonic structural contours maps);
- analysis of relief differentiation (degree of horizontal and vertical relief differentiation);
- morphography techniques.

In the first case, the analysis is conducted for both hypsometric zoning of the territory and assessment of the interconnection between relief and tectonics.

In the second case, the structural interpretation is the following: zones of the increasing dissection degree of relief are identified with the Neogene-Quaternary structural uplift, and zones of depression - with the possible Neogene-Quaternary subsidence.

In the third case, the planned picture of the Earth's surface is investigated based on aerospace materials. Morphography elements, which identify structures in plans, are divided by their form on straightened, arc-shaped and planar.

The main purpose of the structural and geomorphological studies (SGS) during the regional researches conduction was the investigation or rectification of the tectonic structure, which include large oil-gas regions, and local structures. A priori structural and geomorphological information in the software product ArcGIS, as well as satellite images Sich-2, Landsat–7–ETM+, Landsat–8–OLI (Fig.1), shuttle radar topography mission - SRTM and structural contours scheme based on SRTM data (Fig.2) are used in these studies.

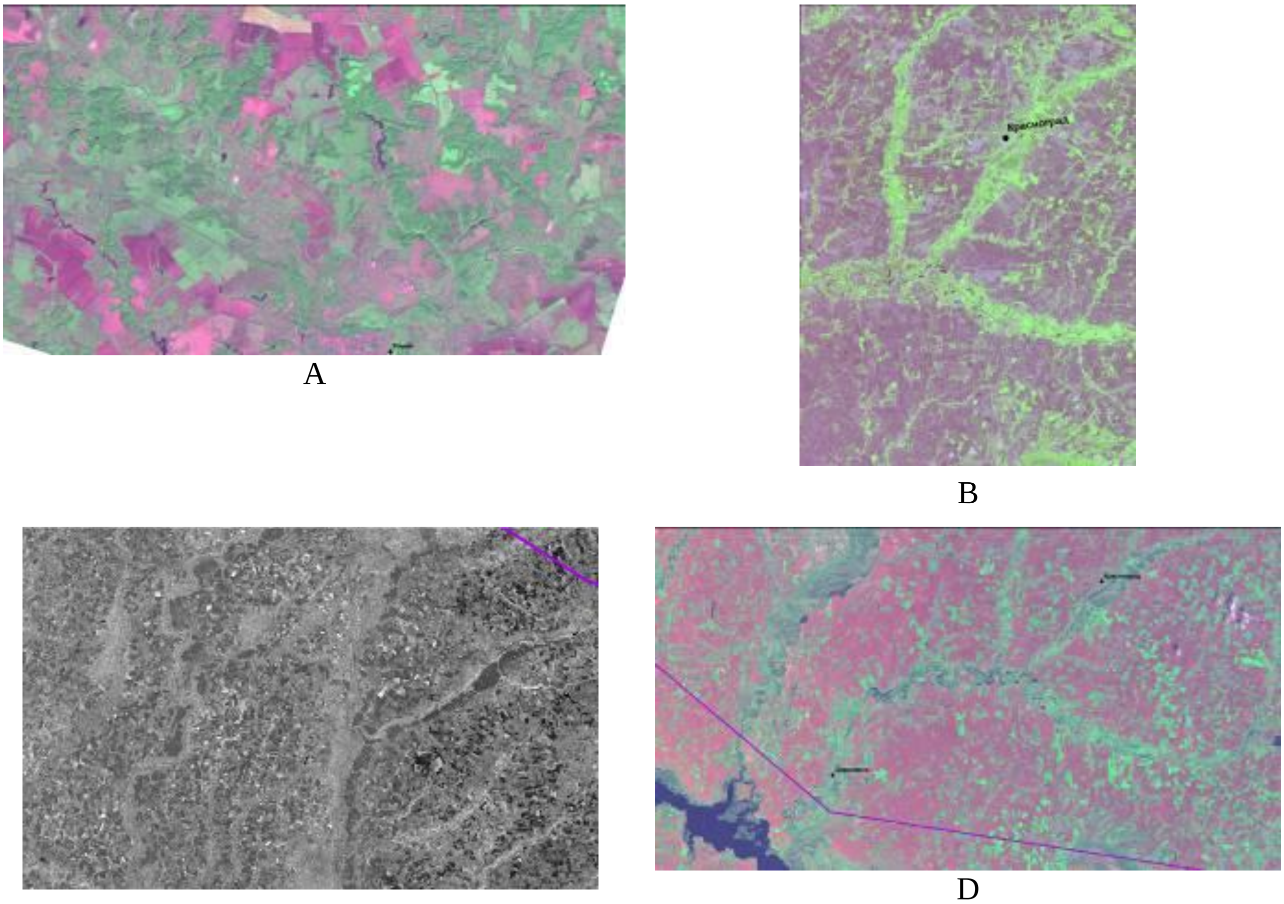

A B C D

Fig.1. The Dnieper-Donets Basin: A, B – satellite imagery Sich-2 (2012); C - satellite image (Landsat–7–ETM+, 2002); D - satellite imagery (Landsat— OLI, 2013)

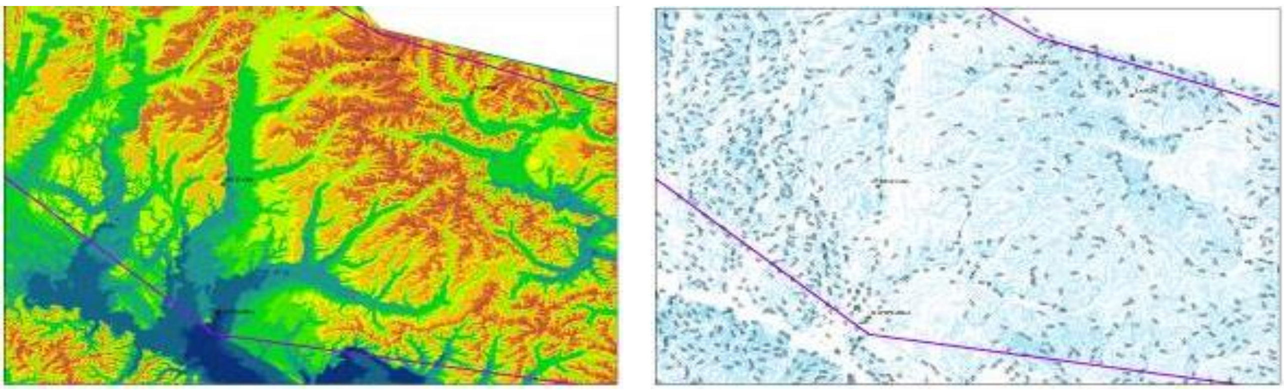

A B

Fig.2. The Dnieper-Donets Basin: A – shuttle radar topography mission image (SRTM); B – scheme the structural contours (based on SRTM)

At the first stage, the scheme of the structural decryption was established based on aforementioned satellite imagery, on which lineaments (Fig.3) and their zones (Fig.4) were marked. The result of these procedures was the structural decryption scheme of the Dnieper-Donets Basin (Fig.5).

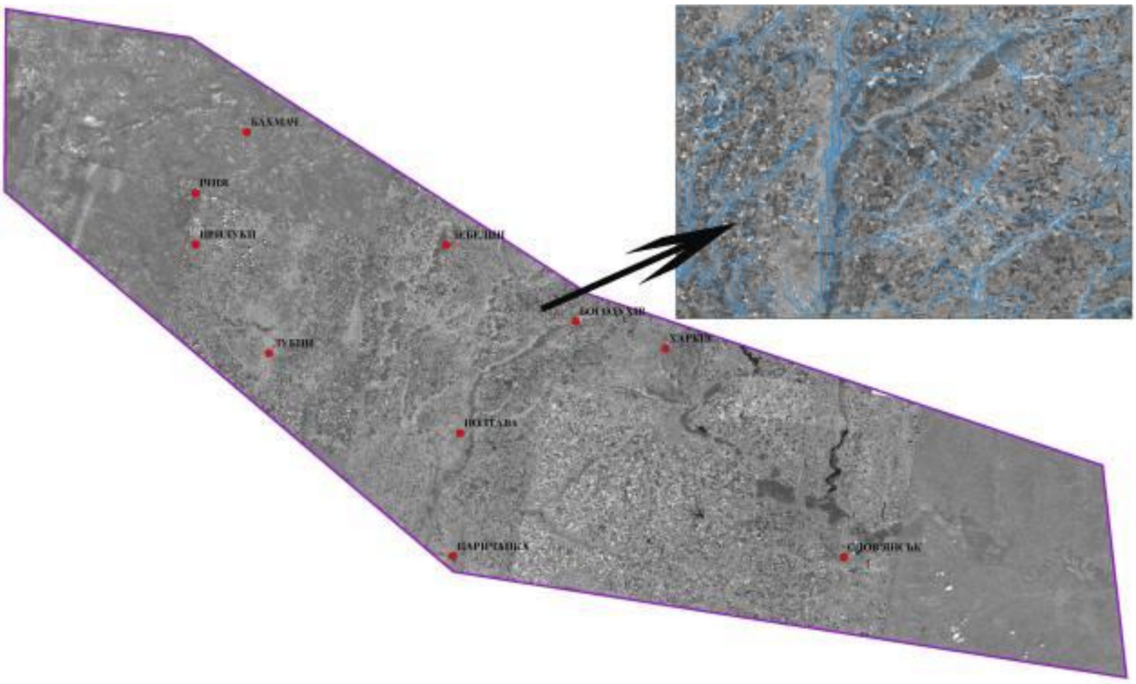

A

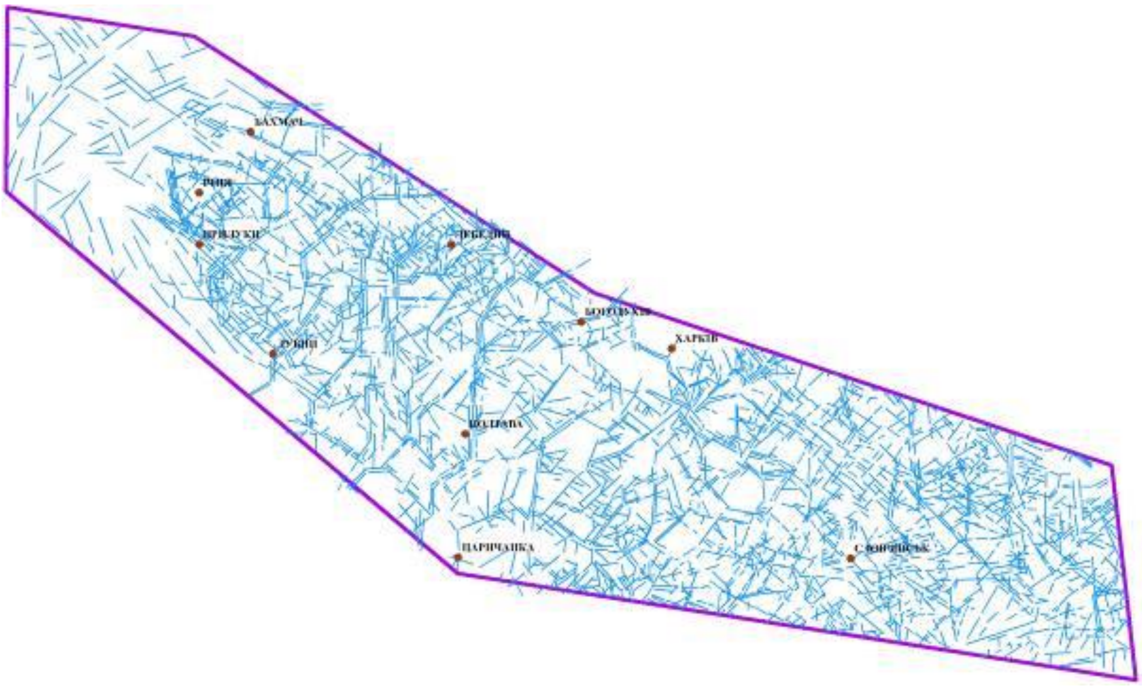

B

Fig.3. The Dnieper-Donets Basin: the scheme of lineaments (B) based on remote sensing from Landsat–7–ETM+ (A)

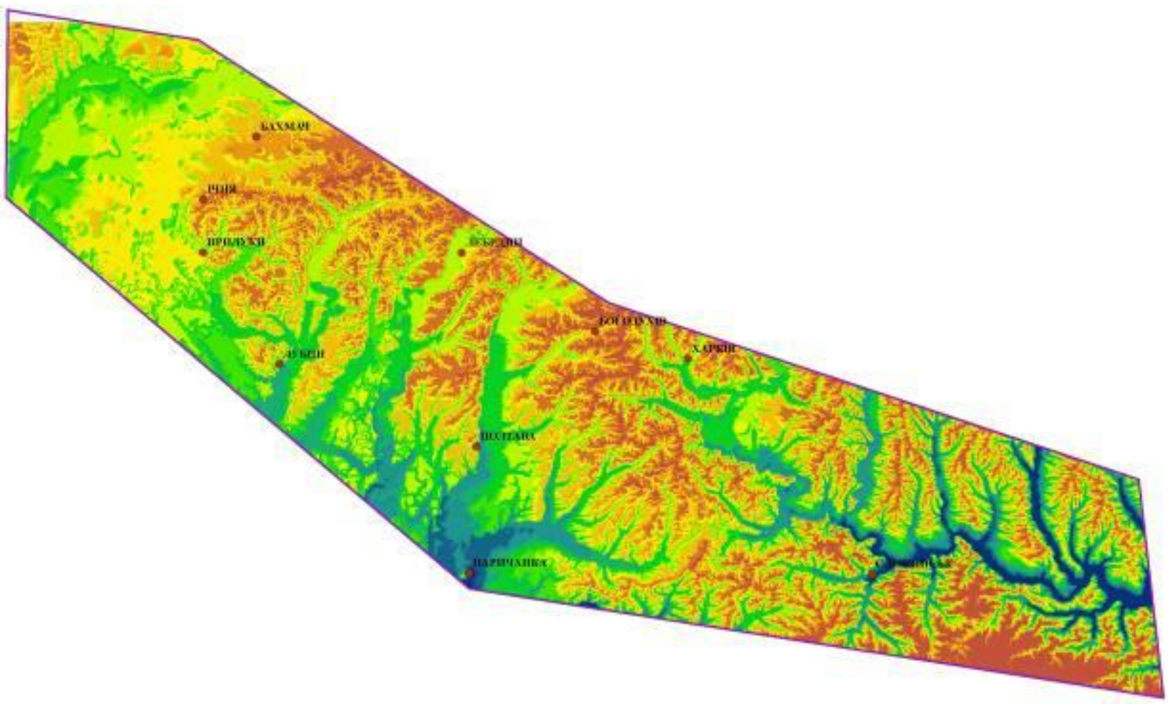

A

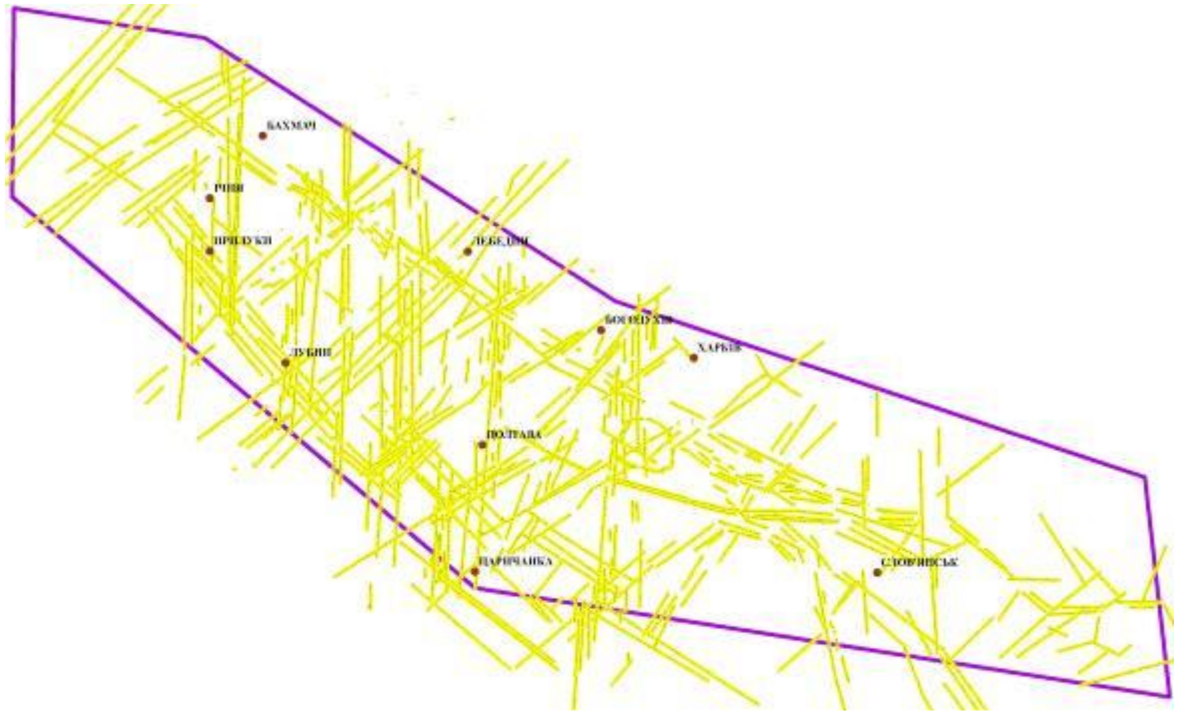

B

Fig.4. The Dnieper-Donets Basin: the scheme of lineaments (B) based on shuttle radar topography mission (A)

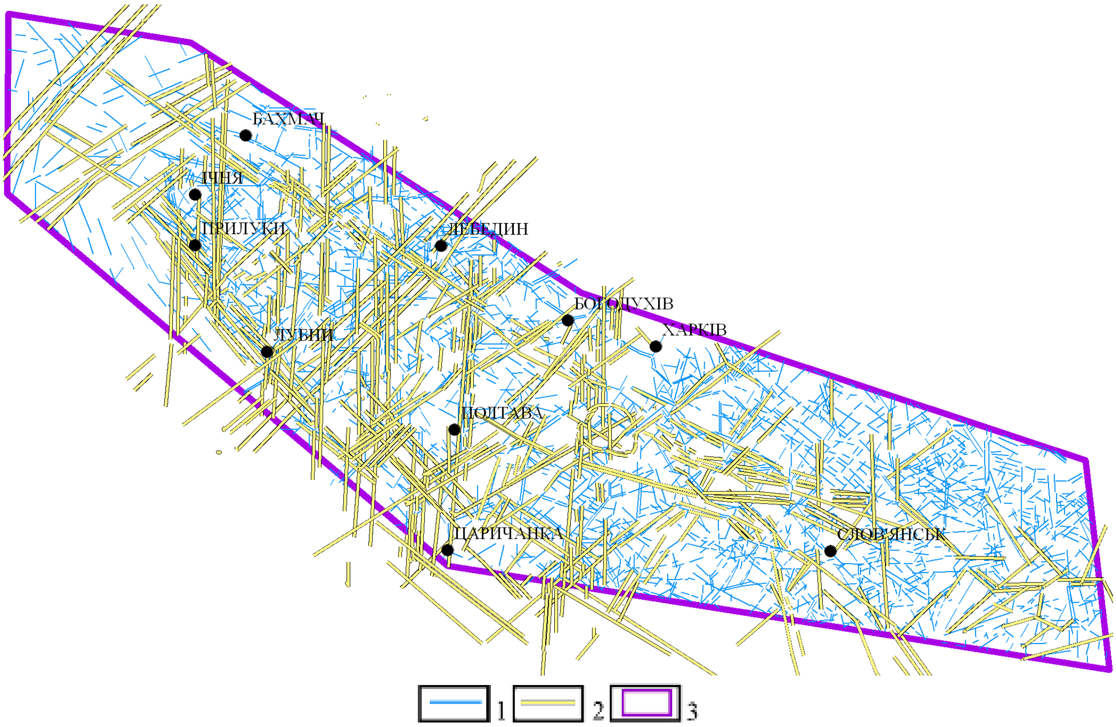

Legend: 1 - lineaments; 2 – lineaments zones; 3 - the research area

Fig.5. The Dnieper-Donets Basin: the resulting scheme of the relief structural identification based on materials of satellite imagery

Thus, there are lineament zones of the north-western strike can be observed as well on the performed scheme. These zones have inherited ravines and valleys, most of which are oriented parallel to the marginal faults of the Dnieper-Donets Basin and longitudinal cuts off power within the northern and southern near edge zones and the northern edge. As a result, there are the following associations were traced:

1) the north-western apophysis of the salt stocks cap rocks connected with these marginal faults;

2) the coming of hydrocarbons out to the day surface connected with intersection nodes with such cross sectional dislocations;

The north-eastern sectional dislocations can be identified less clearly by short extension young erosion topographical formations. Obviously, this is associated with a later activation of neotectonic movements on the surface of ancient faults. Moreover, there are traced the salt stocks u-turn of the Dnieper-Donets Basin in the south-eastern part. Submeridional and sublatitudinal faults more clearly, but still fragmentary, are shown in relief's north-western part of the Dnieper-Donets Basin, where they inherited by the valleys of big rivers that were laid, obviously, by the updated ancient fault structures which may extend from the Ukrainian Crystalline Massif through the Dnieper-Donets Basin in Voronezh anteclise.

At the next stage diagram of the relief vertical differentiation is constructed (Fig.6). For these studies the SRTM is used, which greatly simplifies the process of materials' construction and interpretation [1]. The analysis of the scheme allowed establishing the connection between the degree of vertical differentiation of relief and tectonic movements.

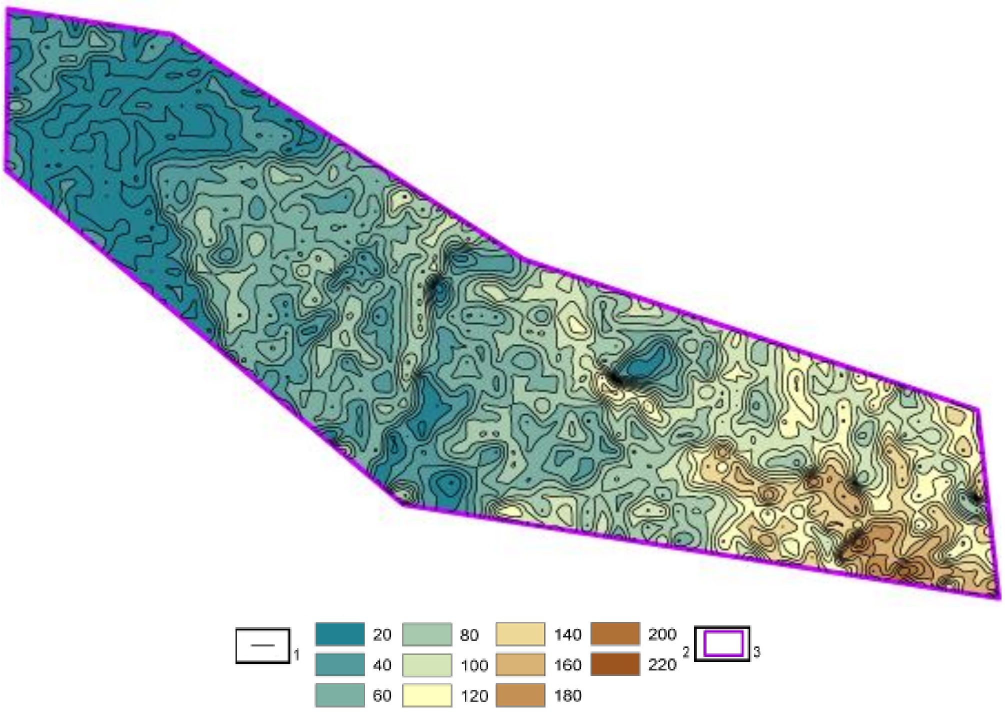

Legend: 1 – structural contours of relief vertical differentiation, m; 2 - level vertical differentiation; 3 – study area

Fig.6. The Dnieper-Donets Basin: the vertical differentiation of relief (based on SRTM)

According to SRTM the authors carried out the hypsometric relief analysis and built the map of morphotectonic structural contours (Fig.7).

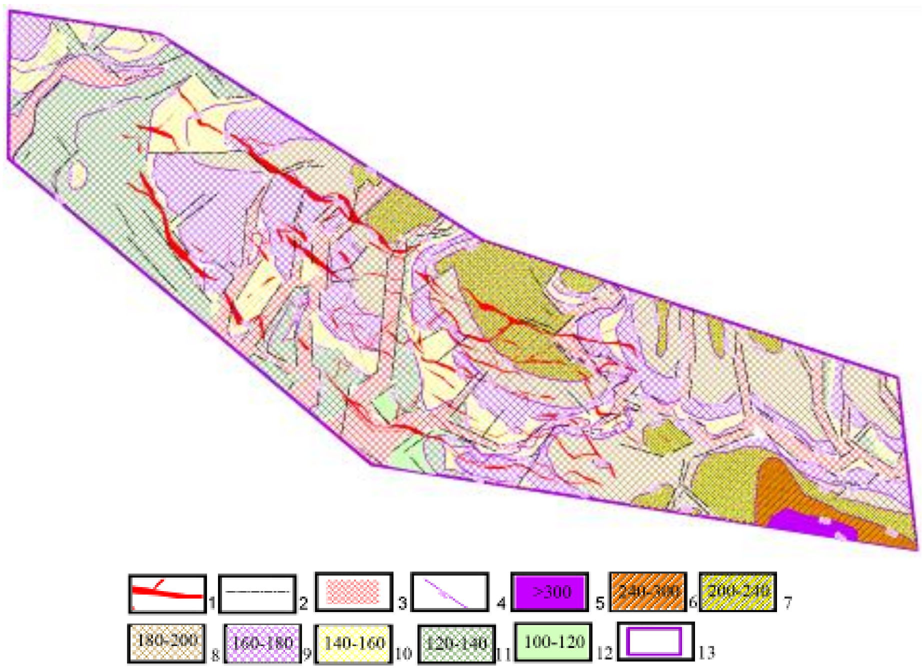

Legend: 1 - faults in the basement; 2 - lineaments and their zones; 3 – unconsolidation zones; 4 - morphotectonic structural contours; 5-12 scale of height, m; 13 – study area

Fig.7. The Dnieper-Donets Basin. The morphotectonic structural contours scheme (based on SRTM)

The method involves the reconstruction of relief. Thus, differently amplitude block structure of the recent relief is defined quite clearly: there are stand out the most elevated blocks, which allows draw conclusions about the positive deformation of the Earth's surface. The neotectonic activity the Dnieper-Donets Basin’s deep structures led the displaying of these structures’ features of relief’s forms depression. Thus, the edges are associated with the uplifted areas of relief, and the depression areas are - with an axial part of the Dnieper-Donets Basin. The structural contours block structure of reconstructed relief with relative range of these blocks motions is performed on the built morphotectonic structural contours scheme as well.

The result of comprehensive research is the scheme of the Dnieper-Donets Basin relative neotectonic activity (Fig.8).

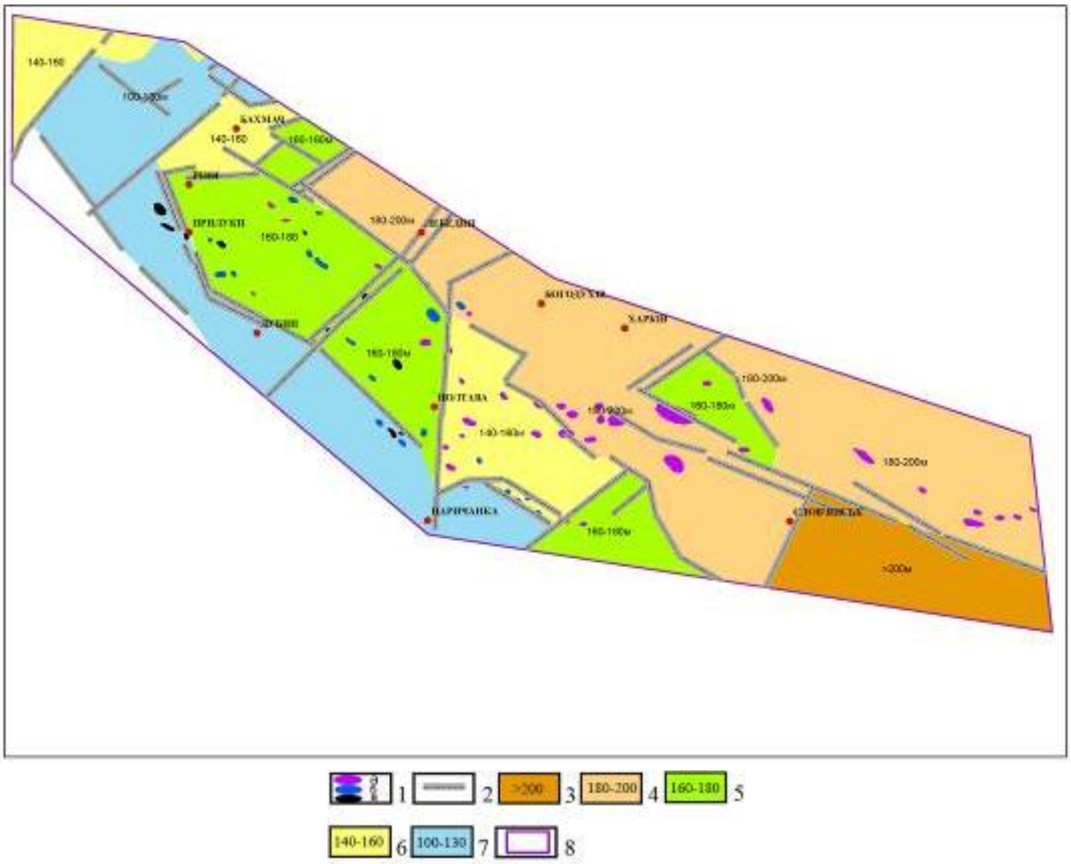

Legend: 1 – deposits: a – natural gas, б – oil-gas, в – crude oil; 2 – blocks' boundaries; 3–7 - scale of the relative neotectonic activity, m; 8 – study area

Fig.8. The Dnieper-Donets Basin. Scheme of the relative neotectonic activity

Our studies provide an opportunity to identify areas that are characterized by varying intensity of neotectonic movements.

The maximum relative amplitude of neotectonic movements - 200 m and more common for the northern edge and the eastern part of the Dnieper-Donets Basin. At the same time, there are the sharp increasing of neotectonic activity and the number of high blocks with high activity while their size reducing in the eastern part. Oil and gas structures in this part of the Dnieper-Donets Basin are characterized by high amplitudes. High values of the neotectonic amplitudes are typical for most of the salt stocks that occur in the recent relief in the form of the positive relief deformations.

Moreover, negative deformations were formed under the stocks that stopped their growth in the Paleogene or had negative direction of movements.

Thus, famous Turutynske, Huhrynsk-Chernetchynske, Yuliyivske and Skvortsivske deposits located within the northern edge and northern near edge zone are confined to regions of the maximum neotectonic activity.

Mean values of relative neotectonic amplitudes - about 160-200 meters - are typical mainly for near edge zone of crystalline basement - Makeyevkske, Lubensk-Isachkivske, Pliskivsk-Lysohorske, Talalaevske, Novotroitske, Radiansk-Koziyivske and others. Therefore, here are concentrated lineaments, which form elongated north-western zones that overlap with less powerful north-eastern zones and the layout of a significant amount of oil, gas condensate and natural gas deposits are related to them.

Within the southern edge of the Dnieper-Donets Basin amplitudes of relative neotectonic movements are much smaller and generally do not exceed 130 meters. However, there are a number of hydrocarbons deposits there and eastern of the Vorskla river district are observed: Livenske, Holubivske, Bohatoyske. Obviously, this is connected with the presence of a significant fractured zone of basement and sedimentary rocks, which may be hydrocarbon transportation routes.

Low values of the relative neotectonic amplitudes of 100-130 m, are occurred on the slopes of deflections and sloping monoclinale of the basement.

Thus, within the studied area of the Dnieper-Donets Basin the following regularity is observed:

- the bulk of hydrocarbons confined to moderate (150-200 m) neotectonic active areas;
- oil deposits are located within the north-western part of the Dnieper-Donets Basin (160-180 m);
- gas condensate deposits are located in the South-eastern part of the Dnieper-Donets Basin (180-200 m).

Consequently, we can conclude that finding of hydrocarbons deposits at the north edge, which is characterized by high amplitudes of relative neotectonic movements, greatly increases its oil and gas prospects due to favorable conditions for the formation of capacitive fracture and fractured-porous reservoirs in the crystalline basement's rocks.

References

[1] Tovstyuk Z.M., Titarenko A.V., Efimenko T.A. Remote sensing neotectonic structure research for oil and gas deposits finding on example of Dnieper-Donets Basin // Proceedings of the 14th Conference of Ukrainian space research. - Uzhgorod Institute of Electron Physics, National Academy of Sciences of Ukraine, 2014, 188 p.

[2] Tovstyuk Z.M., Efimenko T.A. Remote sensing of Earth for neotectonic research on oil and gas perspective structures on the example of the Dnieper-Donets Basin. - Ukrainian Journal of remote sensing №6 2015. - P. - 8-13.

Неотектонические исследования по материалам дистанционного зондирования Земли при поиске структур перспективных на нефть и газ на примере Днепровско-Донецкой впадины

З.М. Товстюк, Т.А. Ефименко, О.В. Титаренко, М.О. Свиденюк

Резюме

В статье рассматриваются разные приемы структурно-геоморфологического анализа для решения задач поиска нефтегазоносных структур на различных стадиях проведения работ (от региональных до детальных). Для Днепровско-Донецкой впадины наиболее приемлемыми оказались следующие: гипсометрический анализ рельефа (построение карт морфотектоизогипс); анализ расчленения рельефа (степень горизонтального и вертикального расчленения рельефа); морфографические приемы. При этих исследованиях используются структурная и геоморфологическая информация в программном продукте ArcGIS, а также космические снимки Сич-2, Landsat-7 ETM +, Landsat-8 OLI, радарная топографическая съемка SRTM и схема изогипс по данным SRTM.

Результатом комплексных исследований стала схема относительной неотектонической активности Днепровско-Донецкой впадины.

ნეოტექტონიკური გამოკვლევები დედამიწის დისტანციური ზონდირების მასალების მიხედვით გაზისა და ნავთობის პერსპექტიული სტრუქტურების ძიებისას დნეპროპეტროვსკ-დონეცკის ქვაბულის მაგალითზე

ზ.მ.ტოვსტიუკი, ტ.ა.ეფიმენკო, ო.ვ.ტიტარენკო, მ.ო.სვიდენიუკი

რეზიუმე

სტატიაში განიხილება სტრუქტურულ-გეომორფოლოგიური ანალიზის სხვადასხვა ხერხები, ნავთობგაზური სტრუქტურების ძიების ამოცანების გადაწყვეტისათვის, სამუშაოების ჩატარების სხვადასხვა სტადიაზე (რეგიონალურიდან დეტალურამდე). დნეპროვსკ-დონეცკის ქვაბულისათვის ყველაზე მისაღები აღმოჩნდა შემდეგი: რელიეფის გიფსომეტრიული ანალიზი(მორფოტექტოიზოგიფსების ანალიზი); რელიეფის დანაწევრების ანალიზი(რელიეფის ჰორიზონტული და ვერტიკალური დანაწევრების ხარისხი); მორფოლოგიური ხერხები. ამ გამოკვლევების დროს გამოიყენება სტრუქტურული და გეომორფოლოგიური ინფორმაცია პროგრამულ პროდუქტში ArcGIS, აგრეთვე კოსმოსური სურათები Сич-2, Landsat-7 ETM+, Landsat-8 OLI, რადარული ტოპოგრაფიული გადაღება SRTM და იზოგიფსების სქემა SRTM-ის მონაცემების მიხედვით.

კომპლექსური გამოკვლევების შედეგია დნეპროვსკ-დონეცკის ქვაბულის ფარდობითი ნეოტექტონიკური აქტივობის სქემა.

Journal of Georgian Geophysical Society,
Issue (A), Physics of Solid Earth, v.17a, 2016, pp. 84-103

Hydrodynamic and geomagnetic anomalies related with preparation of earthquakes in Caucasus

George Melikadze, Tamar Jimsheladze, Genadi Kobzev, Alexandre Tchankvetadze, Marina Devidze

Iv. Javakhishvili Tbilisi State University, M. Nodia Institute of Geophysics

Abstract

During July 2016 - September 2016 several hydrodynamic and geomagnetic anomalies were observed on the multiparametrical monitoring network located on the territory of Georgia. Data were recorded minutely and receiving in real time. Data were analyzed by the special program. In order to exclude the influence of geological factors, the data from various stations were calibraited by the common value of tidal variations. Were analyzed variation and reaction of parameters to the earthquake preparation process, the value of stress field before and after earthquake was calculated as well.

Introduction

Observation of spatial and temporal variability of earth crust's stress-deformation gives a possibility to create some modern methodology for earthquake prediction. In order to monitore the pre and post earthquake anomalies, considering the interaction between hydrodinamic, geophysical and other geodeformation processes (earthquakes, slow tectonic proceses, technogenic and etc), the data from July 2016 till September 2016 have been analyzed by the special program.

Data analysis

Multiparametric data (water level, atmosphere pressure, temperature, geomagnetic variation etc) were recorded with a minute frequency, in the deep boreholes located on the territory of Georgia. Observations were carried out using the specialized equipment providing measurement of deformation up to 10^{-8} degrees (1-2). In order to exclude the influence of geological factors, the data from various stations were rated against the common value of tidal variations (3-4). Variation and reaction of parameters to earthquake preparation process (5-9) were analyzed. The value of stress field by hydrodynamical parameters (10-11) and the stress field variations during preparation of several earthquake processes on the territory of Caucasus were calculated and analyzed:

Earthquake in Akhalkalaki area -21.07.2016 Mag-4.3

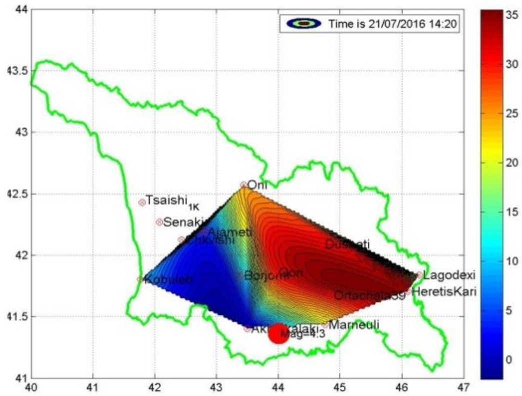

Fig.1.

Hydrogeodeformational field picture on the moment of 21 July 2016 earthquake. The field was created by the trended water level value

Anomaly was revealed on Akhalkalaki station before 21 July 2016 earthquake, 2 days earlier and continued 1day long. The earthquake was in 42km distance from the station.

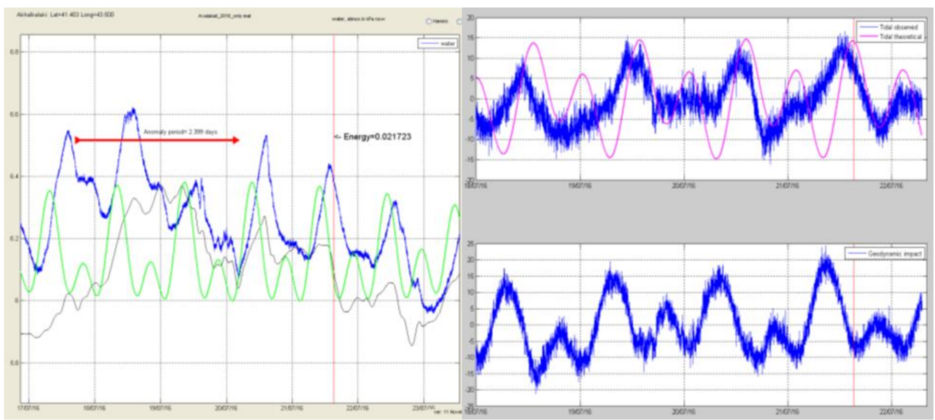

a b

Fig. 2

a- Origin of water level, atmospheric pressure and tidal variations at the Akhalkalaki borehole. Vertical line marks an earthquake moment. On abscise axis time is in hours. b- Speed factor of variations water level and earth tidal and the difference between them.

Anomaly was recorded at Marneuli station, as well.

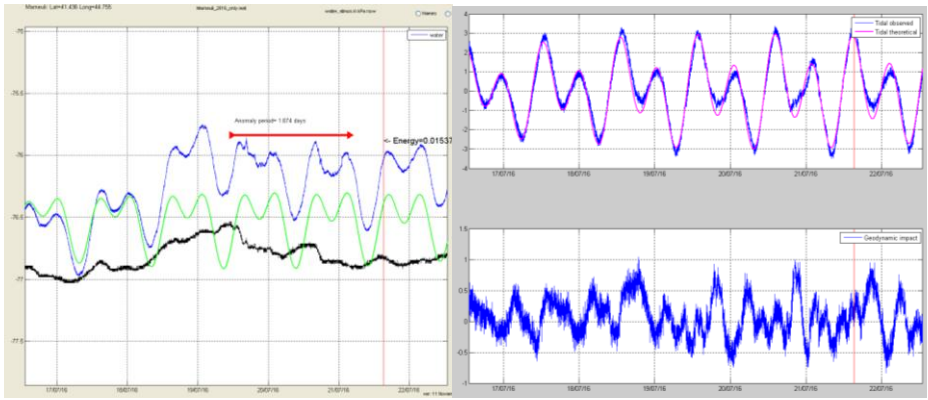

a b

Fig. 3.

a- Water level, atmospheric pressure and tidal variations at the Marneuli borehole (cm). Vertical line marks an earthquake. On abscise axis time is in hours. b- Speed factor of variations water level and earth tidal and the difference between them.

Anomaly of behavior of water level is revealed 2 days earlier before 21.07.2016 earthquake, 62 km from station.

Anomaly was observed in Dusheti geomagnetic observatory 1 day earlier before event of 21 July 2016. The Earthquake occurred in 99 km from a station.

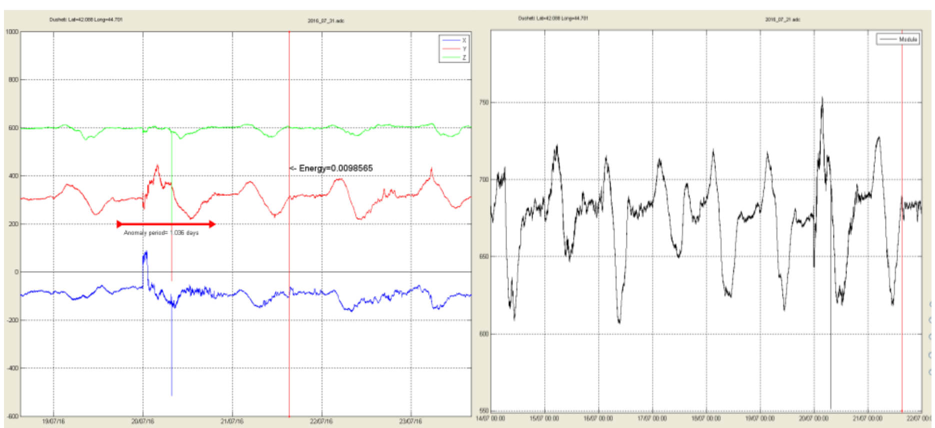

a b

Fig. 4

a- Variations of x,y,z components of the magnetic field. b- Variation of calculated module value.

Earthquake in Kobuleti area-28_07_2016, Mag-3,6.

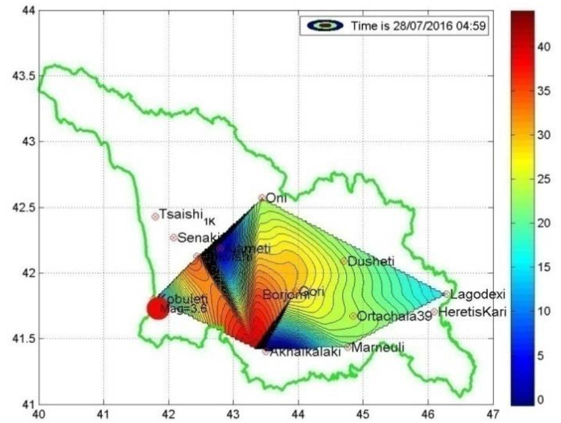

Fig. 5.

Hydrogeodeformational field picture on the moment of 28 July 2016 earthquake. The field was built for the value of trended water level.

Anomaly was observed from the Akhalkalaki station before 28 july 2016 few hours earlier and was continuing also during earthquake and after earthquake period. Earthquake happened in 142 km far from the station.

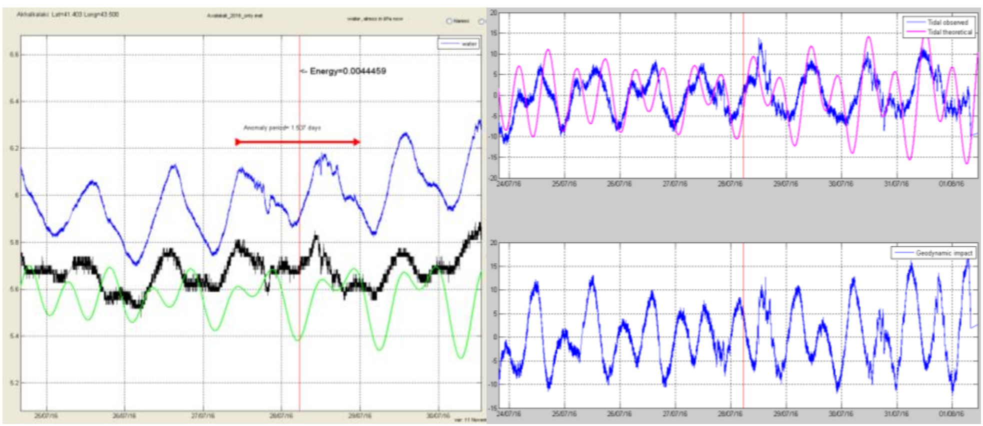

a b

Fig. 6

a - Water level, atmospheric pressure and tidal variations at the Akhalkalaki borehole. Vertical line marks an earthquake. On abscise axis time is in hours. b- Speed factor of variations water level and earth tidal and the difference between them.

.

Anomalies were observed before the earthquake of Kobuleti, as well as on the Ajamenti station, also.

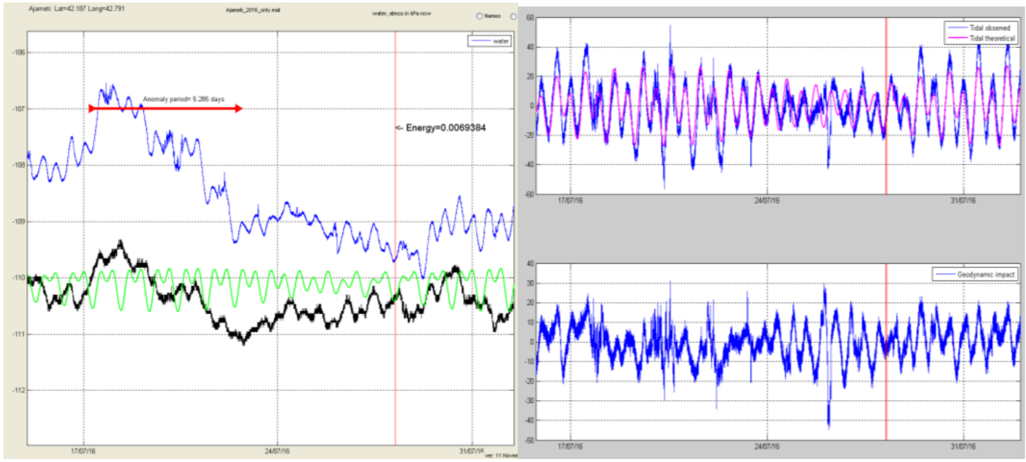

a b

Fig. 7

a - Water level, atmospheric pressure and tidal variations on the Ajameti borehole (cm). Vertical line marks an earthquake. On abscise axis time is in hours. b- Speed factor of variations water level and earth tidal and the difference between them.

At Ajameti station anomaly behavior was 9-10 days earlier before the earthquake. Earthquake epicenter was located in 93 km far from the station.

At Kobuleti station anomaly was observed 4 days earlier before the earthquake. Increasing water level and at the same time falling can be seen on the graph. Derangement continued for 2 days before the earthquake and the variation of water level got his regular face after 2 days. Earthquake epicenter was 9 km away from Kobuleti station.

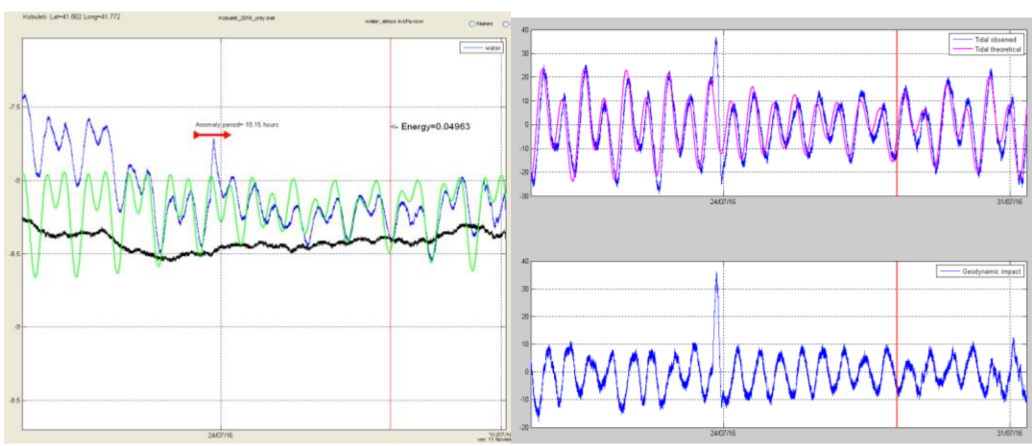

a b

Fig. 8.

a - Water level, atmospheric pressure and tidal variations on the Kobuleti borehole (cm). Vertical line marks an earthquake. On abscise axis time is in hours. b- Speed factor of variations water level and earth tidal and the difference between them.

Anomaly can be seen at Oni station, before 8 days earlier earthquake, as well as at on Ajameti station, water level drop was observed. The Epicenter of the 28 July earthquake occurred 161 km away from Oni station.

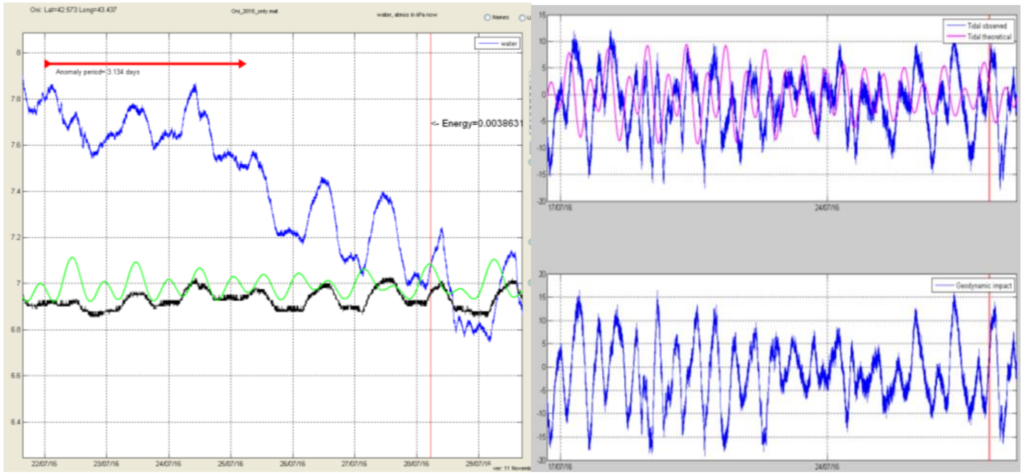

a b

Fig. 9.

a- Water level, atmospheric pressure and tidal variations at the Oni borehole (cm). The vertical line marks an earthquake. On abscise axis time is in hours. b- Speed factor of variations water level and earth tidal and the difference between them.

At Gori station water level drop also was observed. 6 days earlier before the earthquake water level increased. This process continued for 2 days and then began to drop down. Earthquake occurred 175 km away from Gori station

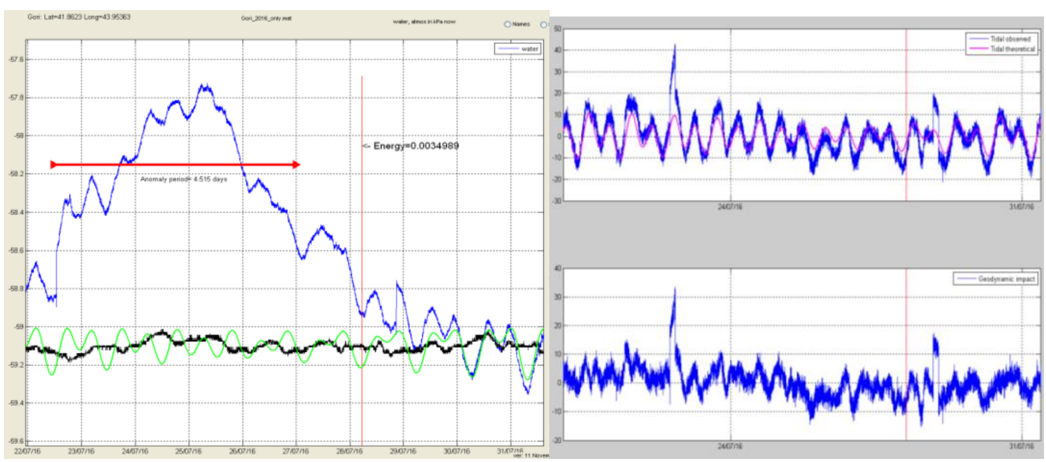

a b

Fig. 10.

a- Water level, atmospheric pressure and tidal variations on the Gori borehole. The vertical line marks an earthquake. On abscise axis time is in hours. b- Speed factor of variations water level and earth tidal and the difference between them.

The level started rising before Kobuleti earthquake on Chkvishi station, 4 days earlier before the earthquake. The epicenter was 65 km away from Chkvishi station.

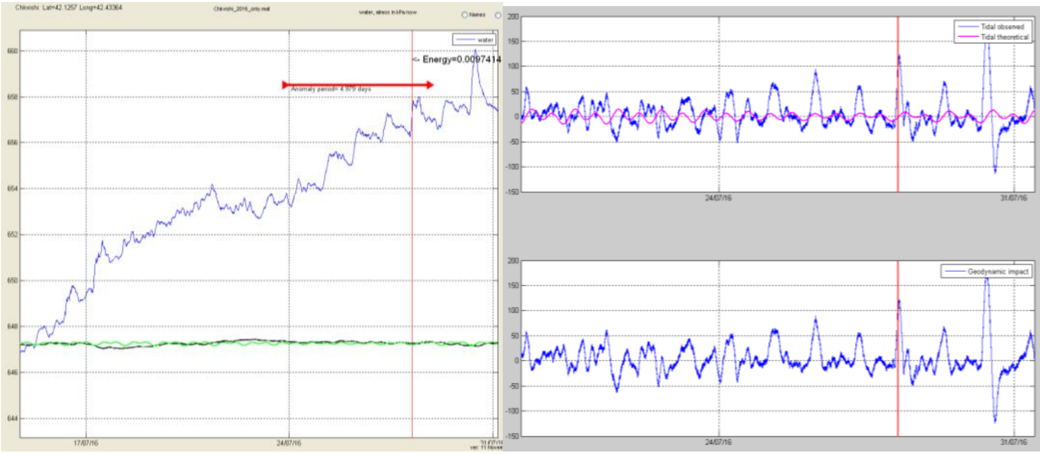

a b

Fig. 11.

a - Water level, atmospheric pressure and tidal variations at the Chkvishii borehole (cm). The vertical line marks an earthquake. On abscise axis time is in hours. b- Speed factor of variations water level and earth tidal and the difference between them.

As we can see on the graph, on 28 July before the earthquake, anomaly was recorded at Tsaishi station, 2-3 days earlier before the earthquake. Epicenter was 77 km away from the station.

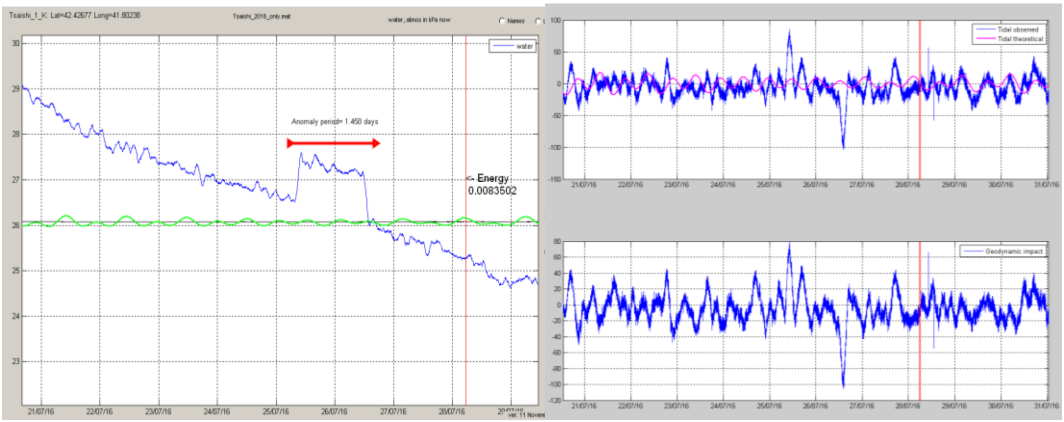

a b

Fig. 12.

a- Water level, atmospheric pressure and tidal variations on the Tsaishi borehole (cm). The vertical line marks an earthquake. On abscise axis time is in hours. b- Speed factor of variations water level and earth tidal and the difference between them.

Anomaly was observed at Dusheti geomagnetic observatory 3 days earlier before the earthquake and continues for 2 days after the earthquake. The earthquake occurred 240 km away from station.

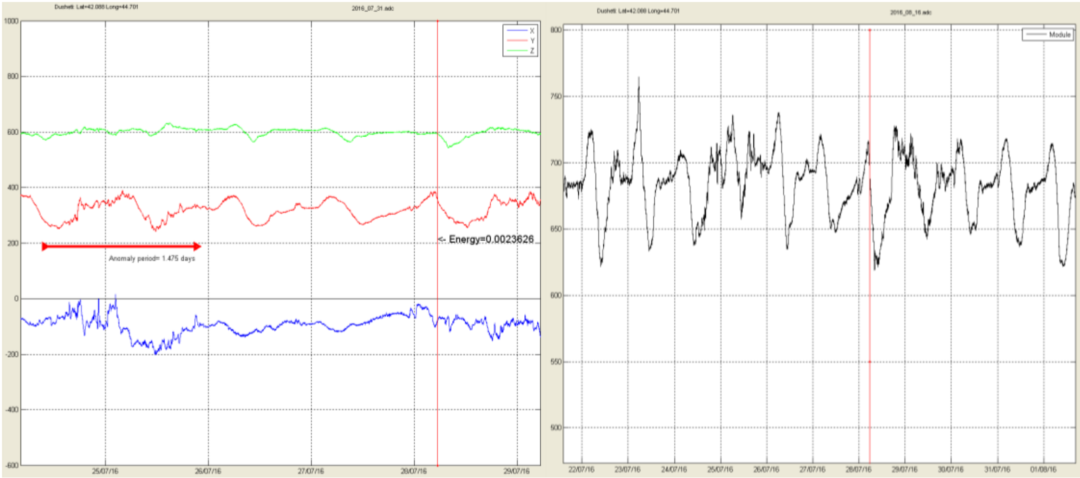

a b

Fig. 13.

a-Variation of x,y,z components of the magnetic field. b- Variation of the module value

Earthquake near Akhalkalaki- 04.08.2016, Mag-3.1

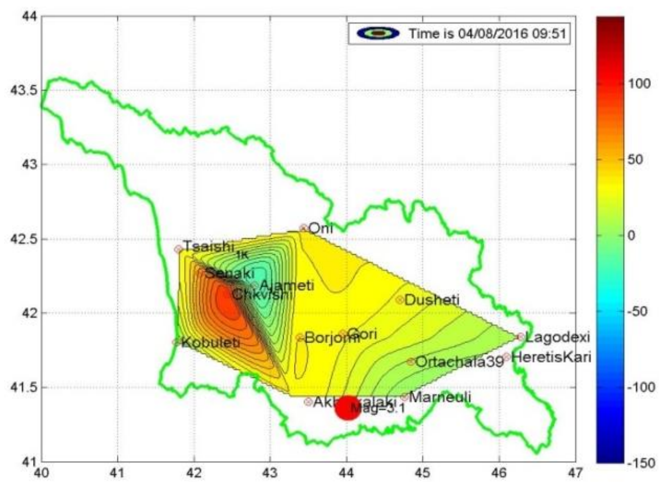

Fig. 14.

Hydrogeodeformational field value observed during the 4 August, 2016 earthquake. The field was created by the value of trended water level.

At the Marneuli station we observed anomaly on 4 August between the earthquake and its aftershock, it was also observed for 1 day after the earthquake. Earthquake occurred 60 km away from the station.

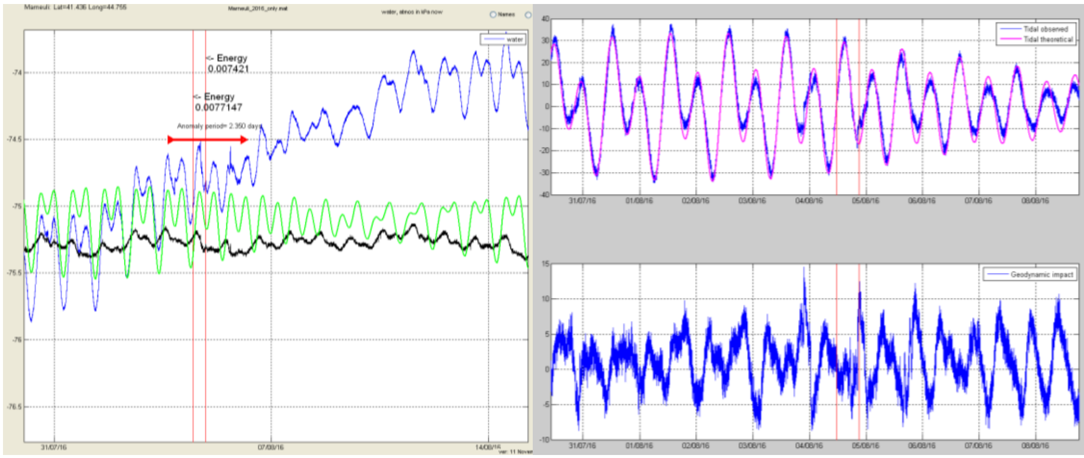

a b

Fig. 15

a- Water level, atmospheric pressure and tidal variations on the Marneuli borehole (cm). The vertical line marks an earthquake. On abscise axis time is in hours. b- Speed factor of variations water level and earth tidal and the difference between them.

At the Gori station, like the one at Marneuli station, anomaly was observed on 4 August before the earthquake and its aftershock. Gori station is in 51 km from the Epicenter.

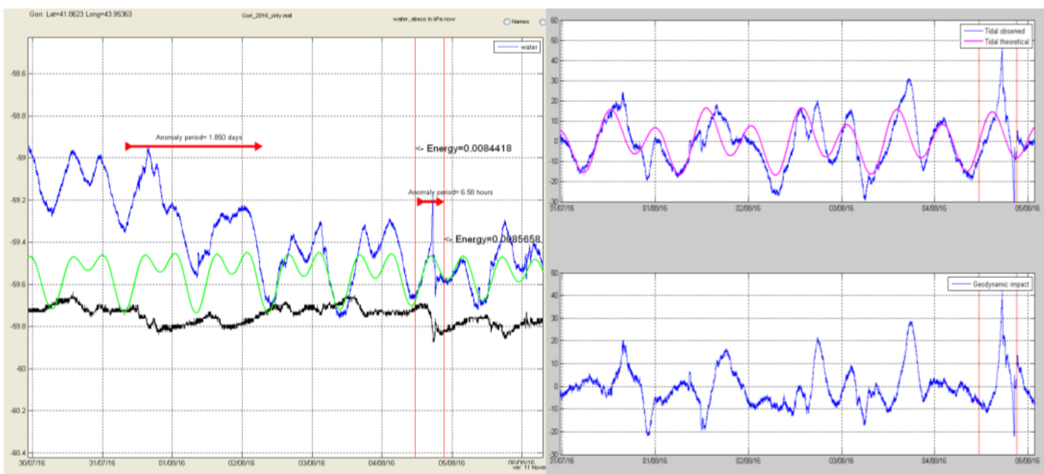

a b

Fig. 16

a- Water level, atmospheric pressure and tidal variations, Gori borehole (cm). The vertical line marks an earthquake. On abscise axis time is in hours. b- Speed factor of variations water level and earth tidal and the difference between them.

Anomaly was observed at Dusheti geomagnetic observatory, starting from 4 August 2016, 2- days prior to the earthquake. The earthquake occurred in 98 km from the station. The anomaly continued for 2 days after the earthquake.

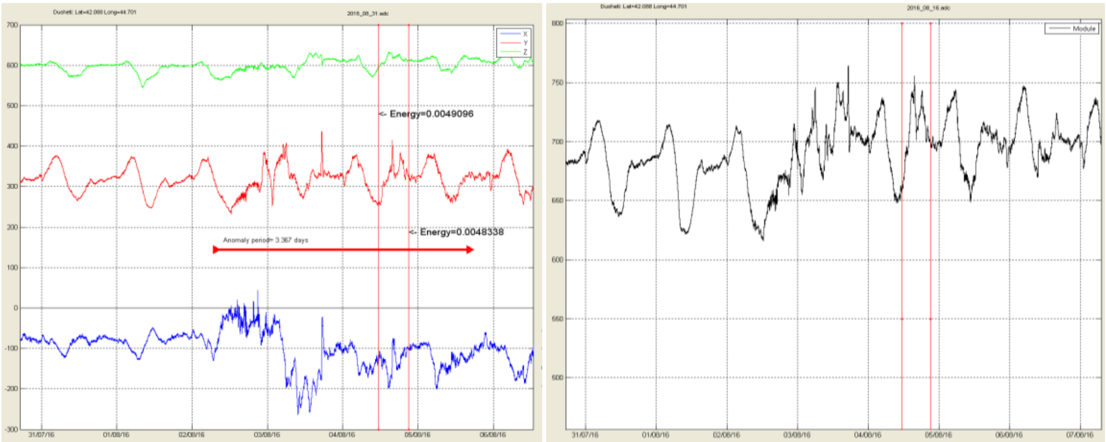

a b

Fig. 17.

a-Variation of x,y z components of the magnetic field. b- Variation of the module value.

Earthquake in Ninotsminda area-15.08.2015, Mag-3.6

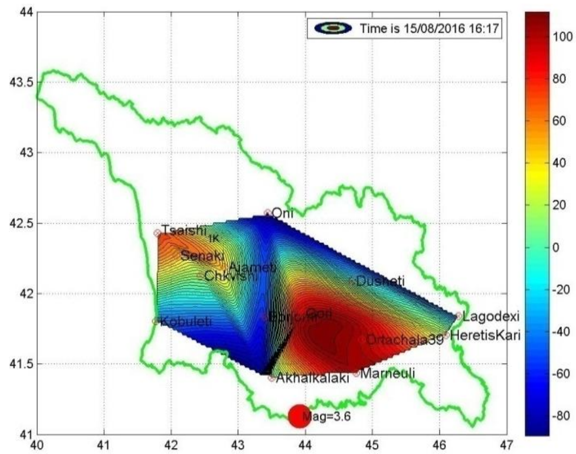

Fig. 18.

Hydrogeodeformational field value during the 15 August 2016 earthquake. The field was plotted for water level trended values.

Anomaly was observed at Ajameti station, on 15 August 2016, before the earthquake. The station is in 150 km from the epicenter of the earthquake. 3-4 days earlier before the earthquake the water level dropped by 40 cm. 1 day earlier before the earthquake we observed sudden rise of the water level by 20 cm. The stressed condition remained after the earthquake as wall.

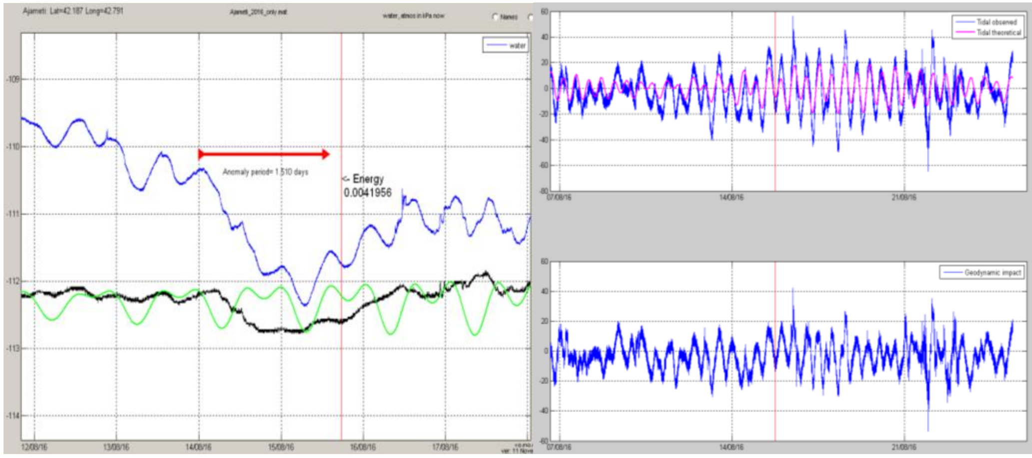

a b

Fig. 19.

a- Water level, atmospheric pressure and tidal variations, Ajameti borehole (cm). The vertical line marks an earthquake. On abscise axis time is in hours. b- Speed factor of variations water level and earth tidal and the difference between them..

In Kobuleti, which is 193 km away from the epicenter, we observed an anomaly 2 days prior to the earthquake.

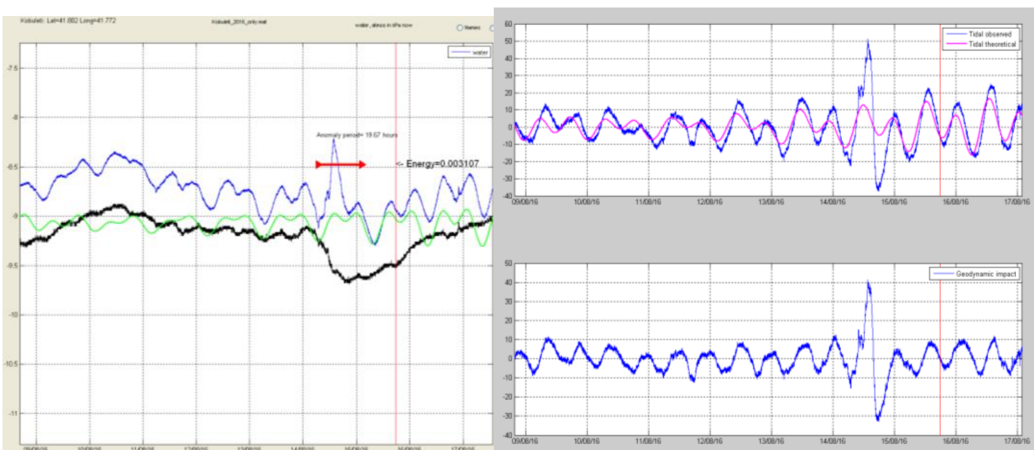

a b

Fig. 20

a- Water level, atmospheric pressure and tidal variations at Kobuleti borehole (cm). The vertical line marks an earthquake. On abscise axis time is in hours. b- Speed factor of variations water level and earth tidal and the difference between them.

The anomaly observed 4-5 days prior to the before earthquake can be seen in the plot. The epicenter was 81 km away from Gori station.

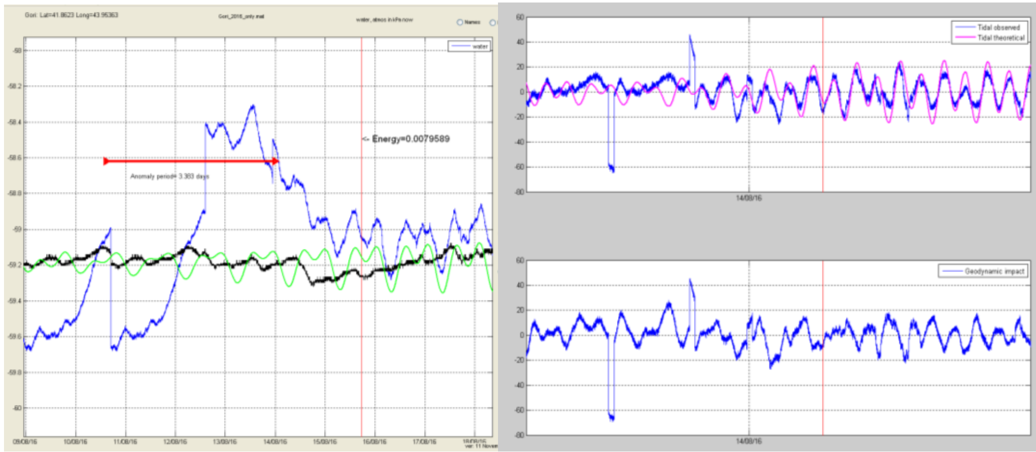

a b

Fig. 21

a - Water level, atmospheric pressure and tidal variations, Gori borehole (cm). The vertical line marks an earthquake. On abscise axis time is in hours. b- Speed factor of variations water level and earth tidal and the difference between them.

At Chkvishi station anomaly was observed 2days prior to the earthquake. The duration of the anomalous period is shown on graphic. Chkvishi station is 165 km away from the epicenter.

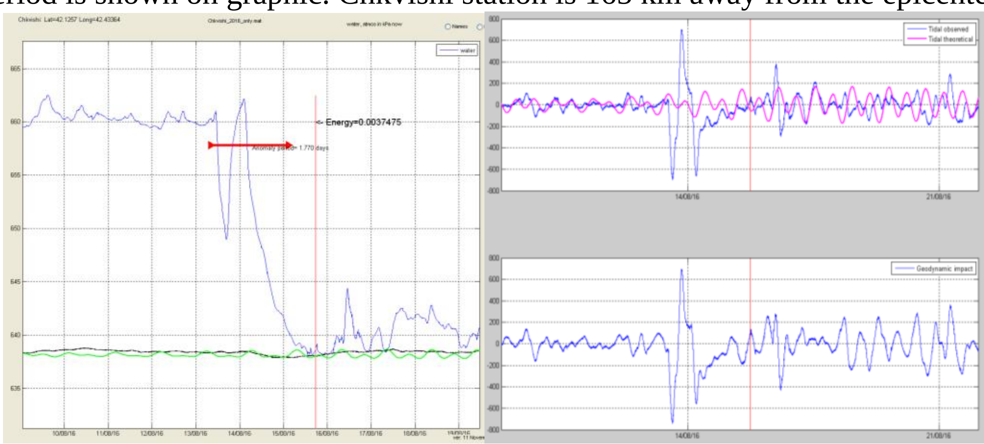

a b

Fig. 22

a- Water level, atmospheric pressure and tidal variations at Chkvishi borehole (cm). The vertical line marks an earthquake. On abscise axis time is in hours. b- Speed factor of variations water level and earth tidal and the difference between them.

At Tsaishi station the anomaly was observed a week prior to the earthquake. Borehole is out flowing and is located 227 km away from the epicenter.

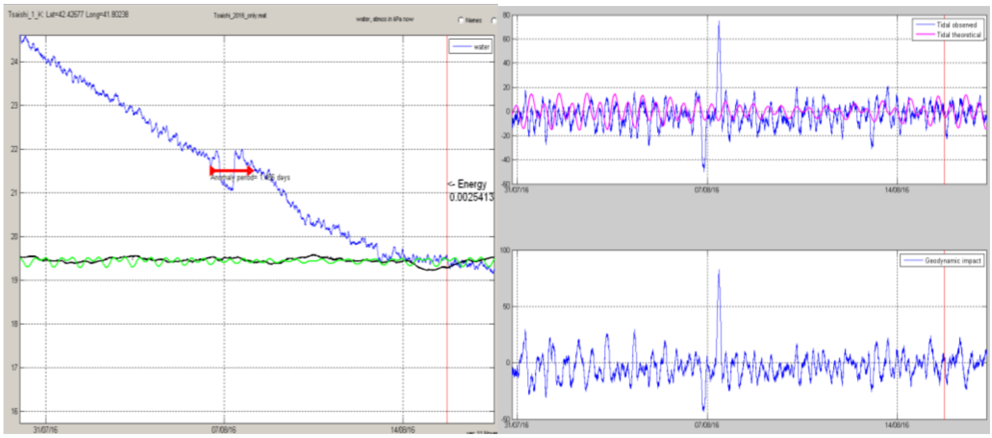

a b

Fig. 23

a - Water level, atmospheric pressure and tidal variations on the Tsaishi borehole (cm). The vertical line marks an earthquake. On abscise axis time is in hours. b- Speed factor of variations water level and earth tidal and the difference between them.

Earthquake in the Gagra region- 02.09.2016 Mag=4

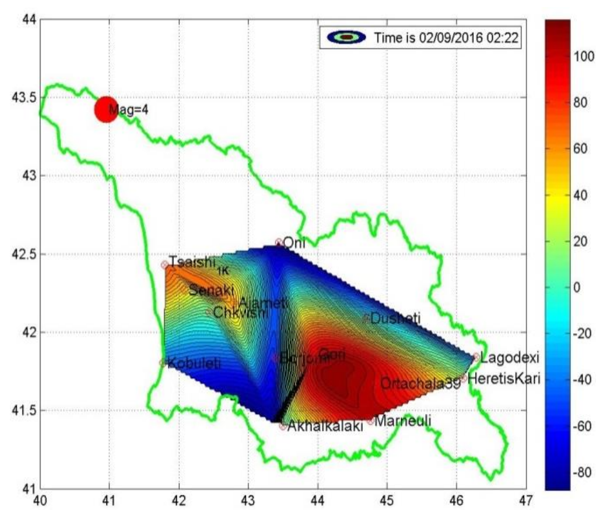

Fig. 24

. Hydrogeodeformational field value during the 02 September 2016 earthquake. The field was built for the water level trended values

2 days prior to the 2 September earthquake we observed the anomaly at Kobuleti station. Kobuleti station is 191km away from the epicenter.

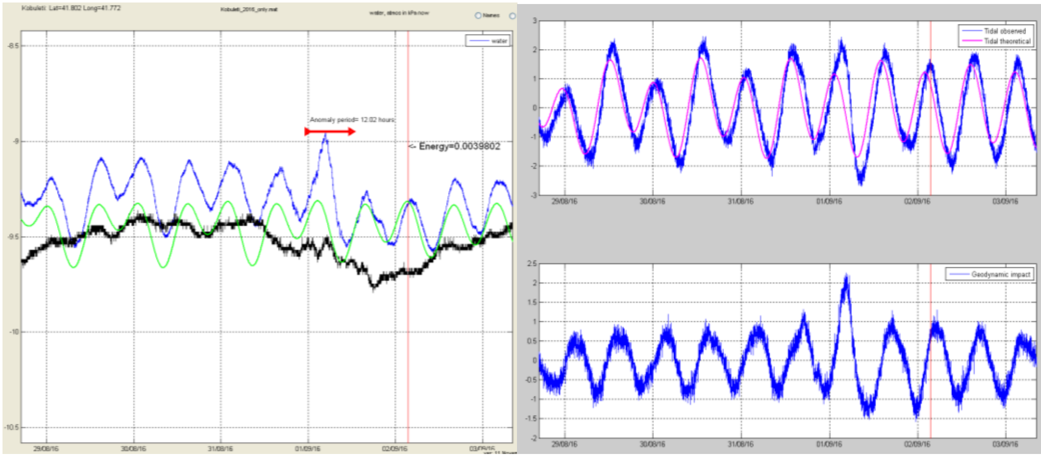

a b

Fig. 25

a- Water level, atmospheric pressure and tidal variations at Kobuleti borehole (cm). The vertical line marks an earthquake. On abscise axis time is in hours. b- Their variations speed graphics and the difference.

We observed anomaly at Ajameti station 1 day prior to the earthquake- water level remained dropped after the earthquake as well.

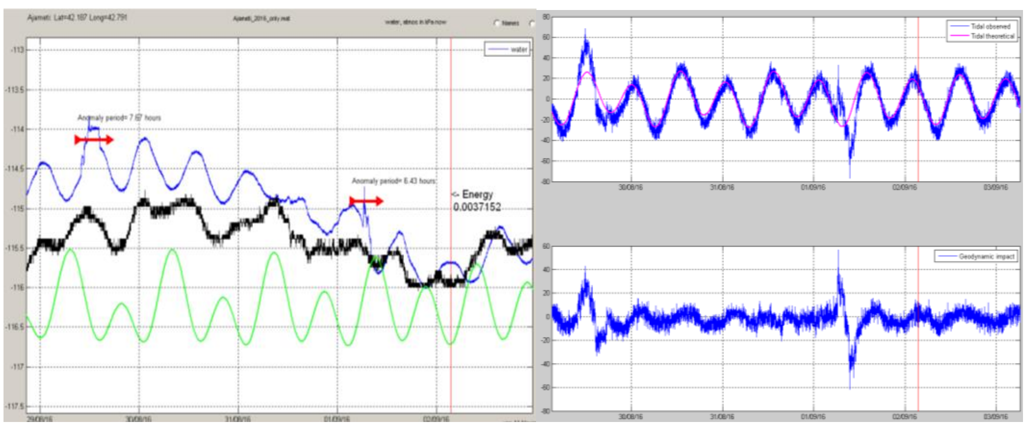

a b

Fig.

Fig. 26

a- Water level, atmospheric pressure and tidal variations at Ajameti borehole. The vertical line marks an earthquake. On abscise axis time is in hours. b- Speed factor of variations water level and earth tidal and the difference between them.

Anomaly was also observed at Chvishi station before the earthquake on 2 September, where like the one in Ajameti, the water level dropped and maintained the level for some time after the earthquake. Chkvishi borehole is 187 km away from epicenter.

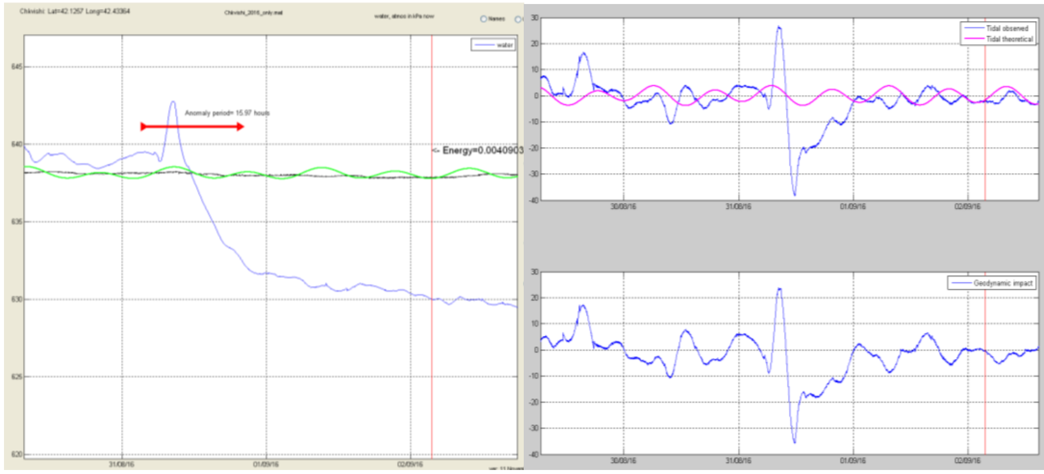

a b

Fig. 27

a - Water level, atmospheric pressure and tidal variations at Chkvishi borehole (cm). The vertical line marks an earthquake. On abscise axis time is in hours. b- Speed factor of variations water level and earth tidal and the difference between them.

Earthquake occurred on the North-West territory of Azerbaijan- 07.09.2016, Mag=4.4

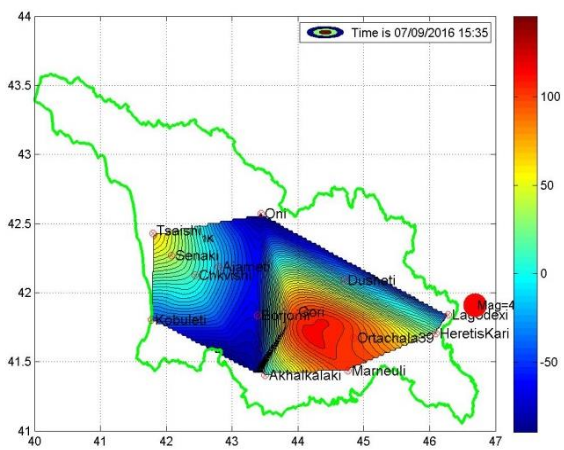

Fig. 28.

Hydrogeodeformational field value during the 07 September 2016 earthquake. The field was built for the trended water level values.

Anomaly was also observed at Dusheti Geomagnetic Observatory, a week prior to the 7 September 2016 earthquake and continued for 6 days. The earthquake occurred in 165 km from the station. The second earthquake in the graph is an aftershock.

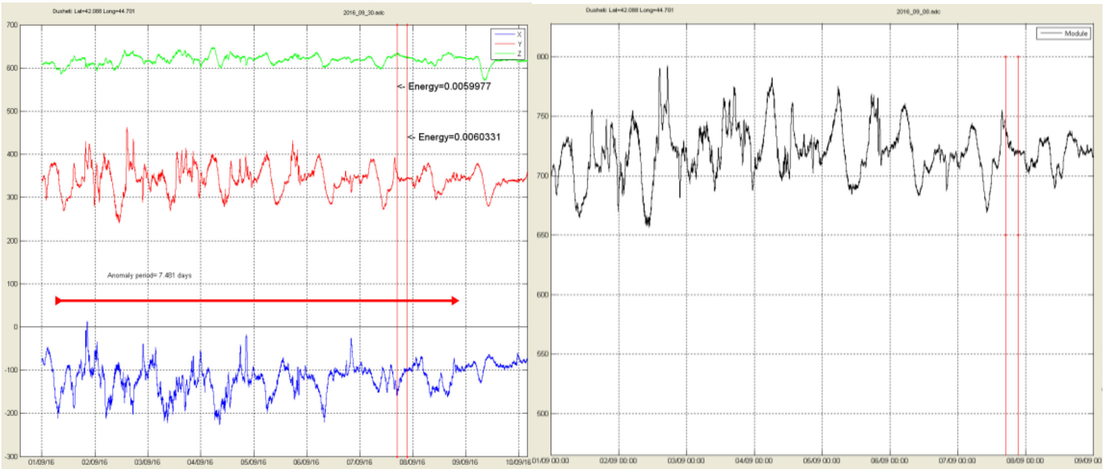

a b

Fig. 29.

a-Variation of x,y,z components of the magnetic field. b- Variation of the module value.

Lagodekhi station is in 35 km from the epicenter. As we can see the graph, the anomaly is observed 2 days prior to the 7 September earthquake.

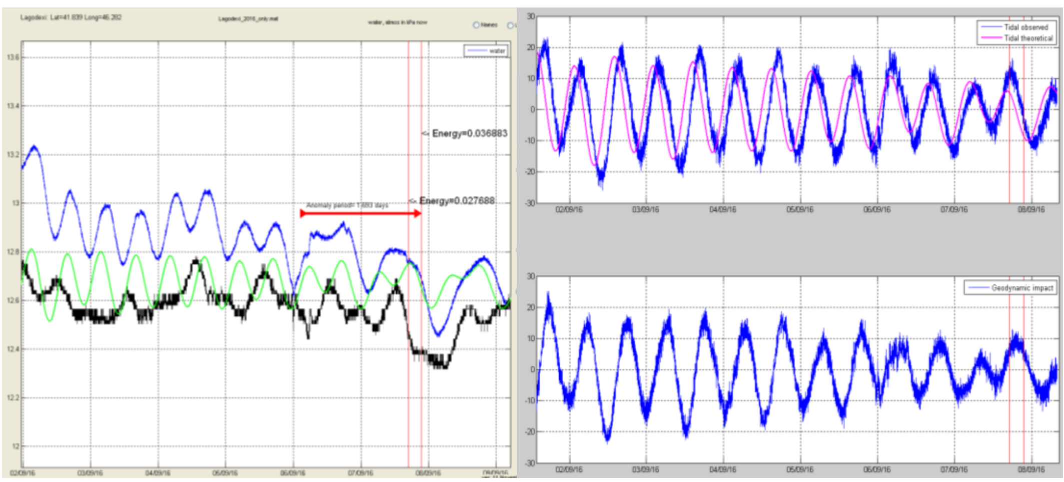

a b

Fig. 30.

a - Water level, atmospheric pressure and tidal variations at Lagodekhi borehole (cm). The vertical line marks an earthquake. On abscise axis time is in hours. b- Speed factor of variations water level and earth tidal and the difference between them.

At Marneuli station, which is 169 km away from the epicenter, the anomaly was observed 2 days prior to the earthquake and lasted during the earthquake as well.

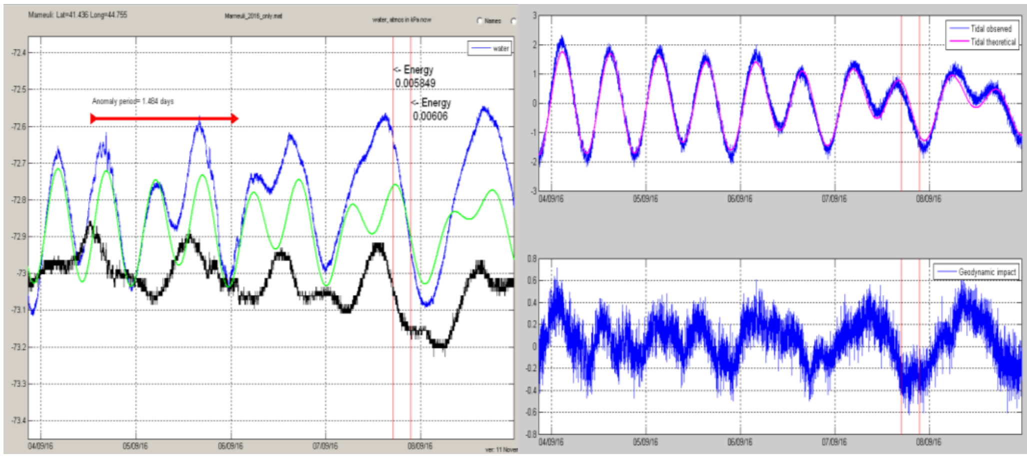

a b

Fig. 31.

a - Water level, atmospheric pressure and tidal variations at Marneuli borehole (cm). The vertical line marks an earthquake. On abscise axis time is in hours. b- Speed factor of variations water level and earth tidal and the difference between them.

Anomaly was also observed 2 days prior to the earthquake at Gori station. Here like in Marneuli, conditions lasted after the earthquake as well. Gori station is 226 km away from the 7 September earthquake epicenter.

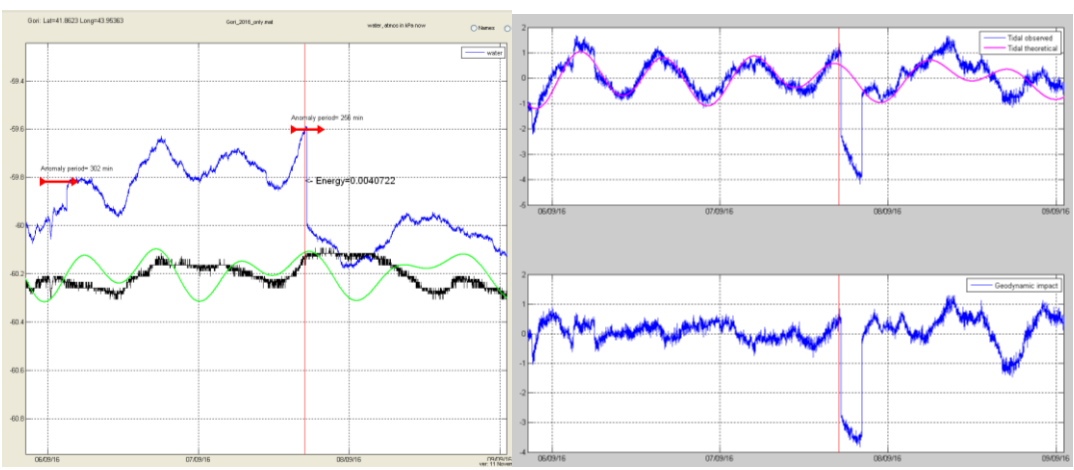

a b

Fig. 32

a - Water level, atmospheric pressure and tidal variations at Gori borehole (cm). The vertical line marks an earthquake. On abscise axis time is in hours. b- Speed factor of variations water level and earth tidal and the difference between them.

4 days prior to the earthquake an anomaly was observed near Chkvishi borehole. Here a typical picture of Chkvishi station is shown before the earthquake expressed in sharp changing of the level. Chkvishi station is away 352 km from the earthquake epicenter, which occurred on 7 September 2016.

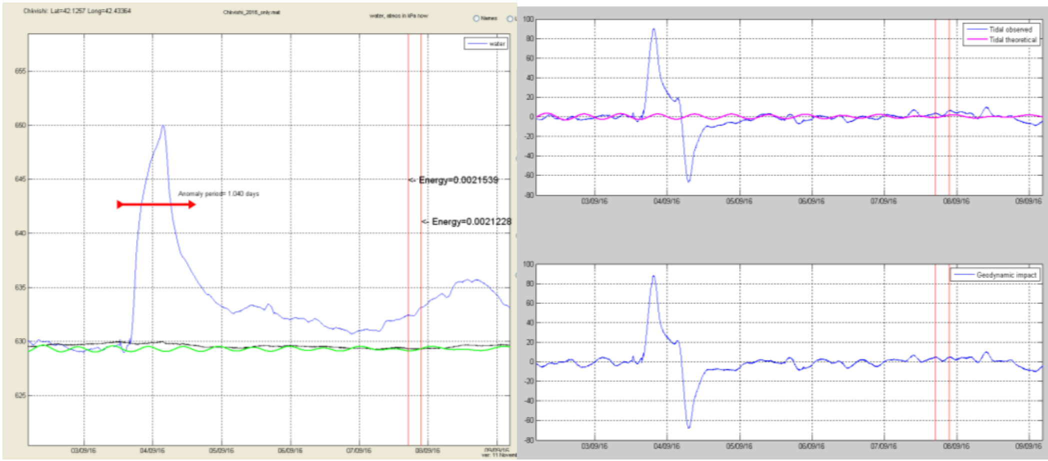

a b

Fig. 33

a - Water level, atmospheric pressure and tidal variations at Chkvishi borehole (cm). The vertical line marks an earthquake. On abscise axis time is in hours. b- Speed factor of variations water level and earth tidal and the difference between them.

Conclusions

The results show that variations in hydrodynamic and geomagnetic parameters are caused by the earth stress. During normal period it change according tidal variation and has “background” value. “Anomalous” variations during preparation period of the seismic event demonstrated change above “background” value, as indicator of tectonic activity. Earthquakes with Magnitude 3-5, occurred during the observed time period on the territory of Caucasus. Character of “anomalies” depended on energy of earthquakes. Period of “anomalies” varied between 2-5 days and the distance of influence changed between 200-500 km from the epicenter.

Acknowledgments: The authors thank the Rustaveli National Scientific foundation for financial support of the project #156/13 “Spatial and Temporal Variability of Geodynamical Field and Its Influence on the Deep Aquifers and Geomagnetic Field**“.**

References

1. G. Melikadze, I. Kobzev, N. Kapanadze, Z. Machaidze, T. Jimsheladze, Analyze of underground water regime factors for determine tectonic component, LEPT Institute of Hydrogeology and Engineering Geology, Collection articles, vol. XYI. Proceeding of Conference Dedicate to the 100-th Anniversary of Professor Josef Buachidze. Tbilisi. 2007

2. N. Dovgal, G.I. Melikadze, Methodology of Creation of Multi-Parametrical Network, Workshop materials “Exploration and exploitation of groundwater and thermal water systems in Georgia, 50-60, 2010, Tbilisi, Georgia, http://dspace.nplg.gov.ge/handle/1234/9081

3. K. Kartvelishvili, G. Melikadze, G. Kobzev “Influence of atmosphere pressure and tidal variation of gravity of the hydrosphere”. Mokheil Nodia Institute of Geophysics, Proceedings of the Institute Geophysics, Volume 65, page 1 69 -173, 2010

4. G. Kobzev, G.I. Melikadze, Methods of hydrogeodynamical analysis for revealing earthquakes precursors, Workshop materials “Exploration and exploitation of groundwater and thermal water systems in Georgia,.60-69, 2010, Tbilisi, Georgia
5. T. Chelidze, T. Matcharashvili, and G. Melikadze, Earthquakes’ Signatures in Dynamics of Water Level Variations in Boreholes, In: Synchronization and Triggering: from Fracture to Earthquake Processes, Eds.V.de Rubeis, Z. Czechowski, R. Teisseyre, Geoplanet: Earth and Planetary Sciences, 2010, Volume 1, Part 3, 287-304, DOI: 10.1007/978-3-642-12300-9_20, Springer.
6. T. Jimsheladze, G. Kobzev, G. Melikadze, N. Zhukova, Geodynamical Impact on the Water Level Variations in the Boreholes, Workshop materials “Exploration and exploitation of groundwater and thermal water systems in Georgia, 69-83, 2010, Tbilisi, Georgia
7. T. Jimsheladze, G. Melikadze, A. Chankvetadze, R. Gagua, T. Matiashvili. The Geomagnetic Variation in Dusheti Observatory Related With Earthquake Activity in East Georgia, Journal of the Georgian Geophysical Society, Issue A. Physics of Solid Earth, vol. 15A, p.118-128, 2012.
8. T.Chelidze, I.Shengelia, N.Zhukova, T. Matcharashvili, G. Melikadze, G. Kobzev. “Coupling of Multiple Rayleigh Waves and Water Level Signals during 2011 Great Tohoku Earthquake Observed in Georgia, Caucasus”.Proceedings of the National Academy of Sciences (Impact Factor: 9.81). 01/2014;
9. G. Melikadze, T. Jimsheladze, G. Kobzev, A. Benderev, E. Botev. “Linear methods of studying the water level variation related with seismicity”.Geophysical Journal International (Impact Factor: 2.72). 01/2014; Physics of Solid Earth, v.17a (Issue (A)):65-75.
10. G.Melikadze, G.Kobzev, T.Jimsheladze. “Some Methods of Analyze Geodynamic Imfuct on the Deep Aquifare”. Journal of Georgian Geophysical Society 01/2014; Physics of Solid Earth, v.17a (Issue (A)):47-52.
11. T. Jimsheladze, G. Melikadze, G. Kobzev “Construction and analysis of the stress state of environment during the preparation of the Racha earthquake 2009” Proceedings of Mikheil Nodia Institute of Geophysics, Tbilisi, Georgia, 2013.

ჰიდროდინამიკური და გეომაგნიტიკური ანომალიები დაკავშირებული კავკასიის მიწისძვრებთან

გიორგი მელიქაძე, თამარ ჯიმშელაძე, გენადი კობზევი, ალექსანდრე ჭანკვეტაძე

ივ. ჯავახიშვილისსახ. თბილისის სახელმწიფო უნივერსიტეტი, მ. ნოდიას გეოფიზიკის ინსტიტუტი

რეზიუმე

2016 წლის ივლისი-სექტემბრის პერიოდში, საქართველოს ტერიტორიაზე განლაგებულ მულტიპარამეტრულ სამონიტორინგო ქსელზე დაფიქსირდა მრავალი ჰიდროდინამიკური და გეომაგნიტური ანომალია. მონაცემები იზომებოდა ყოველ წუთში და იკრიბებოდა

რეალური დროის მონაკვეთში. მონაცემები მუშავდებოდა სპეციალური პროგრამის მეშვეობით. გეოლოგიური ფაქტორების გავლენის გამოსარიცხათ სხვადასხვა სადგურების მონაცემები კალიბრებოდა მიმოქცევითი ვარიაციებით. გაანალიზდა პარამეტერბის ვარიაციები და რეაქციები მიწისძვრის მომზადების პროცესზე და ასევე მიწისძვრის წინ დაძაბულობის ველის რეალური სიდიდეები.

Гидродинамические и геомагнитные аномалии, связанные с землетрясениями Кавказа

Гиоргий Меликадзе, Тамар Джимшеладзе, Генадий Кобзев, Александре Чанкветатдзе

Государственный университет им. Иване Джавахишвили, Институт геофизики им. М. Нодия

Резюме

В период с июля 2016 по сентябрь 2016 был зафиксирован ряд гидродинамических и геомагнитных аномалий при мультипараметрических наблюдениях на мониторинговой сети, расположенной на территории Грузии. Данные записывались ежеминутно и собирались в режиме реального времени. Они были проанализированы с помощью специальной программы. С тем, чтобы исключить влияние геологических факторов, данные с различных станций были откалиброваны с помощью значений приливных вариаций. Осуществлен анализ вариаций и реакция параметра на процесс подготовки землетрясения, а также вычислены значения напряженного поля земли до и после землетрясения.

Information for contributors

Papers intended for the Journal should be submitted in two copies to the Editor-in-Chief. Papers from countries that have a member in the Editorial Board should normally be submitted through that member. The address can be found on the inside front cover.

1. Papers should be written in the concise form. Occasionally long papers, particularly those of a review nature (not exceeding 16 printed pages), will be accepted. Short reports should be written in the most concise form not exceeding 6 printed pages. It is desirable to submit a copy of paper on a diskette.
2. A brief, concise abstract in English is required at the beginning of all papers in Russian and in Georgian at the end of them.
3. Line drawings should include all relevant details. All lettering, graph lines and points on graphs should be sufficiently large and bold to permit reproduction when the diagram has been reduced to a size suitable for inclusion in the Journal.
4. Each figure must be provided with an adequate caption.
5. Figure Captions and table headings should be provided on a separate sheet.
6. Page should be 20 x 28 cm. Large or long tables should be typed on continuing sheets.
7. References should be given in the standard form to be found in this Journal.
8. All copy (including tables, references and figure captions) must be double spaced with wide margins, and all pages must be numbered consecutively.
9. Both System of units in GGS and SI are permitted in manuscript
10. Each manuscript should include the components, which should be presented in the order following as follows:
    Title, name, affiliation and complete postal address of each author and dateline.
    The text should be divided into sections, each with a separate heading or numbered consecutively, as 1.1 (then 1.1.1, 1.1.2 . . .) 1.2 etc.
    Introduction
    State the objectives of the work and provide an adequate short background
    Material and methods
    Provide sufficient detail to allow the work to be reproduced. Methods already published should be indicated by a reference.
    Theory/calculation
    Results
    Results should be clear and concise.
    Discussion
    This should explore the significance of the results of the work, not repeat them. Acombined Results and Discussion section is often appropriate.
    Conclusions
    Alone or form a subsection of a Discussion or Results and Discussion section.
    Acknowledgements. Appendix. Reference.
11. The editors will supply the date of receipt of the manuscript.

CONTENTS

სარჩევი

საქართველოს გეოფიზიკური საზოგადოების ჟურნალი

სერია ა. დედამიწის ფიზიკა

ჟურნალი იბეჭდება საქართველოს გეოფიზიკური საზოგადოების პრეზიდიუმის დადგენილების საფუძველზე

ტირაჟი 100 ცალი

ЖУРНАЛ ГРУЗИНСКОГО ГЕОФИЗИЧЕСКОГО ОБЩЕСТВА

Серия А. Физика твердой Земли

Журнал печатается по постановлению президиума Грузинского геофизического общества

Тираж 100 экз

JOURNAL OF THE GEORGIAN GEOPHYSICAL SOCIETY

Issue A. Physics of Solid Earth

Printed by the decision of the Georgian Geophysical Society Board

Circulation 100 copies